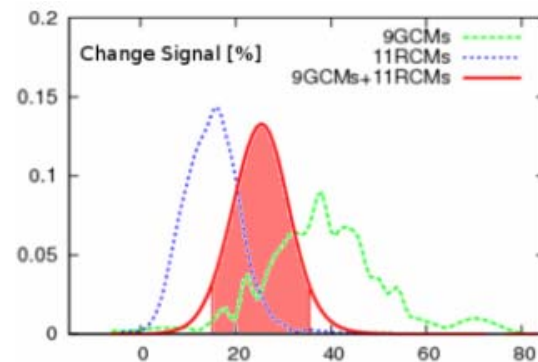
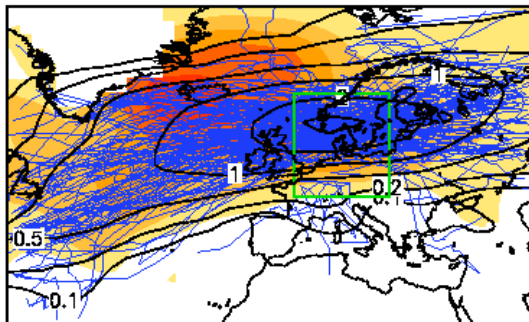


European wind storms, related loss potentials and changes in multi-model climate simulations



DISSERTATION
zur Erlangung des akademischen Grades eines
Doktors der Naturwissenschaften
am Fachbereich für Geowissenschaften
der Freien Universität Berlin

vorgelegt von

Markus G. Donat

Berlin, März 2010

1. Gutachter: Prof. Dr. Uwe Ulbrich

2. Gutachter: Prof. Dr. Ulrich Cubasch

Disputationstermin: 14. Juni 2010

Content

Content	i
Selbstständigkeitserklärung	iii
Abstract	1
Kurzzusammenfassung	3
1. Introduction	5
1.1. Motivation	7
1.2. State of knowledge	8
1.2.1. European storminess: natural variability and trends caused by ACC	9
1.2.2. Uncertainties in climate simulations and ensemble approaches for estimating robustness and increasing confidence	10
1.3. Thesis Objective	12
1.4. Thesis Outline	13
2. Examination of Wind Storms over Central Europe with respect to Circulation Weather Types and NAO phases	17
2.1. Introduction	19
2.2. Data and Methods	21
2.3. Analysis of the large-scale circulation and storm days	26
2.3.1. Classification of daily circulation weather types and detection of storm days	26
2.3.2. CWTs and storm days related to NAO	28
2.3.3. Characteristics of storm events	32
2.4. Summary, Discussion and Conclusions	36
3. European storminess and associated circulation weather types: future changes deduced from a multi-model ensemble of GCM simulations	41
3.1. Introduction	43
3.2. Data and Methods	45
3.3. Analysis of the model simulations	49
3.3.1. Winter mean MSLP field and atmospheric flow	49
3.3.2. Classification of daily circulation weather types	51
3.3.3. Storm day frequencies	52
3.3.4. Atmospheric circulation on storm days	58
3.3.5. Cyclone tracks, pressure patterns and local wind speeds associated with storm events	59
3.3.6. Effects of different model combinations on the ensemble mean ACC signals	64
3.4. Discussion	66
3.5. Summary and Conclusion	68
4. Mid-latitude Cyclones and Storms in an Ensemble of European AOGCMs under Anthropogenic Climate Change	71
4.1. Introduction	73
4.2. Investigation Method and Results	75
4.3. Conclusion and Future Work	77

5. Benefits and limitations of regional multi-model ensembles for storm loss estimations.....	79
5.1. Introduction	81
5.2. Data and Methods.....	83
5.2.1. Data.....	83
5.2.2. Calculation of storm induced losses	85
5.3. Results concerning extreme wind speeds and loss estimates	87
5.3.1. Simulated wind fields	87
5.3.2. Validation with loss data for Germany.....	89
5.3.3. Impact of different model combinations on the ensemble mean performance	93
5.4. Specific considerations of the storm on 13 November 1972 and impacts on the RCM performance measure.....	95
5.5. Summary, Discussion and Conclusion	99
6. Future changes of European winter storm losses and extreme wind speeds in multi-model GCM and RCM simulations.....	105
6.1. Introduction	107
6.2. Data and Methods.....	110
6.2.1. Meteorological Data	110
6.2.2. Calculation of storm induced losses	113
6.3. Extreme wind speeds and related losses estimated from GCM and RCM scenario simulations	116
6.3.1. Analysis of the GCM simulations	116
6.3.2. Analysis of the RCM scenario simulations	125
6.3.3. Multi-model combinatorics: Uncertainty of ACC loss potentials considering all possible model combinations.....	129
6.4. Summary, Discussion and Conclusion	133
6.5. Appendix Chapter 6: Supplementary Material.....	138
7. Conclusions and Outlook.....	143
7.1. Conclusions	145
7.2. Discussion and Outlook.....	151
Bibliography.....	155
Acknowledgements.....	169

Selbstständigkeitserklärung

Hiermit erkläre ich an Eides Statt, dass ich die vorliegende Arbeit selbstständig und ohne fremde Hilfe angefertigt, keine anderen als die angegebenen Quellen und Hilfsmittel benutzt und die den benutzten Quellen wörtlich oder inhaltlich entnommenen Stellen als solche kenntlich gemacht habe. Diese Arbeit hat in gleicher oder ähnlicher Form noch keiner Prüfungsbehörde vorgelegen.

Berlin, 10.03.2010

Abstract

The occurrence of European winter storms and consequential losses is examined on the basis of reanalysis data and multi-model climate simulations, with the aim of learning about potential future changes of wind storm risk in Europe. Considering multi-model simulations conduces to an estimation of the (un-) certainties of change signals. Characteristics of the large-scale atmospheric flow are analysed and examined in conjunction with the occurrence of wind storms in Central Europe. Additionally, extreme wind speeds and the related loss potentials are investigated, applying a loss regression model. Further, the effect of dynamical downscaling on the results is considered with respect to extreme wind and storm loss analysis, and the benefit of combining different climate models to a multi-model ensemble is examined.

Validating the climate model simulations of the recent climate against ERA40-reanalysis data leads to the finding that the models are generally capable of reproducing observed characteristics of atmospheric circulation and wind storm related atmospheric features in the North Atlantic / European region. One limitation, however, is a tendency towards an excess of zonal flow situations and an underestimation of anticyclonic flow in most models.

In future climate scenario simulations, a significantly reduced total number of extra-tropical cyclones is found in the northern hemisphere, whereas considering only extreme cyclones, hotspots of increased activity are found over the eastern parts of the North Atlantic and the North Pacific. Focussing on Central Europe, the large-scale atmospheric flow is characterised by an increased frequency of westerly flow situations, and also an enhanced frequency of storm days is analysed, in ensemble mean between 19 and 33 % for two different measures of storminess. The intensity of cyclones associated with wind storm in Central Europe is increased by about 10 % in ensemble mean in the Eastern Atlantic and in the North Sea. Furthermore, the wind speeds during storm events increase significantly over large parts of Central Europe by about 5 %. Analysing extreme wind speeds and the related loss potentials, enhanced speed values and risk of loss are found over the northern parts of Central and Western Europe, whereas significant reductions are found over southern Europe and the Mediterranean region.

The uncertainty of the change signals is estimated using two different measures. First, the inter-model standard deviation is considered. It is, however, sensitive to outliers and therefore involves relatively large uncertainty ranges, for most signals of a similar magnitude as the signal itself. Secondly, a new measure for uncertainty is proposed based on multi-model combinatorics, considering all possible combinations of available climate simulations and hence taking into account the arbitrariness of model selection for multi-model studies. This approach leads to considerably narrower uncertainty ranges.

Except for limitations for one specific storm event, a distinct benefit to storm loss calculations from dynamical downscaling is shown. The benefit from combining the output of different models was examined systematically, and it is documented that the performance of the ensemble mean is comparable to the best single model, even if weak performing models are included. Further, for larger ensemble sizes the spread between the best and the weakest performing model combination becomes considerably lower, supporting the inclusion of preferably many models in the ensemble. Exclusion of weak models yields only marginal improvements.

Kurzzusammenfassung

Das Auftreten von europäischen Winterstürmen und der damit verbundenen Schäden wird auf Grundlage von Reanalysedaten und Multi-Modell-Klimasimulationen untersucht. Ziel ist es, Aussagen über zukünftige Änderungen des Sturmrisikos in Europa abzuleiten. Die Betrachtung von Multi-Modell-Simulationen ermöglicht es, die (Un-)Sicherheiten der Änderungssignale abzuschätzen.

In dieser Arbeit werden die Eigenschaften der großskaligen atmosphärischen Strömung analysiert und im Zusammenhang mit dem Auftreten von Stürmen in Mitteleuropa betrachtet. Außerdem werden extreme Windgeschwindigkeiten und – durch Anwendung eines Sturmschaden-Regressions-Modells – damit verbundene Sturmschadenpotentiale untersucht. Darüber hinaus wird der Einfluss von dynamischem Downscaling auf die Ergebnisse hinsichtlich extremer Windgeschwindigkeiten und Sturmschadenberechnungen betrachtet, wie auch der Nutzen durch das Kombinieren verschiedener Klimamodelle zu einem Multi-Modell Ensemble.

Die Validation der Klimasimulationen im Vergleich zu ERA40-Reanalysen zeigt, dass die Modelle die beobachteten Eigenschaften der atmosphärischen Zirkulation und die Merkmale im Zusammenhang mit Sturm im Raum Nordatlantik/Europa gut reproduzieren. Ein Defizit der meisten Modelle ist jedoch deren Tendenz zu übermäßig häufigen zonalen Strömungssituationen, während antizyklonale Wetterlagen zu selten simuliert werden.

In Szenariensimulationen des zukünftigen Klimas zeigt sich eine Reduktion der Gesamtanzahl extratropischer Zyklonen auf der Nordhalbkugel, während sich hinsichtlich extremer Zyklonen Gebiete mit erhöhter Aktivität über dem östlichen Nordatlantik und Nordpazifik zeigen. Die großskalige Zirkulation über Mitteleuropa ist durch häufigeres Auftreten westlicher Anströmungsklassen gekennzeichnet, wie auch durch häufigeres Auftreten von Sturmtagen (zwischen 19 und 33% für zwei verschiedene Sturmtagkriterien). Die Intensität der Zyklonen, die zu Sturm in Mitteleuropa führen, ist in den Zukunftssimulationen insbesondere über dem östlichen Atlantik und über der Nordsee erhöht, im Ensemblemittel um ca. 10%. Auch die Windgeschwindigkeiten während der Sturmereignisse nehmen signifikant um etwa 5% zu. Die Analyse von extremen Windgeschwindigkeiten und der damit verbundenen Schadenpotentiale zeigt höhere Geschwindigkeitswerte und auch Schadenrisiken über

den nördlichen Teilen Mittel- und Westeuropas, während sie sich über Südeuropa und dem Mittelmeerraum signifikant verringern.

Die Unsicherheit der Änderungssignale wird mittels zweier verschiedener Maße abgeschätzt. Einerseits wird die Standardabweichung zwischen den Signalen der einzelnen Modelle betrachtet. Diese ist jedoch anfällig gegenüber Ausreißern und zeigt daher relativ große Unsicherheitsbereiche, für die meisten Signale in einer ähnlichen Größenordnung wie das Signal selbst. Zum anderen wird ein neues Unsicherheitsmaß eingeführt, welches auf der Kombinatorik der Multi-Modell-Simulationen beruht, alle Kombinationen verfügbarer Klimasimulationen berücksichtigt, und somit auch der Willkür bezüglich der Modellauswahl Rechnung trägt. Dieser Ansatz führt zu deutlich kleineren Unsicherheitsbereichen.

Abgesehen von Einschränkungen bei einem besonderen Sturm, zeigt sich ein deutlicher Vorteil durch dynamisches Downscaling für die Sturmschadenberechnungen. Der Nutzen durch das Kombinieren verschiedener Modelle wird systematisch untersucht und es wird dokumentiert, dass die Performanz des Ensemblemittels vergleichbar ist mit der des besten einzelnen Modells, selbst wenn Modelle geringerer Qualität miteinbezogen werden. Zusätzlich wird für große Ensembles die Spannbreite zwischen der besten und schwächsten Modellkombination deutlich kleiner, was die Berücksichtigung möglichst vieler Modelle im Ensemble unterstützt. Das Ausschließen schwächerer Modelle bringt nur geringe Verbesserungen.

1. Introduction

1.1. Motivation

Intense winter storms affect Central Europe regularly. For example, severe storms such as those seen in January and February 1990 (e.g. Daria, Vivian, Wiebke, cf. McCallum and Norris, 1990), in December 1999 (e.g. Anatol, Lothar, Martin, cf. Ulbrich et al., 2001; Wernli et al., 2002), and more recently in January 2007 (e.g. Kyrill, cf. Fink et al., 2009) and in February 2010 (storm Xynthia), repeatedly raise public and scientific interest in these natural hazards. Wind storms are the most loss-relevant natural hazards affecting Central Europe. They commonly result in damage to the environment, infrastructure and buildings, disturbances of traffic, may lead to storm surges and may also cause injury or even loss of life. Compared to other meteorological hazards, wind storms affect relatively large areas. This contributes to the large loss amounts caused by those events, accounting for several billion Euros related with individual storms. For example, in Germany 53 (64) % of economic (insured) losses owing to natural hazards are caused by severe winter storms (MunichRe, 1999; Munich Re, 2007). On average, insurance companies have to pay about 900 million € per year in Germany alone as a consequence of storm damage to residential buildings (GDV 2006; 2009).

The gale-force winds affecting Europe during winter generally occur in connection with strong extra-tropical cyclones, the majority of which originate at the polar fronts of the North Atlantic. Normally following a zonal (eastward) track, some of these cyclones can develop to very intense systems if they pass environments featuring suitable growth conditions (such as high baroclinicity, upper-tropospheric divergence, latent heating, cf. e.g. Pinto et al., 2009).

Today there is very high scientific confidence that mankind is about to influence the climate system (IPCC 2007a), primarily by modifying the chemical composition of the earth's atmosphere and by land use changes. Due to industrial activities, but also agricultural and societal actions (e.g. intense mass animal farming and traffic), greenhouse gas (GHG) concentrations in the atmosphere have increased significantly since about 1850. Consequential changes in the radiation budget lead to a global warming, as a higher ratio of energy is remaining in the earth system. This anthropogenic induced climate change, however, not only manifests in higher global mean surface temperatures, but also in shifts of the atmospheric circulations and changes in precipitation regimes. There is a multitude of potential impacts, including

e.g. sea level rises, melting of glaciers, changes in the water cycles and also in the occurrence of extreme events (e.g. floods, droughts, heat waves, storms). With respect to those impacts, the latest Assessment Report of the Intergovernmental Panel on Climate Change (IPCC 2007b) notes: “Impacts due to altered frequencies and intensities of extreme weather, climate and sea-level events are very likely to change” and further, with regard to human health: “Climate change is likely to increase the risk of mortality and injury from wind storms, flash floods and coastal flooding” (Alcamo et al., 2007).

Given the relevance of wind storms in Europe, it is thus of high public and economic interest to quantify and understand long-term changes in their intensity and frequency, and to estimate future changes induced by anthropogenic climate change (ACC). The question of how the occurrence of European wind storms might change under ACC conditions is not only of high interest for the (re-)insurance industry in terms of anticipating future risks of loss, it is also relevant for institutions involved in infrastructure planning (e.g. dike construction, building regulations, etc.) in order to enforce adaptation and enable preparedness.

Numerical climate models are the state-of-the-art tools used to obtain information about potential future climate changes, performing future scenario simulations. Those climate simulations are, however, affected by several uncertainties (see section 1.2.2). Ensemble approaches are often used to learn about the inherent uncertainties, performing a multitude of simulations with the same model, or combining different models to a multi-model ensemble (MME). Thus, the robustness of the results can be estimated and a range of possible future changes can be specified.

1.2. State of knowledge

This section summarises the state of knowledge concerning the two major topics which are combined in this thesis: (1) changes in European storminess as a consequence of ACC and (2) the application of MMEs to estimate the robustness of climate projections. In order to minimise redundancy, here only those fundamental points which are directly relevant to the context of the motivation of the thesis are assembled. Each of the following chapters (prepared as scientific journal papers) will provide a summary of the state of knowledge concerning the specific questions examined therein.

1.2.1. European storminess: natural variability and trends caused by ACC

The occurrence of historical storms can be estimated directly from wind measurements and also indirectly from air pressure records (by considering e.g. spatial pressure differences and assuming geostrophy). Systematic weather observations and records commenced at a few stations in the late 18th century (e.g. Hohenpeißenberg in 1781). Since the late 19th century, the number of weather stations has increased; records in a higher spatial density are available for about the last 100 years. Many of these early stations, however, did not register all meteorological parameters being observed today and concentrated on temperature and precipitation records. Worldwide there are only 52 (8) series of measurements starting before the year 1900 including wind (air pressure) records (source: <http://www.pik-potsdam.de/infothek/sakularstation>, date: 07 March 2010). Based on observations, therefore, historical trends of storminess can be analysed approximately for the last century. Problems with the homogeneity of weather records have to be kept in mind. In contrast to historical temperatures, for example, there is no reliable proxy data established that enables sound reconstructions of the storm climate for the pre-observation era.

Studies analysing trends of storminess during the past century document a large multi-decadal variability in the occurrence of severe winter storms and identify partly ambiguous trends. While there are some studies pointing to an increase of storminess in the recent decades up to the late 1990's (e.g. Weisse et al., 2005; Leckebusch et al., 2008b; Wang et al., 2009), others state that the recent trend may be part of natural variability: also for the early 1900's a high storm activity was analysed and there is no evidence that today's storm climate is different from storm occurrences about 100 years ago (WASA group, 1998; Alexandersson et al., 2000; Barring and von Storch, 2004; Mattula et al., 2008). With respect to monetary (economic and insured) storm losses, clear positive trends are apparent in recent decades (Munich Re 2000; 2007). Barredo (2010), however, associates these trends primarily with positive trends in societal factors, e.g. economic growth and increasing values.

With regard to potential changes in ACC future scenario simulations, a number of studies have recently found indications of more frequent occurrence of intensive cyclones over eastern North-Atlantic (Bengtsson et al., 2006; Lambert and Fyfe 2006, Leckebusch et al., 2006) and an eastward extension of the North Atlantic storm track (Ulbrich et al., 2008). Particularly with respect to extreme cyclones, however, the results appear to depend on the individual methodology and data applied, and partly

ambiguous signals are found (see Ulbrich et al., 2009 and references therein). Increased occurrence of extreme cyclones over the eastern North Atlantic is in accordance with findings of higher extreme wind speeds over parts of Western and Central Europe (Knippertz et al., 2000, Leckebusch and Ulbrich, 2004, Pinto et al., 2007; Gastineau and Soden, 2009). Studies estimating changes to storm losses under ACC conditions found increased risk of losses particularly in Western and Central Europe if no adaptation of buildings to higher wind speeds takes place (Leckebusch et al., 2007; Pinto et al., 2007; Schwierz et al., 2009). Most of these recent studies on future wind storm risk are, however, based on single models or small ensembles and thus potentially biased due to individual model deficiencies. A sound estimation of the uncertainties related with the change signals still remains necessary and will be addressed in this thesis.

1.2.2. Uncertainties in climate simulations and ensemble approaches for estimating robustness and increasing confidence

Climate model simulations are affected by several uncertainties. Besides the uncertainty due to the internal variability of the climate system, the most important uncertainties are often grouped into boundary condition, parameter and structural uncertainties (Tebaldi and Knutti, 2007).

Boundary condition uncertainties include, for example, the uncertainty regarding future societal and technological development, which in turn leads to uncertainties with respect to future GHG emissions. This uncertainty is generally examined by considering different future emission scenarios (e.g. Nakićenović et al., 2000). Parameter uncertainties arise from the fact that sub-grid scale processes (e.g. cloud physics, convection, radiation transfer) are generally not resolved in climate models. Instead, parameterisations are used to depict those processes. Although generally based on expert knowledge and experience, tuning of parameterisations is at least partly subjective and does not necessarily hold for special cases. Structural uncertainties include uncertainties in the numerical schemes for discretization and integration of the model equations, and also incomplete knowledge of Earth system processes, such as the carbon cycle. Parameter and structural uncertainties are also often considered conjoined as modelling uncertainties.

Ensemble approaches based on single or multi-models are used to sample the different uncertainties and to quantify their effects. The effects of internal variability can be quantified by running a model many times from different initial conditions (e.g. Selten

et al., 2004). Perturbed physics ensembles (e.g. Murphy et al., 2004; Collins et al., 2006; Harris et al., 2006) are used to examine the parameter uncertainties. Generally based on single-models, a large number of simulations is performed by perturbing poorly constrained parameters in the climate system.

The idea behind a multi-model ensemble (MME) is to run different models with identical forcing. MMEs primarily sample parameter and structural uncertainties as well as uncertainties owing to internal variability. Thus, by considering results from different models, not only a range of possible climate signals (under a given scenario) and their (un-) certainties can be estimated (e.g. Furrer et al., 2007; Tebaldi and Knutti, 2007). Moreover, individual model errors, uncertainties in the numerical schemes, can be cancelled out, and the increased sample size reduces the uncertainty due to internal variability. A limitation of MME approaches, however, may arise from the fact that different ensemble members often share some common systematic errors by sharing some components and thus may not span the full range of possible results.

The use of ensembles emerged in weather forecasting (Palmer and Hagedorn, 2006), and the superiority of MMEs could be widely demonstrated for weather and seasonal forecasting applications (Hagedorn et al, 2005). On those short time scales, the verification of the MME results is relatively straight-forward, e.g. by skill measures. Nevertheless, also for climate-scale simulations MME approaches can be favourable compared to a single model (cf. Lambert and Boer, 2001; Palmer and Räisänen, 2002; Räisänen, 2007, Collins, 2007).

With regard to analysis of climate change simulations, the expected results are more straightforward for some modelled variables than for others. An increase in the mean global near-surface temperature, for example, is a plausible consequence of increased GHG forcing, and all models reveal positive trends. However, climate sensitivity is different in different models and thus, a range of possible warming is estimated from multi-model simulations (e.g. Knutti et al., 2002; Räisänen, 2005; Furrer et al., 2007). The role of internal variability increases for smaller scales (e.g. Giorgi and Francisco, 2000; Schär et al., 2004), and an additional effect comes from changes in the atmospheric circulation (e.g. van Ulden and van Oldenborgh, 2005). Winter storms are extreme meteorological events acting on rather regional than global scales. Moreover, their occurrence is influenced by complex atmospheric processes, for which the numerical realisations in the climate models may be affected by model-specific

characteristics, leading to different solutions (independently from model to model). Thus, climate change studies on storminess may reveal partly contrary trends in different models, particularly if specific regions are considered. Here, information about the robustness of the results (which can be obtained from a multi-model ensemble) is particularly important for obtaining reliable estimates of future changes and thus enabling preparedness.

1.3. Thesis Objective

The primary objective of this thesis is to estimate how the risk of severe European winter storms (and of related losses) might change under ACC conditions, including an assessment of the robustness of the identified change signals. Therefore, atmospheric conditions found in conjunction with European windstorms, extreme wind speeds and storm loss potentials are investigated on the basis of reanalysis and (global and regional) climate simulation data. By examining multi-model simulations, the robustness of the signals is estimated and uncertainty ranges are determined. In addition to considering multi-model simulations, the robustness of signals is also examined by applying different complementary analysis methods, such as cyclone tracking, weather types and wind speed analyses. Consistent signals in the different metrics will increase the confidence in the results. A further topic is the examination and quantification of the profit of combining models to a MME for climate scale applications, and an investigation of the benefits of dynamical downscaling for storm loss calculations.

Dealing with these issues brings up the following *research questions*, which are investigated in this thesis:

Atmospheric Circulation in Relation to Wind Storms

- What are the preferred atmospheric conditions for the occurrence of (Central) European winter storms? Do state-of-the-art climate models have the capacity to reproduce observed atmospheric characteristics relating to storms?

Anthropogenic Signals

- How do atmospheric features related to wind storms respond to increased GHG concentrations in the climate model simulations?

- What is the consequence of increased GHG forcing on the occurrence of extreme wind speeds in Europe?
- How do loss potentials caused by severe wind storms change under future ACC conditions?

Multi-Model Simulations and Analysis

- How robust are the identified ACC signals concerning the changes in the different individual simulations? What are suitable measures of uncertainty? How large is the uncertainty of the signals?
- What is the benefit of combining different climate simulations into a MME?
- What influence do different ways of constructing the ensemble (e.g. model selection, weighting) have on the MME performance, and on the possible change signals?

Dynamical Downscaling

- What are the benefits and shortcomings of using regional climate models (RCMs) for extreme wind analysis and storm loss calculations?
- Does dynamical downscaling provide any additional information about ACC signals?

1.4. Thesis Outline

The thesis content is divided into 5 chapters, each dealing with a subset of *research questions* raised in section 1.3. All of these chapters are prepared as scientific articles for publication in journals; 3 of these have already been published or accepted for publication, while 2 have been submitted to journals but are still under review.

By virtue of this structure, each chapter can be read largely independently of the others. The structure, however, also entails some recurrence of content in different chapters, as each of the articles contains its own introduction, and furthermore as the data used partly repeat for the different studies.

- In **Chapter 2**, the occurrence of Central European wind storms is investigated with respect to large-scale atmospheric flow and local wind speeds, based on ERA40-reanalysis data. Storm days are identified following two different methods, one

based on large-scale flow characteristics (circulation weather types, CWT), the other on the occurrence of extreme wind speeds in Central Europe. The identified events are then examined with respect to NAO phases and CWTs under which they occur. Pressure patterns, wind speeds and cyclone tracks are investigated for the storm days in general and for storms occurring in different CWT classes. This chapter has been published (online first) in *International Journal of Climatology*¹.

- **Chapter 3** examines wind storm occurrence and its relation to large-scale atmospheric flow conditions, as identified in chapter 2, in a multi-model ensemble of coupled global climate models. In particular, a range of possible changes of frequency and characteristics of European wind storms under future anthropogenic climate change conditions is investigated. This chapter has been accepted for publication in *Climate Research*².
- Occurrence of winter storms is generally linked to severe extratropical cyclones. **Chapter 4** investigates changes in the occurrence of extratropical cyclones in multi-model future scenario simulations. This chapter has been published in *CLIVAR Exchanges*³. Although I am not the lead author of this article, I provided substantial contributions to it. The presented analysis of extratropical cyclones was an important focus of my investigations in the context of this thesis.
- Benefits and limitations for storm loss calculations arising from dynamical downscaling and from combining different models to a multi-model ensemble are examined in **Chapter 5**. After incorporating some requested revisions, this chapter was recently resubmitted to *Climate Research*⁴.
- In **Chapter 6** potential future changes of extreme wind speeds in Europe and related storm losses are investigated on the basis of multi-model simulations with global and regional climate models. Further, a new approach for estimating the uncertainty in multi-model simulations is presented, based on all possible model

¹ Donat MG, Leckebusch GC, Pinto, JG Ulbrich, U. 2009: Examination of Wind Storms over Central Europe with respect to Circulation Weather Types and NAO phases. *International Journal of Climatology*. DOI: 10.1002/joc.1982 (in press)

² Donat MG, Leckebusch GC, Pinto JG, Ulbrich U. 2010. European storminess and associated circulation weather types: future changes deduced from a multi-model ensemble of GCM simulations. *Climate Research* (in press)

³ Leckebusch GC, Donat MG, Ulbrich U, Pinto JG. 2008. Mid-latitude Cyclones and Storms in an Ensemble of European AOGCMs under ACC. *CLIVAR Exchanges* Vol. 13, No. 3, 3-5. ISSN 1026 - 0471.

⁴ Donat MG, Leckebusch GC, Wild S, Ulbrich U. 2010. Benefits and limitations of regional multi-model ensembles for storm loss estimations. *Climate Research* (submitted, revised)

combinations. This study was submitted for publication in *Natural Hazards and Earth System Sciences*⁵.

- The thesis is concluded in **Chapter 7** by summarising the main results from the different studies and by giving a brief discussion and outlook on issues that remained open and may be investigated in future studies.

⁵ Donat MG, Leckebusch GC, Wild S, Ulbrich U. 2010. Future changes of European winter storm losses and extreme wind speeds in multi-model GCM and RCM simulations. *Natural Hazards and Earth System Sciences* (submitted)

2. Examination of Wind Storms over Central Europe with respect to Circulation Weather Types and NAO phases

Abstract

The occurrence of wind storms in Central Europe is investigated with respect to large-scale atmospheric flow and local wind speeds in the investigation area. Two different methods of storm identification are applied for Central Europe as the target region, one based on characteristics of large-scale flow (circulation weather types, CWT), the other on occurrence of extreme wind speeds. The identified events are examined with respect to the NAO phases and CWTs under which they occur. Pressure patterns, wind speeds and cyclone tracks are investigated for storms assigned to different CWTs. Investigations are based on ERA40 reanalysis data.

It is shown that about 80 percent of the storm days in Central Europe are connected with westerly flow and that Central European storm events primarily occur during a moderately positive NAO phase, while strongly positive NAO phases (6.4% of all days) account for more than 20% of the storms. A storm occurs over Central Europe during about 10% of the days with a strong positive NAO index. The most frequent pathway of cyclone systems associated with storms over Central Europe leads from the North Atlantic over the British Isles, North Sea and southern Scandinavia into the Baltic Sea. The mean intensity of the systems typically reaches its maximum near the British Isles. Differences between the characteristics for storms identified from the CWT identification procedure (gale days, based on MSLP fields) and those from extreme winds at Central European grid points are small, even though only 70% of the storm days agree. While most storms occur during westerly flow situations, specific characteristics of storms during the other CWTs are also considered.

2.1. Introduction

Intense winter storms constitute one of the most important natural hazards affecting Central Europe. For example, series of storms like in January and February 1990 (e.g. Daria, Vivian), in December 1999 (e.g. Anatol, Lothar, cf. Ulbrich et al., 2001; Wernli et al., 2002) and more recently January 2007 (e.g. Kyrill, cf. Fink et al., 2009) repeatedly raise public and scientific interest in these natural hazards. Whereas several recent works point to an increase of storminess in the recent decades until the late 1990s (e.g. Leckebusch et al., 2008b; Wang et al., 2009), other authors point out that the recent trend is just part of a decade-long variability and that there is no evidence that storminess over Europe in the early 1900s was different from that in recent decades (WASA group, 1998; Barring and von Storch, 2004; Mattula et al., 2008). As extreme storms are rare events by definition, it is difficult to detect such changes from the events themselves. This paper explores a path for future studies on changes in the large-scale conditions for storm occurrence by taking a closer look at the relation of storms and the large-scale patterns under which they occur.

The association of local weather with cyclones and large-scale flow patterns has been widely examined and applied in climatological studies. Van Bebber (1891), for example, classified cyclone tracks with relevance for Europe, identifying the well-known Vb-track with a high potential for large summer floods in Europe. Within this context, weather typing approaches (Hess and Brezowsky, 1969; Lamb, 1972) are often used to classify large-scale weather situations and relate them to local variables; for instance, the circulation weather types approach (CWTs, see Jones et al., 1993) has been applied to different European regions, often in the context of investigating precipitation-relevant regimes (e.g. Goodess and Palutikof, 1998; Trigo and Dacamara, 2000). Motivated by this successful application, we consider it worthwhile to investigate large-scale atmospheric circulation associated with wind storm events, using a similar approach. For the British Isles and North Sea region, Jenkinson and Collison (1977) assigned the occurrence of gale days to different flow classes, finding a particular relevance of flow from the westerly sectors as well as southerly flow. For Central European storms the westerly flow seems to be particularly important: Schmidtke and Scherrer (1997) suggested west wind storms as the most relevant destructive storm type (in terms of forest losses) affecting Switzerland in winter (besides southerly Foehn storms). Busch et al. (1998) mention westerly/north-westerly flow regimes as an

important criterion for their classification of storm weather situations over the German Bight. Recently, Leckebusch et al. (2008a) showed that a small number of specific weather developments (i.e., temporal evolution of MSLP pattern over 3 days, cf. their Fig. 3) are associated with over 70% of winter storms over Central Europe and especially Germany in recent decades. Hence, these and other studies document that the occurrence of storms over Europe occurred under "preferred" large-scale conditions over the North Atlantic and Europe. A more detailed quantification of the relevance of specific large-scale flow patterns relevant for the occurrence of storm is, however, desirable.

With respect to the dominating variability pattern over the North Atlantic, the North Atlantic Oscillation (NAO, Walker, 1924; Hurrell, 1995), literature provides extended reviews on phenomenology, mechanisms and variability of the NAO, e.g. in Marshall et al. (2001) and Wanner et al. (2001). The link between the NAO phase and the occurrence of intense cyclones has been documented in previous studies (e.g. Serreze et al., 1997). Recently, Pinto et al. (2009) were able to show that an enhanced number of storms over the North Atlantic/European region during positive NAO phases (compared to negative NAO phases) is due to larger areas of suitable growth conditions. Raible (2007) found a NAO+-like pattern in the 500hPa geopotential height field being correlated with the occurrence of extreme cyclones over Northern Europe. With respect to the role of the NAO phase for the occurrence of wind storms, Matulla et al. (2008) mention that on a centennial time-scale the capability of the NAO index to explain storminess across Europe varies in space and with the period considered.

This study aims to achieve a better understanding of the relation between large-scale atmospheric circulation and the occurrence of severe winter storm events in Central Europe, including consideration of the associated extratropical cyclones. Atmospheric circulation is analysed in terms of NAO phase and classified into CWTs with a focus on storm events. While the above-mentioned studies (e.g. Pinto et al., 2009) assign the occurrence of extreme North Atlantic cyclones to the NAO phase during the cyclones' development phase (irrespective of whether they hit Europe or not), a different approach is pursued here: For each wind storm event over Europe, the contemporaneous NAO phase and CWTs are considered in order to deduce their roles for storms in Central Europe. Storm days are identified using two different methods and examined in more detail for relevant circulation classes in order to provide an insight into their synoptic features. For investigating storm-related atmospheric patterns, the main focus is laid on

analysis of the related cyclone tracks and their intensities, on specific patterns of the mean sea level pressure (MSLP) and wind speed.

2.2. Data and Methods

The investigations presented in this study are based on European Center Medium Range Weather Forecast reanalysis (Uppala et al., 2005, hereafter ERA40) for the 40-year period from 1961 to 2000. Mean sea level pressure (MSLP) data and daily maximum wind speeds are used. The latter were derived as the maximum of 4 instantaneous values from 00, 06, 12 and 18 UTC, as no integrated maximum value over all time steps is available from ERA40. This maximum of 4 instantaneous values is expected to be slightly lower than the maximum of all time steps (cf. Pinto et al., 2007a, their figures 3b,c). As almost all severe damage-inducing storm events occur during the winter half year (Klawns and Ulbrich, 2003; Munich Re, 2007), analyses are restricted to the period from October to March. ERA40 reanalysis data have a spatial resolution of about 1.125° (N80) and are also available interpolated on a 2.5° grid. We performed the wind field analyses based on the finer grid, whereas the CWT classification and cyclone tracking (both using MSLP data) were done on the coarser grid. This accounts for the characteristics and data requirements of both methods. We have not used the wind gust data from ERA40 as it has been regarded unreliable over areas of steep orography (Della-Marta et al., 2009a). On the other hand, these authors see the 6-hourly instantaneous wind fields (the same data used here) as apparently largely free from such problems, apart from somewhat too low speed over complex orography.

Large-scale atmospheric circulation is analysed from the characteristics of daily mean MSLP fields (calculated as the mean of four instantaneous output values per day). For the daily flow classification, an objective scheme is used that was initially described by Jenkinson and Collison (1977) and later published by Jones et al. (1993). This scheme is based on the original manual Lamb weather types (Lamb, 1972). Although this method does not consider the temporal evolution of weather situations and the flow analysis is specific for the central point of the investigation area, its objectivity and simplicity make it preferable for this specific application compared to, for example, the subjective Grosswetterlagen classification (Hess and Brezowski, 1969). The only required input parameter is the MSLP field. Originally developed for the region of the British Isles, it was also successfully applied to other European regions and has been widely used in the

literature (see e.g. Buishand and Brandsma, 1997; Goodess and Palutikof, 1998; Trigo and Dacamara, 2000; Demuzere et al., 2008). Here, only the basic features will be recapitulated.

To classify flow characteristics, directional flow (F) and vorticity (Z) are calculated in geostrophical approximation based on the MSLP values of the surrounding $2.5^\circ \times 2.5^\circ$ grid. On the basis of these terms, flow is classified into directional, (anti-) cyclonal or hybrid circulation weather types (CWTs). The directional types are divided into eight sectors of 45° : NE, E, SE, S, SW, W, NW and N. For each day, flow can thus be classified into one of 27 types (8 directional, 1 cyclonal (C), 1 anticyclonal (AC), 8 hybrid cyclonal-directional, 8 hybrid anticyclonal-directional and 1 undefined). Further details can be found in Jones et al. (1993). Here, large-scale flow is classified for Central Europe (figure 2.1a), focusing on 50°N , 10°E . Hybrid weather types are considered each with half as occurrence of directional and half as (anti-) cyclonal flow in terms of frequency counts. Thus, the frequencies of overall 11 classes are determined (8 directional, 1 cyclonal, 1 anticyclonal, 1 undefined). The undefined class could also be omitted. The presented results are equivalent, if the days with undefined CWT (2.5% of all) were classified to the closest of the other CWTs (not shown).

In the classification scheme of circulation weather types (Jenkinson and Collison, 1977; Jones et al., 1993) also a gale index $G = \sqrt{(F^2 + (\frac{1}{2}Z)^2)}$ is defined, considering strength of directional flow (F) and vorticity (Z). Different thresholds for gale days ($G > 30$), severe gale days ($G > 40$) and very severe ($G > 50$) gale days are given for the region of the British Isles. For the Central European investigation area, about 15 gale days per winter season ($G > 30$) are detected in the ERA40 reanalysis data. By calibration towards a slightly higher threshold of $G > 35$, the average number of detected gale days is 5.5 per winter (220 gale days in the ERA40 period 1961-2000). This is reasonable as it roughly reflects the number of extreme and destructive storm events (Munich Re, 1999; Munich Re 2007) and corresponds to the number of severe gale days ($G > 40$) found for the British Isles and North Sea region. Although inevitably subjective, the chosen threshold is considered appropriate as the number of identified gale days corresponds well to storm frequencies considered in other studies (e.g. Klawns and Ulbrich, 2003; Della-Marta et al., 2009a). Owing to the characteristics of our method, a single storm may be associated with several (consecutive) gale days, leading to a slightly higher number of storm days compared to storm events. These gale days based

on the analysis of flow characteristics are hereafter denoted as JC35 ($G>35$). This gale index was also used in other studies, e.g. by Hulme and Jones (1991) and Carnell et al. (1996).

The chosen criterion for gale days considers the characteristics of the daily mean MSLP field, hence estimating the geostrophic component of the large-scale winds (and does not implicitly take into account the incidence of strong winds). The striking and devastating phenomenon in the context of storms is, however, the occurrence of local extreme wind speeds. Therefore, an alternative criterion is applied to identify storm days related to local wind extremes at the ERA40 grid point in the area of interest. This allows a comparison with the storm days found from computation of the gale index G based on large-scale geostrophic flow. The local 98th percentile of daily maximum wind

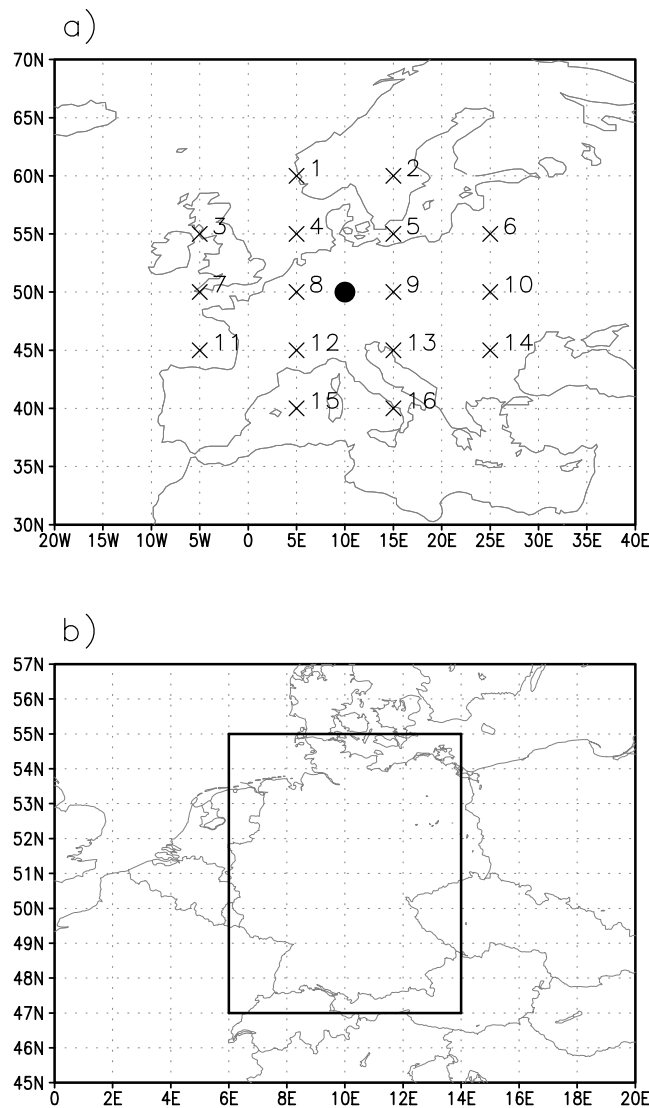


Figure 2.1: Investigation areas
 a) for classification of CWTs and gale days
 b) for detection of storm days SP98

speeds is deemed to be a common threshold for storm damage (e.g. Klawns and Ulbrich, 2003; Leckebusch et al., 2007; Pinto et al., 2007a). In a first step to identify storm days, all exceedances of the local 98th percentile of daily maximum wind speed during winter are registered for the region 6°E-14°E, 47°N-55°N (figure 2.1b). This area roughly corresponds to the area of Germany. As severe windstorms are generally connected to wind fields covering large areas, the local 98th percentile (wind speed threshold) must be exceeded for a minimum number of ERA40 grid points (area threshold). In ERA40 (horizontal resolution ~1.125°) the investigation area for storm detection consists of 49 grid boxes. If the area threshold is calibrated to a quarter of the grid boxes in the investigation area (i.e. 12), a reasonable number of days for consideration of severe storm events are identified as storm days in the ERA40 data. This threshold yields an average of 5.3 storm days per winter half year (214 in the 40-year period 1961-2000). This also corresponds well to the number of JC35 gale days.

Identification and tracking of cyclones is performed by applying an objective algorithm developed by Murray and Simmonds (1991) and adapted to the Northern Hemisphere by Pinto et al. (2005). It is organised in 2 steps: First, cyclones are identified based on the search for the maximum of the Laplacian ($\nabla^2 p$) of MSLP. Under quasi-geostrophic conditions, this is equivalent to the search for extremes of relative vorticity. Subsequently, a tracking algorithm is applied, taking into account the most probable displacement of the cyclone core under the given large-scale conditions and previous path and speed. As this methodology is to be applied to GCM data as well (cf. Donat et al., 2010a), we have chosen to perform the cyclone identification and tracking based on the ERA40 reanalysis data at the 2.5° grid resolutions, in order to enable a later comparison between the ERA40 and GCM-based results (the sensitivity of cyclone statistics to spatial resolution of datasets was explored e.g. in Pinto et al., 2005).

For a more detailed investigation of the characteristics of storm events, the related cyclone track is assigned to each storm day by searching the most intensive cyclone passing a cyclone detection box (i.e. the area where cyclone tracks associated with the event can be expected, defined below) on that date. Intensity is measured in terms of the Laplacian of MSLP. Maximum winds usually occur south of a cyclone core in Central Europe. Thus, for the automatic assignment only those cyclone tracks are considered that pass through the storm day detection area or north of it. The size of the cyclone detection box was calibrated to 0°E-20°E, 47°N-65°N (green box in figure 2.5c). If two

or more consecutive storm days can be related to the same cyclone track, this cyclone is only counted once for the composites of storm cyclones.

It was tested whether the automatic assignment of cyclones produces realistic results for major historical storm events during the years 1990 and 1999. For the storms Daria (Jan 25/26 1990), Herta (Feb 3/4 1990), Vivian (Feb 26/27 1990), Wiebke (Feb 27/28 1990), Anatol (Dec 3 1990) and Martin (Dec 28 1999) the related cyclone tracks were assigned successfully, i.e. in accordance with observations. However, in the case of Lothar (a fast-travelling secondary disturbance south of a strong steering cyclone, Dec 26 1999) the method does not produce the expected result. It assigns the deep steering cyclone to the wind storm, whereas the real track of Lothar is the one with the second highest intensity. This is due to the failure of the reanalysis to include Lothar's pressure anomaly realistically (cf. Ulbrich et al., 2001). Thus, it must be assumed that the automatic procedure may assign stronger steering cyclones to a storm event instead of the secondary cyclone actually causing the storm.

During the whole considered ERA40 period 1961-2000, only for 12 (of in total 220, i.e. $\approx 5\%$) gale days (JC35) no cyclone track can be assigned by this method. In most of these cases there is a strong anticyclone over Northern Europe and easterly flow prevails (i.e., there is no cyclone inside the detection box to assign). A detailed consideration of these cases further showed that wind speeds are comparatively low, barely exceeding the gale index threshold (JC35) or the 98th percentile of wind speed (SP98).

The relation between gale days and contemporaneous NAO phases was also investigated. Therefore, a NAO index for the ERA40 dataset was calculated on a daily basis following Pinto et al. (2009). The NAO pattern is derived from monthly mean data (via Principal Component Analysis of SLP) for the area 90°W-50°E, 20°N-80°N. As expected, the NAO is the leading principal component for this area (Pinto et al., 2009, their Fig. 1). The “daily NAO index” is obtained by projecting the monthly pattern onto the daily SLP data, followed by a 5-day running mean smoothing. This approach for achieving a daily NAO index is similar to the method used by Blessing et al. (2005). To assign storms to NAO phases, the daily NAO index is then classified on the basis of the definitions given in table 2.1 (“neutral”, “positive”, “negative”, “strong positive”, “strong negative”). These NAO classes are the same as used by Pinto et al. (2009). Next, the NAO-index value on the date of storm occurrence (gale day) over central Europe is considered for further analysis. This is a slight departure from the assignment

	Phase	Index Values
NAO--	Strong negative	Index < -1.5
NAO-	Negative	$-1.5 \leq \text{Index} < -0.5$
NAO 0	Neutral	$0.5 \leq \text{Index} < +0.5$
NAO+	Positive	$+0.5 \leq \text{Index} < +1.5$
NAO++	Strong positive	Index $\geq +1.5$

Table 2.1: Definition of NAO phases. Index values based on the first PC for North Atlantic/Europe (90°W-50°E; 20°N-80°N)

to the NAO index as performed by Pinto et al., (2009), which considered the NAO-index value on the day of maximum cyclone development (and not when they affected Europe). Nevertheless, it turned out that the NAO-index class assigned to a storm day is not sensitive to the introduction of a time lag (-1, -2, -3 days, with NAO preceding the storm event).

2.3. Analysis of the large-scale circulation and storm days

2.3.1. Classification of daily circulation weather types and detection of storm days

The relative frequencies of the different CWTs during the winter half year (October-March) are presented in figure 2.2a. Days with anticyclonic flow occur most frequently (31.6%), followed by westerly (22.6%) and cyclonal (10.0%) flow. Atmospheric flow from the whole easterly sector (NE, E, SE) is comparatively rare.

Irrespective of the storm detection method applied, a clear dominance of storm days with westerly flow is recognised for the reanalysis period (figure 2.2b): 80 percent (on average 4.6 days per winter season) of JC35 gale days occur with westerly flow. About 0.2 days per winter season (i.e. approximately one day in five years) occur during each cyclonal, anticyclonal and NW flow; once in ten years (i.e. 0.1 days per winter) a gale day is analysed with easterly or south- westerly flow, respectively. All other CWT classes are apparently irrelevant for the occurrence of gale days. The SP98 storm days show a similar distribution among the circulation classes. Here too, the majority (about 75 percent) occurs with westerly flow. The share of flow from North West in the SP98 storm days is approximately 15 percent and thus higher compared to the JC35 counterpart (approximately 4 percent).

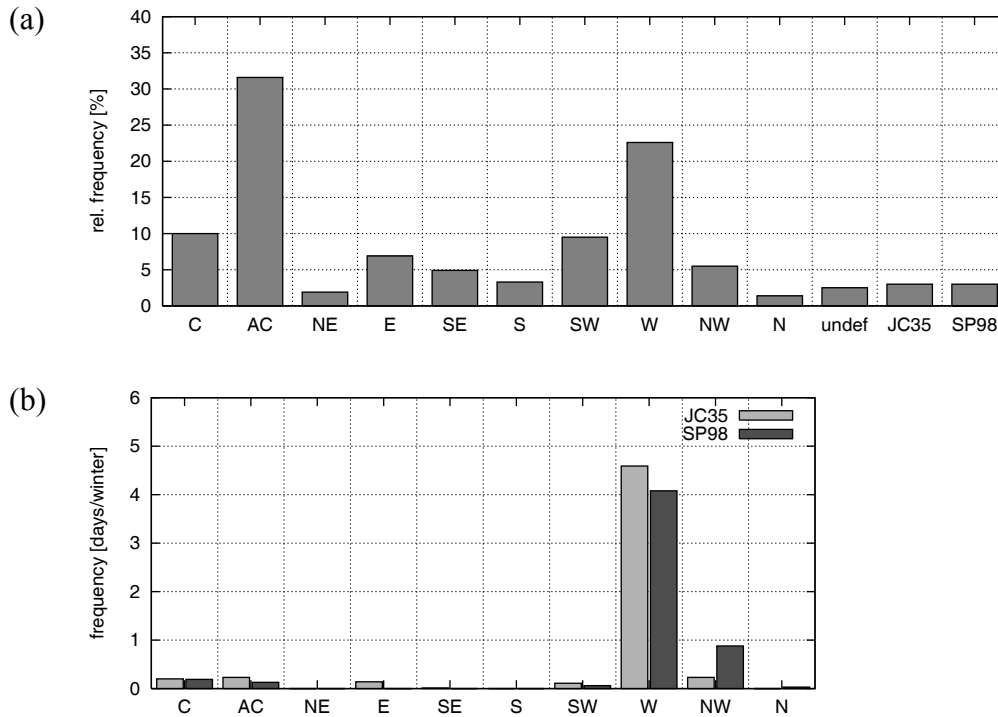


Figure 2.2: CWT and gale/storm day frequencies during winter half year (ONDJFM).

a) relative frequencies (unit: %) for all days

b) CWTs during gale days JC35 (light grey) and storm days SP98 (dark grey), unit: days per winter

At first glance, the occurrence of storm days with anticyclonal flow character might seem unusual (cf. Fig. 2.2). Detailed examination of these days discloses, however, that they are almost exclusively of hybrid type with also westerly or north westerly flow character. In these cases, at the back side of a cyclone a ridge of high pressure extends over Western Europe (Bay of Biscay or France) and thus causes anticyclonal curvature of isobars over Central Europe. The number of 9 gale days (JC35) with anticyclonal character is resulting from 16 days with hybrid flow character (which are each counted as half days for AC and thus are responsible for 8 of the 9 counted days); only one of the gale days occurs with purely anticyclonal flow. From the 16 hybrid anticyclonal gale days, we have 15 that feature westerly flow character and one with NW flow character. According to the SP98 method, all storm days with AC flow detected from ERA40 are of hybrid character with either westerly or north westerly flow. There is no storm day with purely anticyclonal flow.

The similarity of results obtained from the two different methods of storm day identification does not permit a general statement as to which is preferable. The storm events identified by the two different methods coincide to a level of about 70 percent, i.e. about 30 percent of each set are disjoint (typically weaker events). However, in the case of some strong events the detection depends on specific characteristics. For

example, fast-moving storms such as Lothar (Dec 26 1999) can hardly be identified from the daily mean MSLP field (JC35, cf. also Ulbrich et al., 2001, their Fig. 1b), but can clearly be found from daily maximum wind speeds (SP98, cf. also Fink et al., 2009). We will continue to consider both methods equally within section 2.3.

2.3.2. CWTs and storm days related to NAO

The distribution of daily NAO index values in the pre-defined classes is broadly in accordance with a normal distribution. The majority of all days are associated with neutral NAO (38.9%) and slightly positive (25.7%) or slightly negative (21.5%) NAO phases, respectively (Figure 2.3). Days with strong positive (6.4%) and strong negative (7.3%) NAO indices occur with significantly lower frequency. Considering the NAO index values for days in the different CWT classes, we find that each CWT occurred in conjunction with all of the 5 NAO phases in the ERA40 period (with the exception of northerly flow under NAO++). The neutral NAO is the most (or at least second most) frequent phase for each of the CWTs. There are, however, some shifts in the distribution, as flow from the easterly sector (NE, E, SE) occurs much more frequently during negative NAO than in positive phases, whereas flow from the westerly sector (NW, W, SW) is mainly assigned to positive NAO. For cyclonal flow, neutral or slightly negative NAO phases are equally frequent. Days with AC flow tend to occur with neutral or slightly positive NAO indices. For the ERA40 period, no statistically significant trends can be found in the number of winter days assigned to a particular NAO index, or to the number of occurrences of the individual CWTs per winter. Still, the seasonal frequencies of some CWTs are significantly (anti-) correlated with the

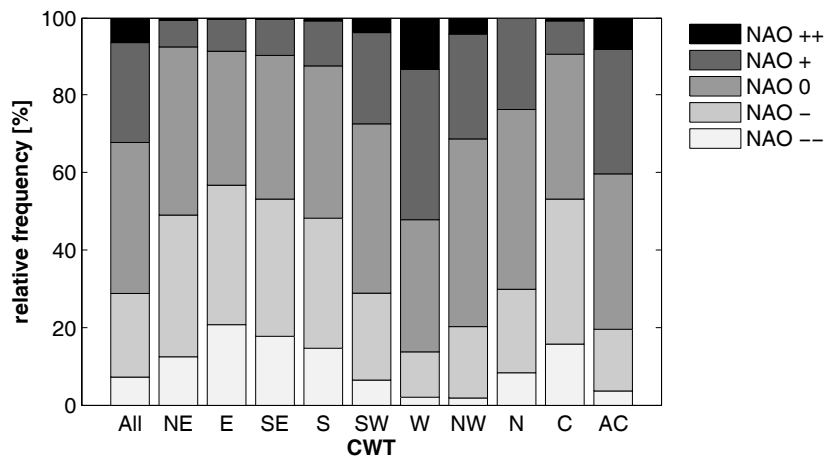


Figure 2.3: Relative frequency of days during the different NAO phases, for all days and for the different CWT classes (unit: percent of days during winter ONDJFM).

winter (ONDJFM) mean NAO index, namely W ($r=+0.50$), AC ($r=+0.50$), C ($r=-0.61$) and E ($r=-0.41$), in agreement with the CWT frequencies during the different NAO classes (cf. figure 2.3).

Considering NAO indices for storm days suggests that a slightly positive phase of NAO seems to represent "optimum conditions" for the occurrence of winter storms in Central Europe with both the JC35 and SP98 approaches (figure 2.4). Some spread is found, though the difference to the distribution for all days (full line) remains clear. The detailed relations between NAO and storm days in the different CWT classes are presented in table 2.2a/b. About 40% of the gale days are during NAO+; about 30% and 23% of gale days occur with NAO0 or NAO++, respectively. Only a few storm days occur during a slightly negative NAO phase (5.1% and 7.7% for SP98 and JC35, respectively), and no storms occur during strong negative NAO phases. Strong positive NAO indices (NAO++) are mainly associated with storms with westerly flow, while the few counts of NAO++ with AC flow are all of hybrid circulation type with W flow. Storm days with SW or NW flow occur with primarily moderate positive NAO. The few gale days with easterly flow occur with neutral to slightly negative NAO phases; also the gale days with cyclonal flow characteristics tend to exhibit neutral to slightly negative NAO. About 10 percent of the days during NAO++ are detected as storm days; for NAO+ the percentage of storm days is about 5%.

While the number of storms occurring with a particular combination of NAO phase and CWT is too small to be evaluated in detail, it can be noted that for several CWTs the percentage of storms occurring during a particular non-neutral NAO phase (cf. table 2.2a,b) generally exceeds the percentage of this combination (figure 2.3), enhancing the

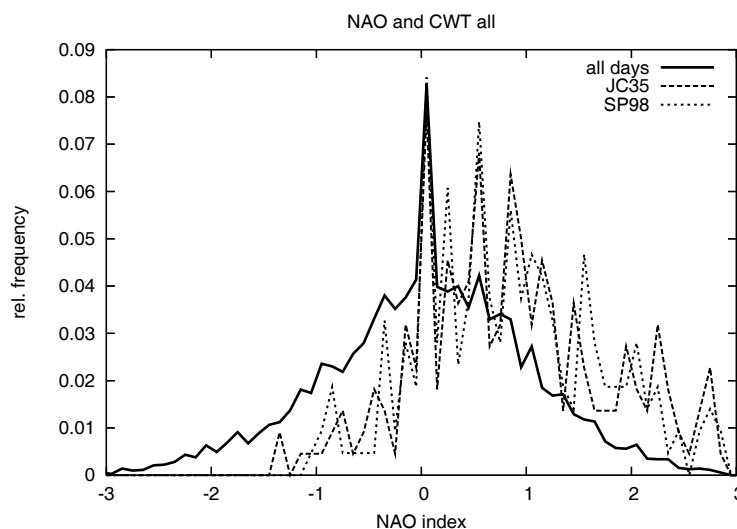


Figure 2.4: Relative frequencies of NAO indices on storm days JC35 and SP98 in comparison to all days.

(a)

	Total number	NAO--	NAO-	NAO 0	NAO+	NAO++
Gale days JC35 (all)	220.0	0	7.7%	29.1%	40.5%	22.7%
JC35 with NE	0	0	0	0	0	0
JC35 with E	5.5	0	63.6%	36.4%	0	0
JC35 with SE	0.5	0	100%	0	0	0
JC35 with S	0	0	0	0	0	0
JC35 with SW	4.5	0	0	88.9%	11.1%	0
JC35 with W	183.5	0	4.4%	28.6%	42.8%	24.2%
JC35 with NW	9.0	0	11.1%	11.1%	77.8%	0
JC35 with N	0	0	0	0	0	0
JC35 with C	8.0	0	50.0%	37.5%	12.5%	0
JC35 with AC	9.0	0	0	16.7%	22.2%	61.1%

(b)

	Total number	NAO--	NAO-	NAO 0	NAO+	NAO++
Gale days JC35 (all)	220.0	0	7.7%	29.1%	40.5%	22.7%
JC35 with NE	0	0	0	0	0	0
JC35 with E	5.5	0	63.6%	36.4%	0	0
JC35 with SE	0.5	0	100%	0	0	0
JC35 with S	0	0	0	0	0	0
JC35 with SW	4.5	0	0	88.9%	11.1%	0
JC35 with W	183.5	0	4.4%	28.6%	42.8%	24.2%
JC35 with NW	9.0	0	11.1%	11.1%	77.8%	0
JC35 with N	0	0	0	0	0	0
JC35 with C	8.0	0	50.0%	37.5%	12.5%	0
JC35 with AC	9.0	0	0	16.7%	22.2%	61.1%

Table 2.2: a) Counts of gale days during the different NAO phases, for all detected days (1st line) and for the different CWT classes for JC 35 gale days. 2nd column: total number of days in CWT class, columns 3 to 7: percent of days in each NAO phase.

b) same as a), but for SP98 storm days

shifts with respect to the normal distribution of NAO phases. Storm days with W or NW flow occur more frequently during positive NAO phases than would be expected from their frequency during these CWTs. The same is true for the few gale days with easterly flow (defined from JC35) and the slightly negative NAO phases. Again, the distribution of storm days in different NAO phases is similar for both storm identification methods. The seasonal frequencies of some CWTs are significantly (anti-) correlated with the winter (ONDJFM) mean NAO index, namely W ($r=+0.50$), AC ($r=+0.50$), C ($r=-0.61$)

and E ($r=-0.41$), in agreement with the CWT frequencies during the different NAO classes (cf. figure 2.3).

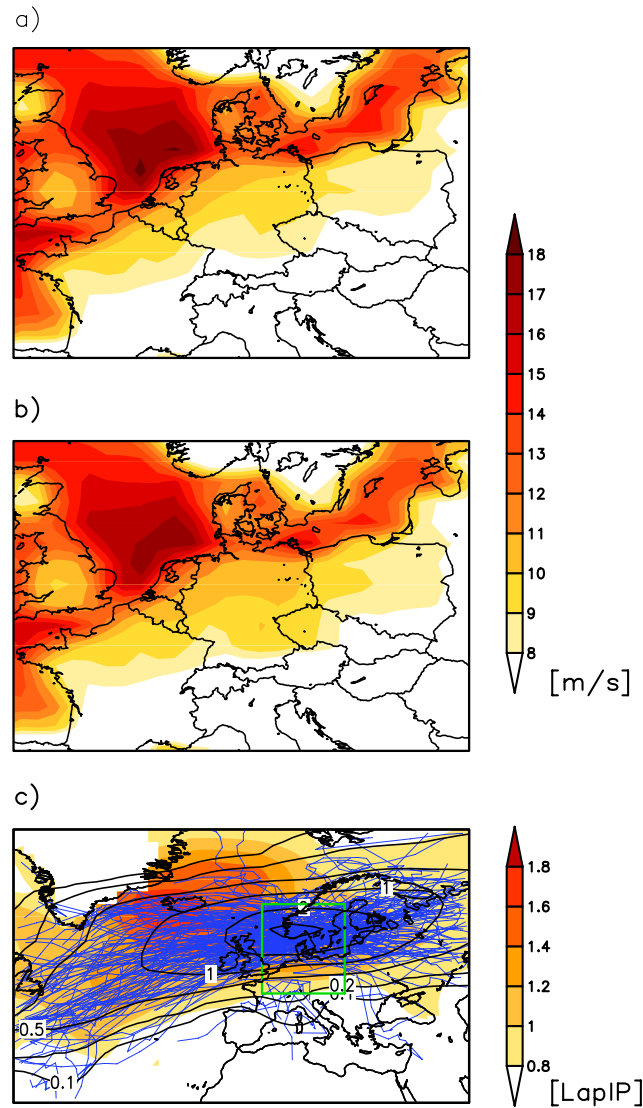


Figure 2.5: Wind speeds and cyclones in relation to storm events

- a) Mean of daily maximum wind speeds during JC 35 gale days in ERA40 reanalysis (unit: ms^{-1})
- b) same as a) but for SP98 storm days
- c) Cyclone tracks assigned to JC35 gale days in ERA40. Contour lines show track densities (unit: tracks/winter), Shaded areas show intensity (Laplacian P, unit: $hPa/(deg.lat)^2$) of the cyclones. Green box: cyclone detection box, i.e. search area for strongest cyclone in relation to gale days.

2.3.3. Characteristics of storm events

Large-scale atmospheric characteristics related to the storm events are considered in more detail in this section. The mean of the daily maximum wind speeds during JC35 and SP98 gale days in ERA40 is presented in figures 2.5a and 2.5b, respectively. Maximum wind speeds are found over the ocean areas, in particular the North Sea and Baltic Sea. Over the Central European inland areas the wind speed values decrease from north to south. The difference between Figs. 2.4a and 2.4b is small. Compared to JC35, SP98 storm days are characterised by somewhat higher wind speeds over Germany. This is due to the definition of SP98 storm days, occurrence of extreme wind speeds in this area being an explicit criterion. As the characteristics for SP98 storm days are very similar to JC35, we concentrate hereafter on presenting detailed analyses of JC35 gale days. The following results are, however, also valid for storm days according to the SP98 criterion.

The track density of cyclones assigned to the storm events is largest over southern Scandinavia (isolines in figure 2.5c), with tracks mostly extending from the North Atlantic into Northern Europe. On average, the intensity (Laplacian P) of the storm-producing cyclones is highest over eastern North Atlantic, between Iceland and British Isles (coloured areas in Fig. 2.5c).

To gain a deeper insight into the relationship between the occurrence of storm situations and the large-scale flow, atmospheric patterns associated with identified gale days in different CWTs will now be considered. Consideration of gale indices and wind speeds revealed that the few gale days with flow from the easterly sector are less relevant not only in terms of their frequency but also in terms of intensity (not shown). Thus, we

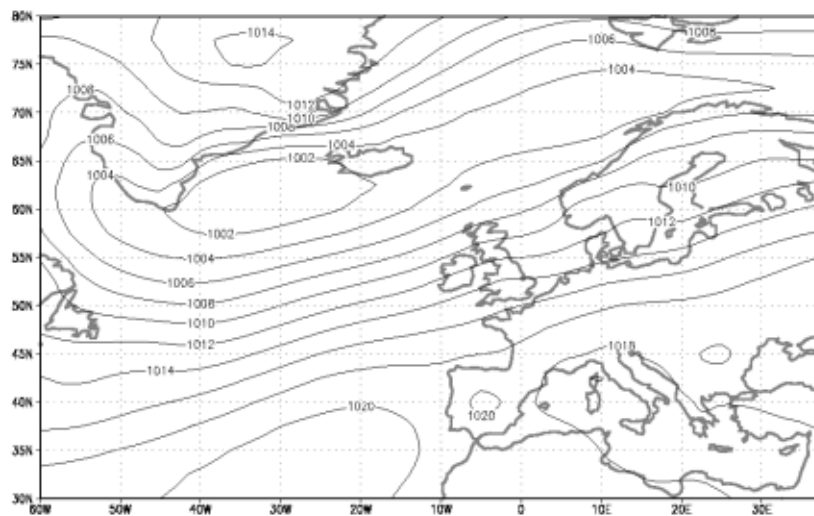


Figure 2.6: Mean MSLP field for winter months ONDJFM in ERA40, 1961-2000 (unit: hPa).

concentrate on gale days occurring in the CWT classes SW, W, NW, C and AC. Anomalies of MSLP patterns from the winter mean state (cf. Fig. 2.6), wind speeds and associated cyclone tracks for JC35 gale days in these classes are presented in figure 2.7. Note that results with respect to CWTs other than W are computed from a comparatively low number of events. Nevertheless, the pressure anomalies for the composites of storm days are significantly stronger compared to the composites of all days in each CWT class (cf. Fig. 2.7, left side).

- Storm days with W flow (figure 2.7a): The position of mean low pressure is over the northern North Sea, whereas high pressure prevails over South-West Europe. This reflects the definition of this CWT over Central Europe, but also shows the extension of low pressure anomalies to Scandinavia. The plots of associated cyclone tracks correspond well to those presented in figure 2.5 for all gale days, as the total volume is dominated by those with W flow. The same reasoning leads to the absence of major deviation from the wind distribution averaged over all events (Fig. 2.7a, right column). A high correlation ($r=0.75$) was found between the seasonal frequency of W storm days and the seasonal frequency of all W days (i.e. irrespective whether storm day or not). Further, the frequency of storm days with W flow reveals also a significant correlation with the seasonal NAO index. Most of the severe historical storms occurred in this class, such as “Daria” (Jan 25/26 1990), “Wiebke” (Feb 28 1990) or “Anatol” (Dec 3 1999; cf. Ulbrich et al., 2001).
- Storm days with NW flow in the Central European investigation area (figure 2.7b) seem to be of enhanced relevance for eastern Central Europe, as highest wind speeds occur over inland areas of Poland and the eastern part of Germany during storms in this CWT class. Also over the North Sea, high mean values of maximum daily wind speeds are found compared to storms in other classes. The mean pressure minimum is located over the Baltic Sea; the mean position of highest pressure is over the Bay of Biscay. Cyclones move on a ridge-like path from North Atlantic to North Sea and then further east over Scandinavia to the Baltic Sea. The mean intensity of cyclones is relatively high far into eastern parts of the tracks; e.g., Laplacian P values higher than $1.2 \text{ hPa}/(\text{deg.lat})^2$ are found over the Baltic Sea, helping to explain the high wind speeds in eastern areas (cf. Fig. 2.7b, right panel). Representative for this class is the storm “Ornella” (Jan 10 1995). It travelled quickly on a pathway from North Atlantic,

south of Iceland towards South Sweden and to the Baltic Sea and reached a minimum pressure of 965 hPa. At the same time, a strong anticyclone (1045 hPa) was located over the eastern Atlantic. The steep pressure gradient between both systems caused a strong NW-flow. In List (Island of Sylt) wind speeds of up to 39 m/s were measured (Berliner Wetterkarte, 1995). Severe gusts also occurred over inland areas (particularly in eastern parts of Germany, e.g. Schwerin 28 m/s, Potsdam 25 m/s, Goerlitz 25 m/s).

- Storm days with SW flow (figure 2.7c): The minimum of averaged MSLP is located over eastern Atlantic, close to the British Isles, whereas there is high pressure over Southern Europe. Cyclones associated with storms with SW flow at the surface when they reach Central Europe typically reach their maximum intensity over or close to the UK. Wind speeds are highest over Western Europe; the eastern part of Central Europe is less or not affected by those events. An example of a storm in this class is the extratropical cyclone “Oralia” (Oct 30 2000). This was a rapidly developing secondary disturbance, moving fast around a relatively deep (960 hPa) stationary depression over Scotland. Oralia reached a minimum pressure of 940 hPa over the North Sea and caused gale-force winds over the German Bight. Here, the light vessel “TW EMS” registered a gust of 39 m/s (Berliner Wetterkarte, 2000). Also over western and Central European inland areas strong gusts were measured (e.g. Vlissingen 27 m/s, Trier 28 m/s, Aachen 27 m/s).
- Storm days with C flow (figure 2.7d): The localised pressure anomaly over Central Europe can be related to the definition of this CWT. The tracks of the associated cyclones are approaching Europe partly from the west and partly from the Mediterranean area. Cyclones are relatively weak over Central Europe (with maximum intensities over the central North Atlantic), and so are maximum wind speeds. In Central Europe the impact of storms in this class is thus weaker than on average (figure. 2.7d). A storm situation identified in this class occurred e.g. on Feb 01 1986. With a cyclone over the western Mediterranean, a shortwave trough moved northwards to the Alps. North of the Alps there were strong southerly foehn winds with gale-force gusts (Zugspitze 37.5 m/s, Augsburg 20 m/s), while over Central and Northern German areas strong easterly winds occurred (Helgoland 28 m/s, Schwerin 20 m/s, Hannover 19 m/s (Berliner Wetterkarte, 1986)).

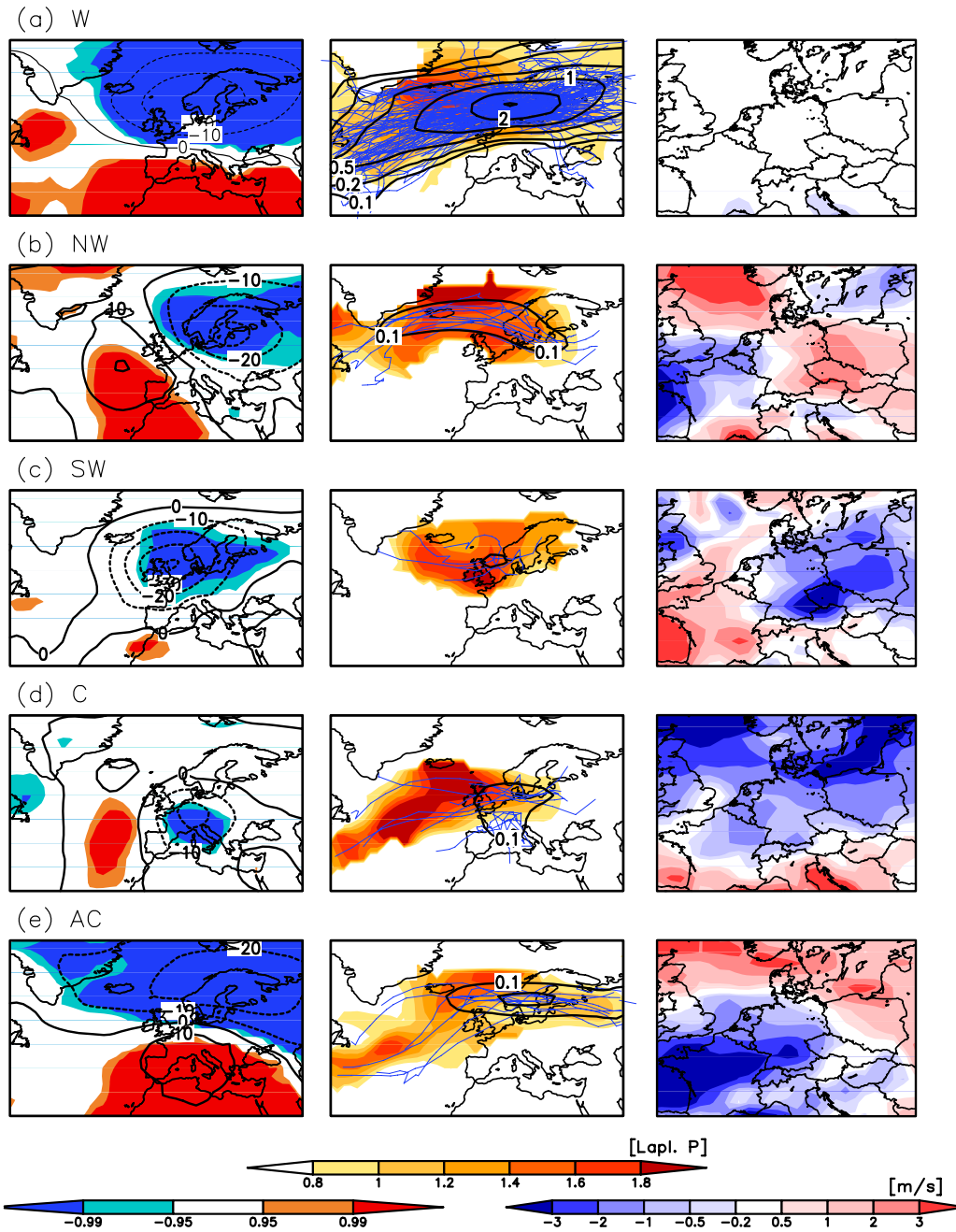


Figure 2.7: Atmospheric features in relation to JC35 gale days in ERA40, separated for relevant CWTs.

Left column: Anomaly of mean MSLP field for storm days in each CWT class from the respective mean MSLP field for winter in figure 2.6 (unit: hPa). Shaded areas indicate zones where the pressure anomalies are significantly higher (red) or lower (blue) compared to all days in each CWT class (Student t-test);

Middle: related cyclones (blue lines=tracks, black contour lines=track density, unit: tracks/winter; shaded areas=mean intensity of cyclones, Laplacian P, unit: hPa/(deg.lat)²);

Right column: anomaly of mean of daily maximum wind speed on storm days in each CWT class from mean of daily maximum wind speed on all storm days in figure 2.5a (unit: ms⁻¹).

- Storm days with AC flow (figure 2.7e) are connected to cyclones on a more northerly track. The mean depression is located over Scandinavia and the Baltic Sea, high pressure over southern Europe. Such a situation typically occurs on the

back side of a cyclone, when relatively high pressure can extend northwards as far as Central Europe, leading to an anticyclonic bend of isobars (almost all of the storm days in this class are of hybrid type with W/NW flow, cf. section 2.3.1). Associated cyclones propagate far eastwards, and their intensity is still relatively high ($\text{Lapl. } P > 1.0 \text{ hPa}/(\text{deg.lat})^2$) over Baltic States and Northern Russia. Thus, also storm days of this class are connected with high wind speeds particularly over eastern Central Europe and Eastern Europe. Note that the storm days classified as (hybrid) AC over Germany are likely to have directional (W or NW) characteristics over this region. Besides the single storm situation with purely anticyclonic flow characteristics (Dec 09 1980) already described in section 2.3.1, the storm “Verena” (Jan 13 1993) is another example identified in this class. This storm day, however, has hybrid AC and W flow characteristics. It is related to a rapidly developing cyclone that travelled quickly from the North Atlantic, over southern England (where it deepened more than 10 hPa in 3 hours), along the coasts of the North and Baltic Seas towards the Baltic States. On its back side emerged a high pressure ridge over western Europe, causing the hybrid anticyclonic flow. Gale-force wind speeds were measured at the coast as well as over inland areas (Helgoland 39 m/s, Schwerin 38 m/s, Duesseldorf 34 m/s (Berliner Wetterkarte, 1993)).

Thus, using a gale day definition focused on Central Europe, the different CWTs associated with the storms yield different specific characteristics of the synoptic situation. An extension of high wind speeds into eastern central Europe, for example, can be found in connection with NW flow or hybrid AC flow, as the cyclones still retain a relatively high intensity over the Baltic Sea. By contrast, during SW flow situations cyclones often lose intensity earlier (e.g. due to landfall) and do not move so far east, explaining a focus of highest wind speeds over the western parts of Central Europe. The vast majority of storms, however, occur with westerly flow over Central Europe.

2.4. Summary, Discussion and Conclusions

In this paper, we identified storms over Central Europe by two different methods: One is based on the relatively simple CWT approach, with storm events defined from a gale parameter originally developed by Jenkinson and Collison, 1977 and Jones et al., 1993.

The other is defined from local winds at ERA40 grid points in Germany exceeding the 98% percentile threshold which is relevant for storm damage. Only 70% of the storm events identified by the two methods were identical, but no large differences were found with respect to the assignment of storms and a daily NAO index, and with respect to the association of storms and the CWTs on storm days. The days differing between the two methods primarily concern weaker events. Despite the partial disjunction of both sets of storm days, the associated atmospheric features such as large-scale atmospheric flow in terms of NAO and CWTs, cyclone tracks and assigned wind speeds turn out to be very similar. Thus, we conclude that the gale index is a simple but suitable parameter to identify damaging storm events in this region. This permits future investigations on storms in multi-model ensembles based on this simple measure.

The vast majority of Central European storm days is associated with westerly flow regimes (about 80%) and with a positive NAO phase, the latter being computed on a daily basis. Only between 5 and 7% of storm days (depending on the specific storm definition) have occurred in conjunction with modestly negative NAO phases, and none with a strongly negative NAO index value. Neutral NAO phases are somewhat underrepresented in the occurrence of storms, as the majority of events occur during a modestly positive phase. Strong positive NAO phases (only 6.4% of all days) have a share of more than 20% of the storms. Thus, about 10 percent of all days with a strongly positive NAO index and about 5% of those with a modestly positive index are associated with a storm over central Europe. It should be kept in mind that, on the other hand, the cyclones themselves play a major role in steering the NAO phase (e.g. Benedict et al., 2004). Thus, the existence of cyclone systems over the North Atlantic itself has an influence on the NAO index (e.g. Schneidereit et al., 2007). Our results complement previous studies on the relation between storms and NAO (e.g. Pinto et al., 2009) which investigated the occurrence of deep cyclones for different NAO phases, but did not account for the affected regions. The results seem to be in line with studies on storms and on the NAO in climate change experiments suggesting an increasing NAO index and an increasing storminess with increasing GHG forcing (e.g. Pinto et al., 2007b).

Distinguishing the different CWTs for the days of storm occurrence, the results for the most relevant westerly flow are very similar to the overall results. They are characterised by cyclones travelling from the North Atlantic to the British Isles, the

North Sea and southern Scandinavia. On average, the intensity of the cyclones related to storms has its maximum over the eastern North Atlantic, between Iceland and the British Isles.

Whereas storm days with W flow are of highest relevance in terms of their frequency, storm days with NW flow seem to be of highest relevance in terms of their intensity. In the observed set of storms, highest wind speeds over (Central European) inland areas and also over the North Sea occur for storm days in this class. The associated cyclones follow a ridge-like path north of the British Isles into the North Sea, and their intensity remains relatively high far eastwards into the Baltic Sea. Nevertheless, most of the severe and historically very loss-intensive storms are associated with W flow. The comparatively lower average wind speed for storm days with westerly flow is apparently due to a large number of weaker events in this class. This is distinct for NW flow, for which only a comparatively smaller number of weaker events are found. This result could be a sampling phenomenon, but a physical background associated with storm cyclone tracks predominantly travelling over sea cannot be excluded. Cyclones associated with NW storms travel over sea before and are thus still comparatively intense when affecting Central Europe. By contrast, cyclones on more southern tracks (associated with other flow classes such as W) typically make landfall earlier and lose intensity accordingly.

The relatively simple CWT approach in conjunction with the two storminess identification methods presented here provides realistic and reasonable results for the investigation of storm situations. The results obtained for the relation of wind storms and tropospheric conditions agree with findings from other studies on, for example, the occurrence of storms primarily during positive NAO phases (Raible, 2007; Pinto et al., 2009) or the importance of westerly flow for storms affecting Central Europe (Schmidtke and Scherrer, 1997; Busch et al., 1998). Additionally, the presented CWT approach allows for quantification of storm events as well as of the different flow classes and its related atmospheric features.

Flow directions typically change during the passage of a cyclone from SW flow on its front side when the cyclone approaches, rotating further to W to NW on the back side of the cyclone. Thus, it is expected that for consecutive storm days the same cyclone track may contribute to the composites of different flow classes (for example, SW, W and NW). Consecutive storm days (as identified here) related to different CWTs occur, but only rarely. During the 40-year reanalysis period, e.g. for JC35, there are 55 cases of

consecutive storm days, only 7 of which feature changes of flow direction (generally from W to NW). Leckebusch et al. (2008a) investigated weather situations leading to storm in Central Europe by means of a cluster analysis that also considers the temporal evolution over three days. Surveying the pressure patterns associated with the primary storm clusters (their figure 3) confirms that the geostrophic flow direction over Central Europe undergoes only small changes during the three day episodes and further illustrates the dominance of westerly flow.

The stability of these relationships covered by comparatively few events will be investigated on the basis of GCM simulations in a companion study (Donat et al., 2010a). In addition, possible future changes of atmospheric circulation and storminess under increased greenhouse gas conditions will be investigated, considering a multi-model ensemble of climate simulations.

A further quality of the present study is its detailed investigation of atmospheric conditions and cyclone systems related to storm events. Such a detailed examination on the relation between storms affecting Central Europe and associated atmospheric features may help to enhance understanding of European storm events. The detailed factors influencing the development and pathway of cyclones close to Europe need to be investigated in further studies. This is desirable in order to understand particular characteristics of cyclones related to storm days of different CWTs, e.g. the ridge-like characteristic of cyclone tracks and their relatively high intensity associated with NW storms.

Acknowledgments

This work was supported by the ENSEMBLES project, funded by the European Commission's 6th Framework Programme through contract GOCE-CT-2003-505539. We particularly thank Stefan Zacharias (Univ. Cologne) for computing the daily NAO index for the ERA40 dataset. We kindly thank ECMWF, DWD (German Weather Service) and DKRZ (German Climate Computing Centre) for ERA-40 data use and availability. We are also grateful to two anonymous reviewers for their detailed comments, which helped to focus the manuscript and improve its clarity.

3. European storminess and associated circulation weather types: future changes deduced from a multi-model ensemble of GCM simulations

Abstract

A range of possible changes of frequency and characteristics of European wind storms under future climate conditions is investigated on the basis of a multi-model ensemble of 9 coupled global climate model (GCM) simulations for the 20th and 21st centuries following the IPCC SRES A1B scenario. A multi-model approach conduces to an estimation of the (un-)certainties of the identified climate change signals. General changes of large-scale atmospheric flow are analysed, the occurrence of wind storms is quantified, and atmospheric features associated with wind storm events are considered. Identified storm days are investigated according to atmospheric circulation, associated pressure patterns, cyclone tracks and wind speed patterns. Validation against reanalysis data reveals that the GCMs are in general capable of realistically reproducing characteristics of European circulation weather types (CWTs) and wind storms. Results are shown with respect to frequency of occurrence, storm-associated flow conditions, cyclone tracks and specific wind speed patterns.

Under anthropogenic climate change conditions (SRES A1B scenario) increased frequency of westerly flow during winter is found over the central European investigation area. The number of detected wind storm days increases between 19 and 33 % in the ensemble mean for two different measures of storminess, only one GCM revealing less storm days. The increased number of storm days detected in most models is disproportionately high compared to the related CWT changes. Mean intensity of cyclones associated with storm days increases by about 10(\pm 10) % in ensemble mean in the Eastern Atlantic, near the British Isles and in the North Sea. Accordingly, wind speeds associated with storm events increase significantly by about 5(\pm 5) % over large parts of central Europe, mainly on days with westerly flow. The impact of different ensemble constructions that leave out an outlier model or include multiple runs of one particular model is discussed.

3.1. Introduction

Mid-latitude wind storms are the most loss-relevant natural hazard in central Europe, causing 53 (64) percent of economic (insured) losses in Germany (Munich Re, 1999; Munich Re, 2007). It is thus of high public and economic interest to quantify and understand long-term changes in their intensity and frequency in the recent past, and to estimate future changes induced by anthropogenic climate change (ACC).

With respect to the past century, studies investigating trends of European storm activity produce ambiguous results. Some point out that no longer term reliable trends could be identified and that an increased storm activity in recent decades (e.g. Leckebusch et al., 2008b) prior to the 1990s could be partially due to natural variability (Barring and von Storch, 2004, Mattula et al., 2008). Alexandersson et al. (2000) document that another period of high storm activity (similar to the 1990s) occurred in the late 19th century. Recently, Wang et al. (2009) identified positive trends of storminess for specific regions of the Northeast-Atlantic if only the winter season was considered.

Analysing windstorms under future ACC, published results seem to agree better, at least with respect to European storm risk: Knippertz et al. (2000) found an increase in extreme wind events for Europe, associated with a rising number of deep cyclones towards the end of the 21st century. Leckebusch et al. (2006) investigated cyclone activity and extreme wind speeds in a multi-model ensemble and found increased activity of extreme cyclones for western parts of central Europe. For one particular climate model (ECHAM5), Bengtsson et al. (2006) found increased cyclone intensity over parts of the eastern North Atlantic (cf. their figure 10). Pinto et al. (2007b) demonstrated that the simulated change in storms in this model is associated with alterations of the flow characteristics over the North Atlantic, in particular an extension of the upper tropospheric jet stream into Europe. Lambert and Fyfe (2006) analysed cyclone counts in an ensemble of 15 climate models and found in all models an increased number of extreme cyclones in winter in both hemispheres and a slightly reduced total cyclone number with increased greenhouse gas (GHG) forcing.

Considering large-scale atmospheric conditions associated with the occurrence of storms, a relation with a positive phase of the North Atlantic Oscillation (NAO) pattern was found in different studies (e.g. Raible, 2007, Pinto et al., 2009). On the other hand, the cyclones themselves play a major role in steering the NAO phase (e.g. Benedict et al., 2004; Schneidereit et al., 2007). Focusing on storms affecting central Europe,

moderate positive NAO phases were identified as optimum for the occurrence of such events (Donat et al., 2009). Studies on possible future changes of NAO under ACC conditions often reveal a shift to a more positive phase, as documented by Stephenson et al. (2006) considering a GCM ensemble.

Examining model projections of future climate, climate scientists are faced with different uncertainties which can be grouped into sensitivity to the initial conditions and to boundary conditions, model uncertainties and uncertainty due to internal variability (statistical uncertainty). Model uncertainty can be explored by using multi-model ensembles. On the seasonal timescale, the multi-model performance has been documented as superior compared with single-model performance (Hagedorn et al., 2005). Also for climate-timescale applications, a multi-model ensemble can be favourable compared to a single model (cf. Palmer and Räisänen, 2002; Räisänen, 2007; Collins, 2007; Tebaldi and Knutti, 2007, Donat et al., 2010b). Multi-model ensembles sample initial condition, parameter as well as structural uncertainties in the model design.

The aim of this study is to learn about potential future changes of large-scale flow conditions over central Europe under anthropogenic climate change conditions, in particular with respect to storm frequencies, intensities and characteristics. The robustness of the analysed climate change signals is estimated on the basis of a multi-model ensemble of state-of-the-art coupled global climate models. This allows for avoiding specific uncertainties in the signal arising from use of only a single model and to present a range of possible changes. The present study adds several new aspects to recent studies investigating future changes in the climatologies of extratropical cyclones (cf. Leckebusch et al., 2006; Lambert and Fyfe, 2006; Pinto et al., 2007b) or extreme wind speeds (cf. Leckebusch and Ulbrich, 2004; Pinto et al., 2007a; Gastineau and Soden, 2009). It explores changes in the frequency of wind storm events and flow types, also investigating the atmospheric conditions that are explicitly associated with the occurrence of wind storms. Thus, the robustness of the identified climate change signals is discussed on the basis of multi-model simulations and additionally by comparing them to different analysis methods from the aforementioned studies.

This paper is organised as follows. The data and methods are described in chapter 3.2. Validation of 20th century simulations and analyses of future changes in large-scale flow, occurrence of storm days and related atmospheric patterns are presented in chapter 3.3, as well as a discussion of impacts of different ensemble compositions on the results.

In chapter 3.4 the results are discussed in comparison to previous studies and chapter 3.5 summarizes the most important conclusions from our study.

3.2. Data and Methods

As almost all synoptic-scale wind storm events associated with severe damage occur during boreal winter (Klawns and Ulbrich, 2003; Munich Re, 2007), our analyses concern the period from October to March. Investigations presented in this study are based on an ensemble of 9 GCM simulations with 6 different GCMs (ENSEMBLES project setup, see table 3.1). From each simulation, we consider a period representing recent greenhouse gas forcing conditions during the last decades of the 20th century (20C) and a projection of future climate at the end of the 21st century according to the SRES A1B scenario (A1B). The simulations of recent climate are validated against results from ERA40 reanalyses (Uppala et al., 2005), as presented in a recent study (cf. Donat et al., 2009). The length of the available simulation periods differs between the model simulations (table 3.1), in particular for the A1B forcing period. Climate estimates computed over relatively short periods (20 years) may be affected by multidecadal variability, which is produced inherently by the GCMs (and which is also present in the real world). Bearing in mind that this effect may cause differences between individual simulations, the considered ensemble of in total 340 years of 20C climate and 240 years of A1B scenario simulations should provide a stable basis for our investigations. Data at high temporal resolution (instantaneous 6-hourly MSLP fields) as required for the cyclone tracking approach were available from the simulations carried out in the ENSEMBLES project. We could not extend our database to the larger set of CMIP3 models (stored at PCMDI), as they do not archive the high resolution data for periods of two or more decades.

Mean sea level pressure (MSLP) data and daily maximum wind speeds are used for the analyses in this study. The daily maximum of wind speed is stored in almost all data sets as the wind speed maximum of all integration time steps. However, this quantity is not available for the DMI-ECHAM5OM1, BCCR-BCM2 and CNRM-CM3 simulations. For these three data sets, we derived the daily maximum as maximum value of 4 instantaneous values from 00, 06, 12 and 18 UTC. This maximum of 4 instantaneous values was shown to be only slightly lower than the actual maximum (cf. Pinto et al., 2007a).

Model	Institute	Resolution atmosphere	20C.	SRES A1B	No. of considered runs	References
BCCR-BCM2	Bjerkness Centre for Climate Research	T63,L45	1960-1999	2080-2099	1	Furevik et al., 2003
CNRM-CM3	Météo France/Centre National de Recherches Météorologiques	T63,L31	1981-2000	2081-2100	1	D. Salas-Mélaia et al., 2005 (personal communication)
DMI-ECHAM5	Danish Meteorological Institute	T63, L31	1961-2000	2071-2100	1	Jungclaus et al., 2006
FUB-EGMAM	Freie Universität Berlin, Institut für Meteorologie	T30, L39	1961-2000	2081-2100	1	Manzini and McFarlane, 1998 Legutke and Voss, 1999 Huebener et al., 2007
IPSL-CM4	Institut Pierre Simon Laplace	2,5°x3,75°, L19	1961-2000	2071-2100	1	Marti et al., 2005
MPI-ECHAM5	Max Planck Institute for Meteorology	T63, L31	1961-2000	2071-2100	3	Jungclaus et al., 2006
METO-HC-HadGEM1	UK Met Office, Hadley Center	1,25°x1,875°, L38	1960-1999	2070-2099	1	Johns et al., 2006 Martin et al., 2006 Ringer et al., 2006

Table 3.1: ENSEMBLES GCM simulation data included in this study.

The ensemble of GCM simulations considered here is dominated by the ECHAM5 model (4 of the 9 simulations are based on this model), and the presented results could be biased owing to the dominance of this particular model. As we prefer to include as many GCM simulations as possible in our ensemble, we generally took all 9 available simulations into account to compute the ensemble mean. This approach is motivated by the finding that the change signals from the individual realisations with ECHAM5 reveal a considerable spread. Nevertheless, the results will also be discussed for the case that only one of the ECHAM5 simulations contributes to the ensemble (cf. section 3.3.6).

In a previous study, the relation between wind storm occurrence in central Europe, large-scale flow and associated atmospheric structures (i.e. related cyclones, patterns of MSLP and wind fields) was investigated on the basis of ERA40-reanalysis data (Donat et al., 2009; hereafter D09). The same methodologies and thresholds are used here (see below). Large-scale atmospheric circulation is classified into daily circulation weather types (CWTs, see Jones et al., 1993). This methodology was successfully used to examine storm events in the central European investigation area (D09), and is suitable to process the large amounts of data in a multi-model ensemble. The only required input parameter is the daily mean MSLP field. To classify the large-scale flow characteristics,

directional flow and vorticity are calculated in geostrophical approximation based on the MSLP differences around the central point (grid points used for the CWT calculation are shown in figure 3.1). On the basis of these terms, flow is classified into directional, (anti-) cyclonal or hybrid CWTs. The directional types are divided into eight sectors of 45°: NE, E, SE, S, SW, W, NW and N. For each day, flow can thus be classified into 1 of 27 types (8 directional, 1 cyclonal (C), 1 anti-cyclonal (AC), 8 hybrid cyclonal-directional, 8 hybrid anti-cyclonal-directional and 1 undefined). For the CWT counts, the hybrid weather types are considered each with half as occurrence of directional and half as (anti-) cyclonal flow. Thus, the frequencies of overall 11 classes are determined (8 directional, 1 cyclonal, 1 anticyclonal, 1 undefined). Further details can be found in Jones et al. (1993). Here, the investigation area is centred over central Europe (50°N, 10°E; cf. figure 3.1). Gale days are detected based on a gale index

$$G = \sqrt{F^2 + \left(\frac{1}{2}Z\right)^2}$$

(unit: hPa) that considers strength of directional flow (F) and vorticity (Z). With a threshold of $G > 35$ a reasonable number of severe gale days for the central European investigation area is detected, based on ERA40 reanalysis (D09). For reasons of comparability, this threshold will also be used here to analyse the GCM simulations. Gale days based on this definition are hereafter denoted as JC35.

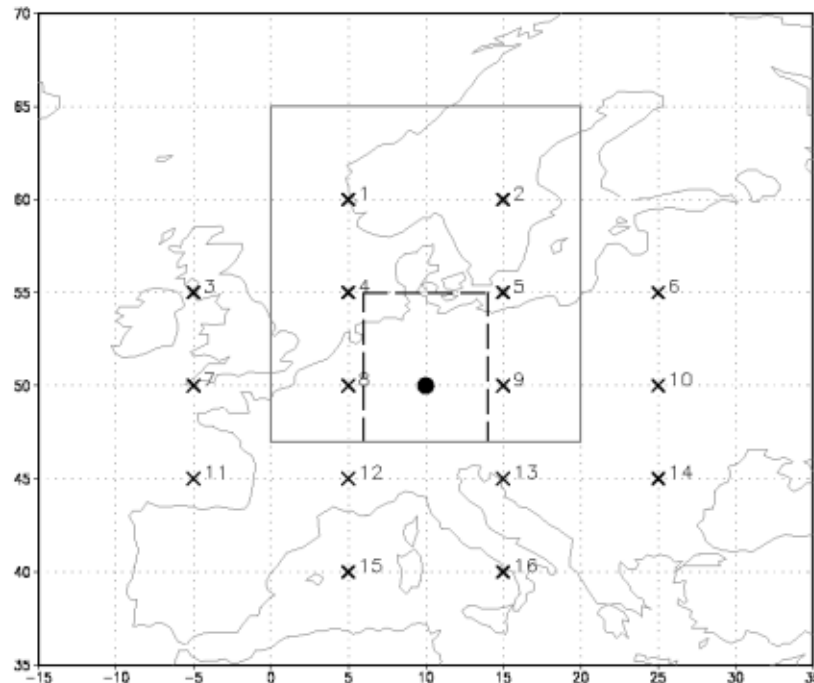


Figure 3.1: Investigation areas for classification of CWTs and gale days (16 points - marked "x" - for calculation of the geostrophic flow at the black central point), detection of storm days SP98 (dashed black box) and for the assignment of cyclone tracks to the wind storm days (solid grey box).

Alternatively to this criterion for storm day identification, which is based only on characteristics of large-scale flow (and does not explicitly take into account the incidence of strong winds), a second criterion considering the occurrence of extreme wind speeds is applied. The local 98th percentile of daily maximum wind speeds is deemed to be a common threshold for occurrence of storm damage (e.g. Klawe and Ulbrich, 2003; Leckebusch et al., 2007; Pinto et al., 2007a) and is thus also used here as a threshold for the identification of storm events. If it is exceeded in at least 25 percent of the central European investigation area (dashed black box in figure 3.1, the day is classified as a storm day. The relative definition of the threshold in this criterion assures comparability in two respects: it permits comparison of different GCMs even if the absolute wind speeds have a systematic error. It also allows the models to be considered simultaneously in spite of the different wind values used (maximum of 4 instantaneous values or highest simulated value on a day). The 25% of area requirement is checked by counting the number of central European grid boxes in dependence of the spatial resolution. In ERA40 (horizontal resolution $\sim 1.125^\circ$), the investigation area for storm detection consists of 49 grid boxes, so the local 98th percentile criterion must be fulfilled in at least 12 grid boxes on the same day. In ECHAM5 ($\sim 1.9^\circ$), the spatial threshold is 4 out of 16 grid boxes, and in the coarsest model (FUB-EGMAM ($\sim 4^\circ$)) it is only one out of 4 grid boxes. Hereafter SP98 is used as an acronym for wind storm days identified based on the exceedance of the 98th percentile of daily maximum wind speeds.

Cyclone systems are identified and their pathways are tracked by means of an objective algorithm developed by Murray and Simmonds (1991) and adapted to Northern Hemisphere cyclone characteristics (Pinto et al., 2005). It is based on 6-hourly MSLP fields and organized in 2 steps: At first cyclones are identified by searching for the maximum of the Laplacian ($\nabla^2 p$) of MSLP. Under quasi-geostrophic conditions, this is equivalent to the search for extremes of relative vorticity. Subsequently, a tracking algorithm is applied, which takes into account the most probable displacement of the cyclone core under the given large-scale conditions and previous path and speed. Tracks with a lifetime shorter than 24h are removed in a further step. While this tracking methodology is only one of many currently available (cf. Ulbrich et al., 2009), it performs well in comparison to other similar methods (Raible et al., 2008). In addition to previous studies (Pinto et al., 2007b; Leckebusch et al., 2008c), here cyclone tracks are explicitly related to storm events in central Europe. This is done by searching the

most intensive cyclone passing across the cyclone detection box that was calibrated to 0°E-20°E, 47°N-65°N (solid grey box in figure 3.1) during an identified storm day.

3.3. Analysis of the model simulations

3.3.1. Winter mean MSLP field and atmospheric flow

As air flow on the scale considered here is primarily a consequence of pressure gradients, this section concentrates on the analysis of MSLP patterns. For 20th century forcing, the winter mean MSLP field of the GCM simulations (figure 3.2a, ensemble mean of 9 GCM runs) reproduces the characteristic pattern with low pressure from the mean Icelandic low to the North Sea and high pressure over the Azores and southern Europe, as it is also found from ERA40 reanalysis data (cf. D09, their Fig. 6). In the area of the mean Icelandic low as well as in the high pressure zone over the Azores, absolute pressure values are slightly higher in the multi-model ensemble mean compared to ERA40 (figure 3.2b). The Azores high in the multi-model mean additionally extends further eastwards than observed, leading to a significantly higher MSLP over the whole Mediterranean region. Slightly too low mean pressure (reaching -2 hPa) is found near the British Isles. Consequently, the meridional pressure gradient over central and western Europe is stronger in the climate model simulations than in ERA40-reanalysis; thus, mean westerly flow is on average expected to be enhanced in the GCMs. For example, the mean pressure difference between northern Scotland and northern Spain is about 20% higher in the GCM ensemble compared to ERA40.

Regarding the MSLP fields of the individual models (not shown), it turns out that higher pressure values over the Mediterranean leading to overly strong pressure gradients over central Europe are especially found in the simulations with IPSL-CM4 (here, mean MSLP is about 5hPa too high over southern Europe), CNRM-CM3, BCCR-BCM2 and FUB-EGMAM. The other two models (HadGEM1, ECHAM5) reproduce better the characteristic climatological pressure patterns that are relevant for central Europe.

The changes of the mean pressure field in simulations for the end of the 21st century (following the SRES A1B scenario) are shown in figure 3.2c. The ensemble mean reveals significantly enhanced pressure values (by up to 2.5 hPa) over large areas of southern Europe and significantly decreased pressure over northern Europe (by -3 hPa). This leads to a higher meridional pressure gradient over central and western Europe

compared to simulations of the recent climate. Consequently, an increase in mean westerly flow may be expected as part of the climate signal.

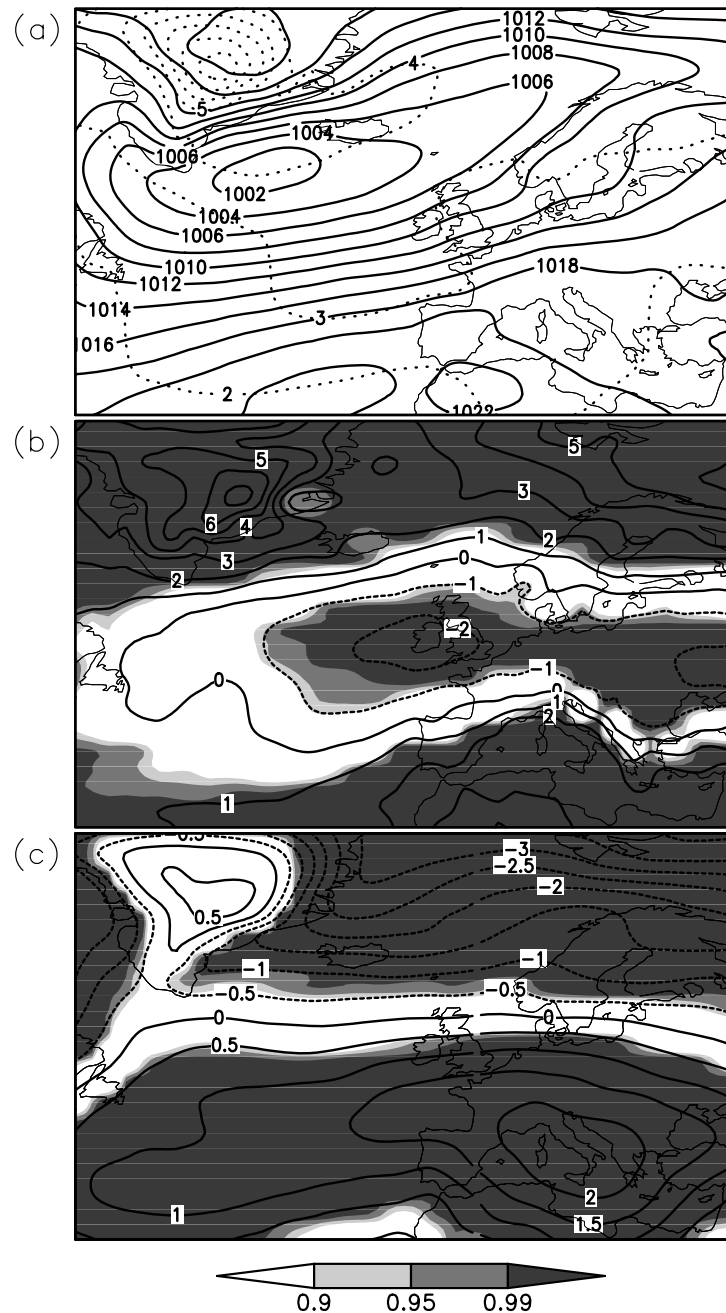


Figure 3.2: Mean MSLP fields during winter half year (ONDJFM).

- a) GCM ensemble mean (solid lines) of the 20C simulations (unit: hPa). The inter-model standard deviation between the fields in the different ensemble members is indicated by the dotted lines
- b) Difference of GCM ensemble mean for 20C from ERA40 reanalysis. The magnitude of differences is displayed by contour lines (unit: hPa), significance level by colours (Student t-test)
- c) ACC signal GCM ensemble mean A1B-20C. Differences are displayed by contour lines (unit: hPa), significance level by colours (Student t-test).

A similar climate change signal can be found in almost all individual model simulations (not shown), leading to a high statistical significance of the change signal in the ensemble mean ($P > 0.99$ in terms of interannual variability over large parts of Mediterranean and southern Europe, according to a local Student t-test). As expected from the lower number of years in the individual models' signals, the individual changes in general have a lower statistical significance.

Fundamentally different signals compared to the ensemble mean and to the majority of the ensemble members are found in the simulations with HadGEM1 and IPSL-CM4. In the HadGEM1 simulation the pattern of change is shifted northwards: maximum increase of pressure is found over the Bay of Biscay, decreasing pressure can only be detected in the very north of Scandinavia. The IPSL-CM4 shows an essentially contrary signal compared to the model ensemble. Here, MSLP is increased over the Northern Atlantic and over large areas of the European continent. MSLP values are decreased over the Atlantic south of 40°N . Consequently, the mean meridional pressure gradient over Europe is reduced in this model for enhanced greenhouse gas forcing.

The increased winter mean meridional pressure gradient over western and central Europe in most of the individual GHG runs and in the ensemble mean indicates a change to a more positive mean state of the NAO (as e.g. discussed by Stephenson et al., 2006), resulting in a more westerly mean large-scale flow. To analyse the flow characteristics for single days and especially for storm events, an objective scheme for classifying daily circulation weather types is applied in the next step.

3.3.2. Classification of daily circulation weather types

The relative frequencies of the different CWTs during the winter half year (October-March) are presented in table 3.2a for ERA40 reanalysis and for the GCM 20C simulations. In the reanalysis data (cf. D09), days with anticyclonic flow occur most frequently (31.6%), followed by westerly (22.6%) and cyclonal (10.0%) flow. Atmospheric flow from the whole easterly sector (NE, E, SE) is relatively rare during winter. To analyse the agreement between the ERA40 and the GCM derived CWT frequencies for the present-day forcing periods, we use the root mean square error (RMSE) as a measure of agreement (column 15 in table 3.2a). RMSE is calculated on the basis of the differences between the individual class frequencies in each model, in comparison to ERA40. HadGEM1 shows the best agreement with reanalysis (RMSE=1.2%), whereas IPSL-CM4 (5.6%) and CNRM-CM3 (8.2%) show the largest

discrepancies. Nearly all GCM simulations show an overestimated number of days with westerly or cyclonal flow, whereas the frequency of anticyclonic days is underestimated by all models but HadGEM1. Particularly IPSL-CM4 and CNRM-CM3 (the two GCMs with the highest RMSE) show a conspicuously overestimated frequency of westerly flow days.

Ensemble mean frequencies of the different CWTs were calculated by averaging the results from all considered GCMs (figure 3.3a and the last row of table 3.2a) and reveal a generally good agreement with the ECMWF reanalysis under present-day forcing (20C), but with an underestimation of AC flow frequency and an overestimation of flow from the whole westerly sector.

For the GHG forcing period at the end of the 21st century, all simulations (except for IPSL-CM4) reveal a significantly enhanced frequency of westerly flow (table 3.2b), which is in line with the winter mean MSLP signals mentioned in section 3.3.1. Further, all simulations show reduced frequency of cyclonal flow and with the exception of HadGEM1 also of easterly flow days. This is also true if changes for the whole easterly sector (NE, E, SE) are added up. In the ensemble mean – as in the majority of the regarded models – there is a significantly increased frequency of westerly flow (relative change +16%), less frequent occurrence of cyclonal (-21%) and easterly flow (-27%).

3.3.3. Storm day frequencies

With respect to the occurrence of storms under present-day forcing conditions, the ensemble average frequency of gale days (JC35 criterion) is realistic (about 7% higher than in ERA40). Individual models range between 40% (BCCR-BCM2) and 120% (MPI-ECHAM5, run 1) of the observational gale day frequency, except for the IPSL-CM4 simulation which produces more than twice the ERA40 value (table 3.2a). Using the SP98 method, a somewhat higher ensemble mean frequency of storms is obtained, compared to JC35 (17% more than ERA40, cf. table 3.2a, figure 3.3a). The differences between storm frequencies produced using the two criteria are large for some of the simulations, whereas the number of storm days had been found to be about equal between JC35 and SP98 using the ERA40 data (D09). For SP98, the inter-model differences are much smaller than for JC35. This is because the relative wind speed threshold used in the definition of SP98 is exceeded (by definition) in 2% of days in the present-day climate in any single model and grid box.

Table 3.2a: Relative frequencies of CWT classes and storm days in ERA40 and GCM 20C simulations (unit: percent of days during winter ONDJFM). The Root Mean Square Error (RMSE) was calculated for each model based on the 11 CWT classes counts (columns 2-12), in comparison with the respective class frequency in ERA40.

	C	AC	NE	E	SE	S	SW	W	NW	N	U	JC35	SP98	RMSE
ERA40	10.0	31.6	1.9	6.9	4.9	3.3	9.5	22.6	5.5	1.4	2.5	3.0	3.0	
MPI-ECHAM5_1	12.6	25.4	2.3	5.3	4.8	3.6	10.5	25.0	6.6	1.7	2.2	3.6	3.5	2.3
MPI-ECHAM5_2	13.2	25.7	2.1	4.9	4.3	3.9	11.1	24.1	6.8	1.8	2.1	3.3	3.4	2.3
MPI-ECHAM5_3	13.0	26.3	2.0	4.1	3.8	4.5	11.7	24.5	6.6	1.5	1.9	3.5	3.5	2.3
IPSL-CM4	9.9	21.9	1.6	2.7	1.7	2.1	11.5	36.9	8.3	1.9	1.6	6.7	3.5	5.6
FUB-EGMAM	12.4	21.8	2.2	3.3	2.3	2.8	11.7	29.8	9.7	2.3	1.6	2.4	4.5	4.2
DMI-ECHAM5OMI	13.0	26.2	2.4	5.2	5.2	3.9	10.5	22.9	6.7	1.7	2.1	3.4	3.4	2.0
CNRM-CM3	14.5	14.0	1.3	2.8	2.2	2.0	11.5	42.1	6.0	1.1	2.5	1.8	3.5	8.2
BCCR-BCM2	18.1	18.0	2.5	5.6	3.7	3.6	10.7	26.0	6.7	1.6	3.3	1.2	3.1	5.0
HadGEM1	9.4	30.4	1.9	6.2	3.7	2.8	10.8	25.5	4.8	1.2	3.3	3.3	3.2	1.2
Ensemble Mean (+/-STD)	12.9 (±2.5)	23.3 (±5.0)	2.0 (±0.4)	4.5 (±1.3)	3.5 (±1.2)	3.2 (±0.9)	11.1 (±0.5)	28.5 (±6.6)	6.9 (±1.4)	1.6 (±0.4)	2.3 (±0.6)	3.2 (±1.5)	3.5 (±0.4)	3.4

Table 3.2b: Climate change signals A1B-20C of CWT classes and storm days in the ensemble of GCMs. Changes on a significance level higher than 0.90 are highlighted by italic, bold numbers (Student's t-test)

	C	AC	NE	E	SE	S	SW	W	NW	N	U	JC35	SP98
MPI-ECHAM5_1	-2.0	+1.1	-0.8	-2.0	-1.6	-0.3	+1.4	+4.3	+0.4	-0.2	-0.2	+1.0	+1.4
MPI-ECHAM5_2	-1.9	+0.1	-0.2	-1.7	-1.0	-0.8	+1.2	+4.8	-0.2	-0.2	-0.2	+0.6	+0.8
MPI-ECHAM5_3	-0.6	-2.1	+0.1	-0.3	-0.4	-0.7	-0.6	+4.2	-0.1	+0.3	+0.3	+0.7	+0.1
IPSL-CM4	-1.5	+4.8	0	-0.7	+0.4	+0.5	+0.3	-2.7	-0.9	-0.2	-0.1	-1.1	-0.3
FUB-EGMAM	-3.1	-0.6	-0.7	-0.7	-0.7	-1.5	+1.1	+7.4	0	-0.4	-0.7	+1.4	+3.0
DMI-ECHAM5	-2.5	+2.0	-0.6	-2.6	-2.2	-0.7	+0.1	+5.4	+1.3	+0.2	-0.1	+0.6	+0.5
CNRM-CM3	-6.7	+5.6	-0.1	-1.1	-1.1	-0.6	-1.5	+6.3	-0.1	-0.2	-0.7	+2.3	+1.8
BCCR-BCM2	-5.8	+0.7	-0.7	-2.2	-0.6	-1.2	+0.6	+10.0	+0.3	-0.2	-0.7	+0.1	+1.0
HadGEM	-0.3	-1.6	-0.3	+0.9	+1.2	-0.4	-2	+2.1	+0.6	0	-0.2	0	+2.1
Ensemble Mean (+/-STD)	-2.7 (±2.2)	+1.1 (±2.7)	-0.4 (±0.3)	-1.2 (±1.1)	-0.7 (±1.0)	-0.6 (±0.6)	+0.1 (±1.2)	+4.6 (±3.5)	+0.1 (±0.6)	-0.1 (±0.2)	-0.3 (±0.3)	+0.6 (±0.9)	+1.2 (±1.0)

Table 3.3a: Gale days JC35 in ERA40 and 20C, occurring in the different CWT classes (unit: days per winter). The last column shows the total number of gale days (i.e. the sum of days in the different classes).

	C	AC	NE	E	SE	S	SW	W	NW	N	undef.	total
ERA40	0.20	0.23	-	0.14	0.01	-	0.11	4.59	0.23	-	-	5.50
MPI-ECHAM5_1	0.61	0.34	0.01	0.16	0.04	0.03	0.23	4.89	0.25	-	-	6.55
MPI-ECHAM5_2	0.41	0.18	-	0.11	0.06	-	0.16	4.75	0.40	-	-	6.08
MPI-ECHAM5_3	0.50	0.34	-	0.01	0.04	-	0.40	4.76	0.40	-	-	6.45
IPSL-CM4	0.25	0.79	-	0.14	0.03	-	0.44	9.63	0.86	-	-	12.13
FUB-EGMAM	0.24	0.16	0.01	0.03	-	-	0.30	3.29	0.25	-	-	4.28
DMI-ECHAM5	0.71	0.26	-	0.19	0.05	-	0.29	4.36	0.36	-	-	6.23
CNRM-CM3	0.03	0.05	-	-	-	-	0.05	3.13	0.05	-	-	3.30
BCCR-BCM2	0.15	0.09	-	0.06	-	-	0.09	1.68	0.06	-	-	2.13
HadGEM	0.05	0.20	-	0.11	-	-	0.13	5.39	0.08	-	-	5.95
Ensemble Mean	0.33	0.27	-	0.09	0.02	-	0.23	4.65	0.30	-	-	5.90
(+/-STD)	(±0.23)	(±0.21)	(±0.01)	(±0.07)	(±0.02)	(±0.01)	(±0.13)	(±2.07)	(±0.24)	(±)	(±)	(±2.65)

Table 3.3b: ACC signal gale days JC35 A1B-20C. Changes on a significance level higher than 0.90 are highlighted by italic, bold numbers (Student's *t*-test)

	C	AC	NE	E	SE	S	SW	W	NW	N	undef.	total
MPI-ECHAM5_1	0.07	-0.14	-0.01	-0.10	0.06	-0.03	0.03	<i>1.61</i>	<i>0.38</i>	-	-	<i>1.88</i>
MPI-ECHAM5_2	-0.13	-0.08	-	-0.01	-0.06	-	0.10	1.32	-0.18	-	-	0.96
MPI-ECHAM5_3	0.13	-0.12	-	0.12	-0.02	-	-0.25	<i>1.42</i>	-0.13	-	-	1.15
IPSL-CM4	0.17	-0.05	0.05	0.01	0.01	-	-0.04	<i>-2.16</i>	-0.08	-	-	<i>-2.09</i>
FUB-EGMAM	0.14	-0.01	-0.01	-	0.03	-	-0.03	<i>2.49</i>	0.03	-	-	<i>2.63</i>
DMI-ECHAM5	0.02	-0.03	-	-0.07	-0.02	-	-0.10	<i>1.30</i>	0.04	-	-	1.14
CNRM-CM3	-	0.13	-	0.03	-	-	0.05	<i>4.10</i>	-0.05	-	-	<i>4.25</i>
BCCR-BCM2	-0.05	-0.04	-	-0.06	-	-	0.01	0.38	0.04	-	-	0.28
HadGEM	0.10	-0.05	-	0.02	-	-	0.01	-0.22	0.09	-	-	-0.05
GCM Ensemble	0.05	-0.04	0.00	-0.01	0.00	0.00	-0.02	<i>1.14</i>	0.01	-	-	1.13
(±0.10)	(±0.08)	(±0.02)	(±0.06)	(±0.03)	(±0.01)	(±0.01)	(±0.10)	(±1.74)	(±0.16)	(±)	(±)	(±1.77)

Table 3.3c: like 3.3a), but for SP98 storm days

	C	AC	NE	E	SE	S	SW	W	NW	N	undef.	total
ERA40	0.19	0.13	-	-	-	-	0.06	4.08	0.88	0.03	-	5.35
MPI-ECHAM5_1	0.70	0.24	0.01	0.01	-	0.09	0.13	3.43	1.63	0.13	-	6.35
MPI-ECHAM5_2	0.54	0.16	0.06	-	0.04	0.05	0.11	3.51	1.49	0.11	-	6.08
MPI-ECHAM5_3	0.45	0.21	0.05	0.01	0.03	-	0.18	3.54	1.61	0.20	0.03	6.30
IPSL-CM4	0.23	0.15	-	-	0.01	0.08	0.21	4.90	0.65	0.03	-	6.25
FUB-EGMAM	0.24	0.56	-	-	-	-	0.61	5.18	1.40	0.06	-	8.05
DMI-EH5OM1	0.63	0.10	0.05	-	0.03	0.04	0.19	3.51	1.36	0.23	-	6.13
CNRM-CM3	0.58	0.28	-	0.13	0.08	0.03	0.13	4.45	0.70	-	-	6.35
BCCR-BCM2	0.46	0.53	0.21	0.16	-	0.03	1.38	2.53	0.10	0.14	-	5.53
HadGEM	0.10	0.14	-	0.03	-	-	0.11	5.04	0.39	0.03	-	5.83
Ensemble Mean	0.43	0.26	0.04	0.04	0.02	0.03	0.34	4.01	1.04	0.10	-	6.32
(+/-)STD	(±0.20)	(±0.17)	(±0.07)	(±0.06)	(±0.03)	(±0.03)	(±0.42)	(±0.91)	(±0.58)	(±0.08)	(±0.01)	(±0.70)

Table 3.3d: like 3.3b), but for SP98 storm days

	C	AC	NE	E	SE	S	SW	W	NW	N	undef.	total
MPI-ECHAM5_1	0.17	0.03	0.02	-0.01	0.00	0.03	0.01	1.74	0.38	0.16	-	2.52
MPI-ECHAM5_2	0.10	-0.05	-0.06	0.03	-0.04	-0.02	0.04	1.14	0.15	0.07	-	1.36
MPI-ECHAM5_3	0.07	-0.03	-0.05	-0.01	-0.03	0.02	-0.08	1.03	-0.55	-0.08	-0.03	0.27
IPSL-CM4	0.06	0.12	-	-	-	-0.08	0.22	-0.67	-0.15	-0.03	-	-0.52
FUB-EGMAM	0.06	0.44	-	-	-	-	0.91	3.65	0.40	-0.06	-	5.40
DMI-EH5OM1	0.03	0.03	-0.05	0.02	-0.01	-	-0.05	0.60	0.50	-0.09	-	0.98
CNRM-CM3	-0.18	-	-	-0.13	-0.08	-	0.18	3.88	-0.43	-	-	3.25
BCCR-BCM2	-0.31	-0.15	0.19	-0.06	-	-0.03	0.88	1.55	-0.05	-0.14	-	1.88
HadGEM	0.10	0.20	-	0.03	-	-	0.07	2.43	0.91	-0.03	-	3.71
GCM Ensemble	0.01	0.07	0.01	-0.02	-0.02	-0.01	0.24	1.71	0.13	-0.02	-	2.09
(+/-)STD	(±0.15)	(±0.17)	(±0.07)	(±0.05)	(±0.03)	(±0.03)	(±0.38)	(±1.44)	(±0.47)	(±0.09)	(±0.01)	(±1.84)

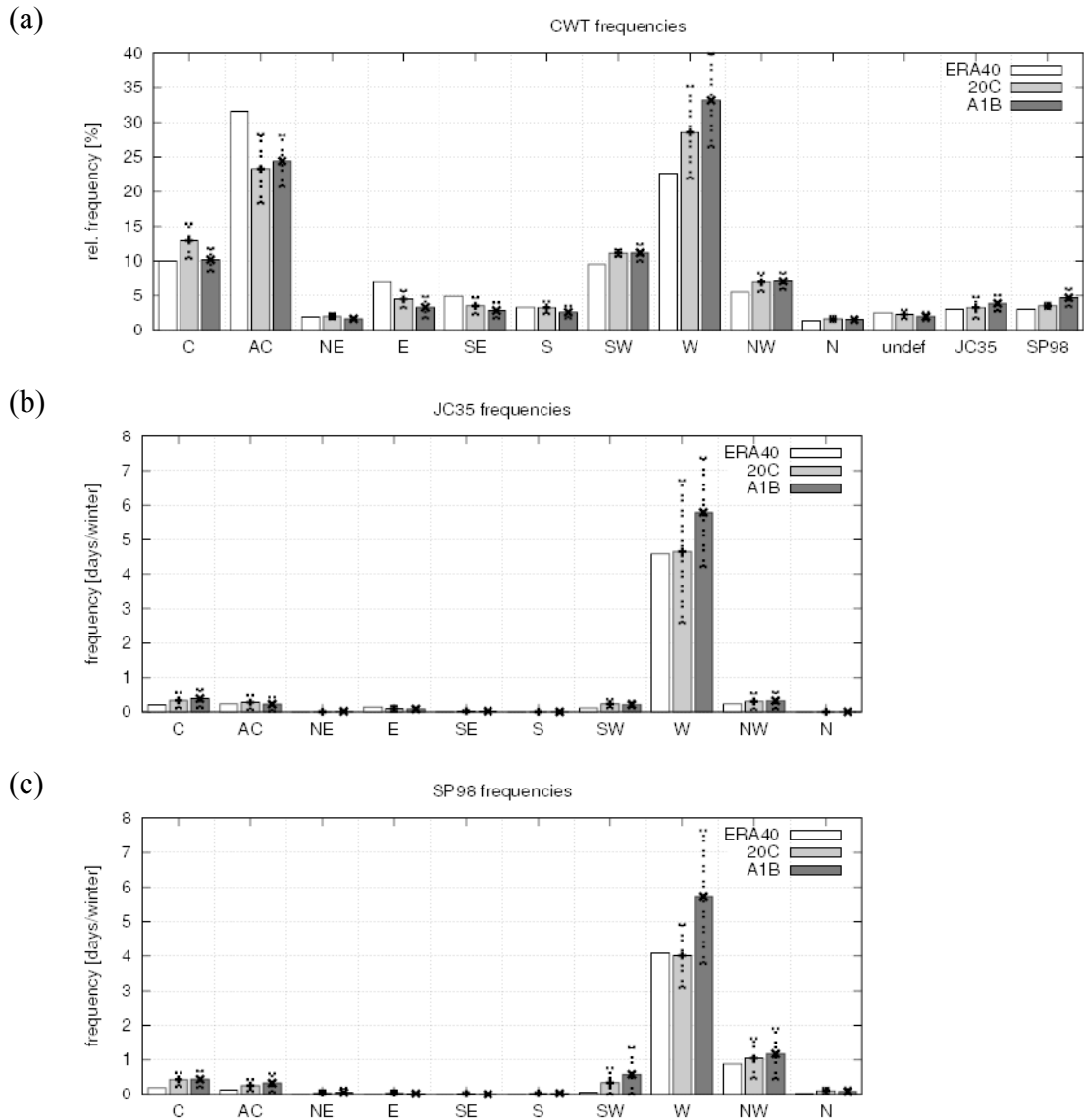


Figure 3.3: CWT and gale/storm day frequencies during winter half year (ONDJFM). The bars show frequencies in ERA40 (white), 20C simulations ensemble mean (light grey) and A1B simulations ensemble mean (dark grey). Uncertainty bars on ensemble mean indicate the inter-model standard deviation between the different ensemble members.

- a) all days (unit: percent of days during winter ONDJFM)
- b) CWTs during gale days JC35 (unit: days per winter ONDJFM)
- c) CWTs during storm days SP98 (unit: days per winter ONDJFM)

Almost all ensemble members show an enhanced frequency of gale days in the A1B forcing period. In ensemble mean, a relative increase of JC35 of about 19 percent is detected (table 3.2b, column 13, and figure 3.3a). Only IPSL-CM4 shows a relative decrease of gale days (-15%), which is in agreement with the winter mean flow signal which is in opposition to all other simulations considered. For this GCM, the A1B gale frequency is thus close to the respective numbers for the other runs. This contributes to a reduced model spread of JC35 in the future climate period (cf. figure 3.3a).

Considering change signals of SP98 storm days, the 98% wind speed threshold of the individual 20C climate is maintained also for the future periods. In terms of vulnerability assessment due to extreme wind speeds, this corresponds to an approach without adaptation of loss thresholds to changed climatic conditions (cf. Leckebusch et al., 2007; Pinto et al., 2007a). The occurrence of SP98 storm days is enhanced in eight out of nine ensemble simulations (significant on the 90%-level in six of them (Student's t-test), cf. table 3.2b, column 14). Only the IPSL-CM4 reveals a decrease of storminess (though not significant). In ensemble mean the number of SP98 storm days shows an increase of about 33% (figure 3.3a).

3.3.4. Atmospheric circulation on storm days

A clear dominance of storm days with westerly flow is found for the ensemble of the 20C GCM simulations, using both the JC35 (figure 3.3b and table 3.3a) and the SP98 criterion (figure 3.3c and table 3.3c). This agrees well with results based on ERA40 reanalysis data (cf. D09). Note that for easier interpretation frequencies of storm days in table 3.3 are given in days per winter half year. The simulated role of several other CWTs is partly different from the ERA40 estimates (with respect to both JC35 and SP98). Note, however, that the number of occurrences is still small compared to westerly flow.

The changes of storm day frequencies in the future scenario simulations are almost exclusively linked with changed frequency of storms with westerly flow (SP98: table 3.3d and figure 3.3c). According to the JC35 method, the ensemble mean storm day frequency is enhanced by 19%; considerable changes are only found for storm days with W flow (table 3.3b and figure 3.3b). Also considering the individual ensemble members, the number of JC35 gale days with flow from the west is significantly increased in six simulations; in 5 of them by approximately 20 percent. In CNRM-CM3 it is even doubled. Only IPSL-CM4 shows (in conjunction with the reduced total frequency of gale days, cf. section 3.3.3.) a significant decrease of those gale days with westerly flow. In two ensemble members (HadGEM1 and BCCR-BCM2) only small and non-significant changes are detected.

With the SP98 detection method, a strongly enhanced total number of storm days found in ensemble mean (+33%) as well as in almost all ensemble members (table 3.3d) is again linked with changed numbers of storm days with westerly flow. In 7 out of 9 ensemble members, significantly more storm days with flow from the west are detected.

Most of the models show an increase of about 30 to 50 percent in this class; only in IPSL-CM4 a small and non-significant reduction is found.

The enhanced storm day frequency is only partly explained by the CWT frequency changes. If the ratio of storm days in each CWT class remained unchanged for the future scenario climate, changes in CWT frequencies would contribute to relative increases of only 11% (9%) for JC35 (SP98), compared to the identified total increases of 19% (33%). An additional contribution comes from changing ratios of storm days in the different CWT classes. For example, considering the most relevant westerly flow class, the percentage of storm days in all days (irrespective if storm day or not) increases, in ensemble mean from 9.4% to 10.1% using the JC35 criterion and from 7.9% to 9.5% for SP98 (corresponding to relative increases of 7% and 20%, respectively). This result agrees with Pinto et al. (2010), who provided evidence that the frequency of intense storms within their storm clusters significantly increases in future climate conditions for the ECHAM5 runs.

3.3.5. Cyclone tracks, pressure patterns and local wind speeds associated with storm events

Simulated atmospheric features in relation to JC35 and SP98 storm events, such as associated cyclone tracks and wind speed patterns during the identified storm days, generally agree with those found for reanalysis data, in particular the maximum wind speeds over the North Sea and the Baltic Sea (figure 3.4a/b, compare D09, their figure 5) and the decrease towards lower wind speeds over inland areas. The latter is, however, more pronounced than in ERA40. Additionally, the isotachs over inland areas in the GCM ensemble have a more zonal orientation compared to ERA40. Although some of the ensemble members feature lower wind speeds (e.g. BCCR, CNRM, IPSL, not shown) and others overestimate wind speed values (e.g. FUB-EGMAM), the ensemble mean reveals a remarkable accordance of absolute wind speed values on gale days compared to ERA40 reanalysis wind speed values.

The observed track density pattern of "storm cyclones" (i.e., cyclones related to storm days, D09, their figure 5c) is well reproduced in the ensemble mean of GCM 20C simulations (figure 3.4c), as well as the spatial pattern of their mean intensity. For the latter, the maximum values between Great Britain and Iceland are about 20% lower than in ERA40, whereas there is a larger area in the GCM ensemble where the mean intensity of storm cyclones has medium values over the central North Atlantic

(Laplacian P $0.8-1.2 \text{ hPa}/(\text{deg.lat})^2$). This difference to the reanalysis data is primarily related to the lower spatial resolution of the GCMs in comparison to the reanalysis data (cf. e.g. Pinto et al., 2006).

Even when considering the atmospheric features associated with storm days in the individual CWT classes (figure 3.5a-e), the GCM ensemble is able to reproduce the characteristics of storm events for each circulation class as found for ERA40 (cf. D09, their figure 7). Regarding the MSLP patterns associated with JC35 storm events for the

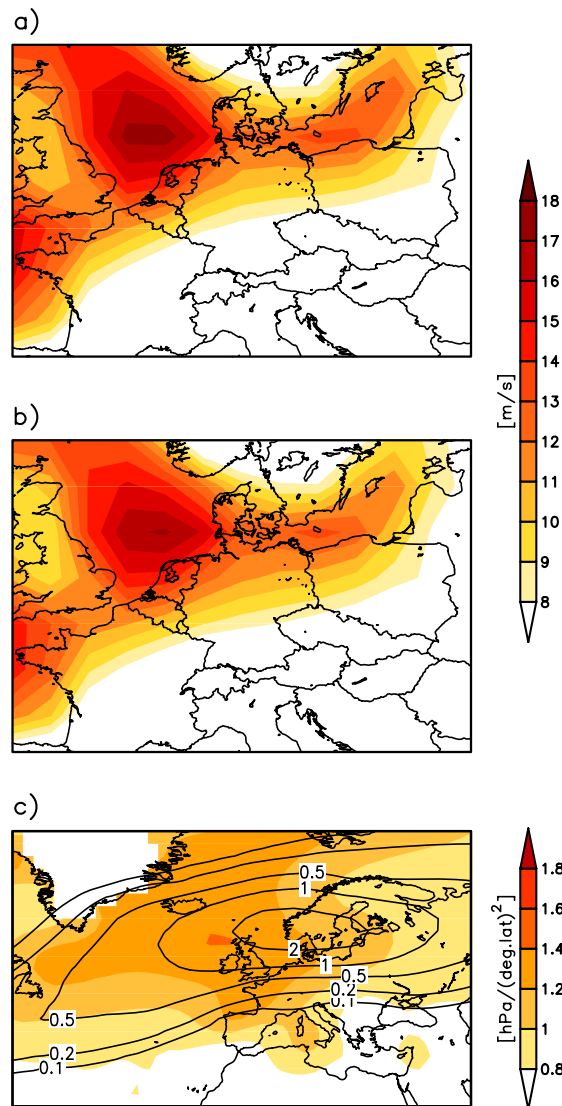


Figure 3.4: Wind speeds and cyclones in relation to storm events.

- a) Mean of daily maximum wind speeds during JC 35 gale days for the ensemble mean of GCM 20C simulations for (unit: ms^{-1})
- b) same as a) but for SP98 storm days
- c) Ensemble mean cyclone track density (isolines, unit: tracks/winter) and intensity (shaded, Laplacian P, unit: $\text{hPa}/(\text{deg.lat})^2$) of cyclones assigned to JC35 gale days in GCM 20C simulations. For smoothing, track density and intensity values are calculated for areas with a radius of 7.5 deg lat. around each grid point. Shading in areas with orography above 1500 m is suppressed.

individual CWT classes (left column in figure 3.5), agreement is expected from the definition of CWTs and storms for the central European area. Furthermore, agreement is also found for typical pathways of the storm cyclones and their intensity (middle column in figure 3.5) when assigned to the different CWT classes. For example, the ridge-like cyclone tracks and relatively high cyclone intensities over the Baltic Sea associated with high wind speeds over central Europe that were analysed for storm days with NW flow are also found in the climate model simulations. Also the wind anomalies associated with the CWTs on storm days (right column in figure 3.5, computed as deviations from the average of maximum wind speeds on all gale days shown in figure 3.4a) correspond well to the patterns that were also found for reanalysis data (compare with D09, their figure 7). In particular, above-average wind speeds in large parts of central Europe are analysed for storm days with NW flow (figure 3.5b), while storm days with SW flow are associated with high wind speeds particularly over western France (figure 3.5c). The composite for storm days with cyclonic flow (figure 3.5d) reveals above-average wind speeds over southern Europe. Storm days with AC flow in central Europe (which are primarily of hybrid CWT classes with W and NW flow, respectively; cf. D09) are associated with high wind speeds particularly over Scandinavia and the northern part of the North Sea. In conclusion, this validation reveals that typical atmospheric patterns associated with storm events in reanalysis data are well reproduced by the GCM ensemble. This is valid not only with respect to CWT frequencies but also for cyclone pathways and intensities and the spatial distribution of wind speeds.

With respect to the A1B simulations, the enhanced number of gale days in most simulations must be reflected by a higher number of cyclones related to storm just by the definition of storm cyclones. It is found that the track density is increased only along the maximum of track densities found for today's climate (figure 3.6a, compare to figure 3.4c). North and south of this zone very little change is found. Thus, this analysis reveals an accentuation of cyclones related to European storms, concentrated on the characteristic pathway over eastern North Atlantic, via the British Isles, North Sea and southern Scandinavia.

The intensity of storm cyclones (measured in terms of the Laplacian of MSLP) increases significantly (by up to 5-10 percent) under increased GHG forcing in a zone from North Atlantic to western central Europe (figure 3.6b). Consequently, and in accordance with this finding, the mean of maximum wind speeds during these storm

days is significantly higher by approximately 5 percent over large parts of Europe (figure 3.6c). Increased wind speeds related to storm days are found in all models at least over parts of central Europe (not shown). Even in the IPSL-CM4 simulation,

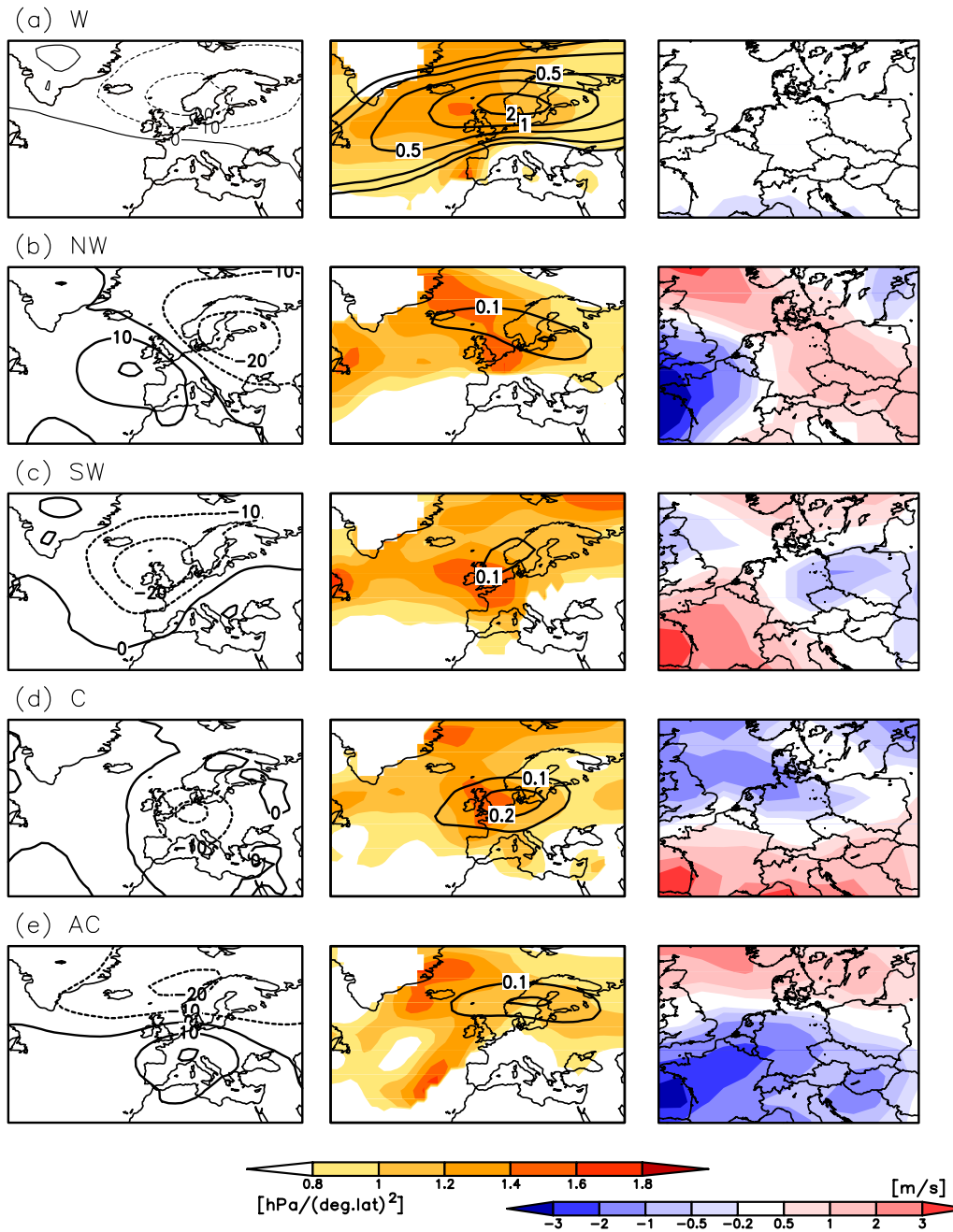


Figure 3.5: Atmospheric features in relation to JC35 gale days in the ensemble of GCM 20C simulations, separated for relevant CWTs. Left column: Anomaly of mean MSLP field for storm days in each CWT class from mean MSLP field for winter in figure 3.2a (unit: hPa); Middle: related cyclones (black contour lines=track density, unit: tracks/winter; shaded areas=mean intensity of cyclones, Laplacian P, unit: hPa/(deg.lat)²). For smoothing, track density and intensity values are calculated for areas with a radius of 7.5 deg lat. around each grid point. Shadings in areas with orography above 1500 m are suppressed. Right column: anomaly of mean of daily maximum wind speed on storm days in each CWT class from mean of daily maximum wind speed on all storm days in figure 3.3a (unit: m s⁻¹).

where reduced frequency of storm days was analysed, the mean of daily maximum wind speed during storm events is increased (not shown).

As a measure of uncertainty, the inter-model standard deviations of the change signals are regarded (contour lines in figures 3.6a-c). They turn out to have the same order of magnitude as the ACC signals, associated with the sensitivity of the standard deviation

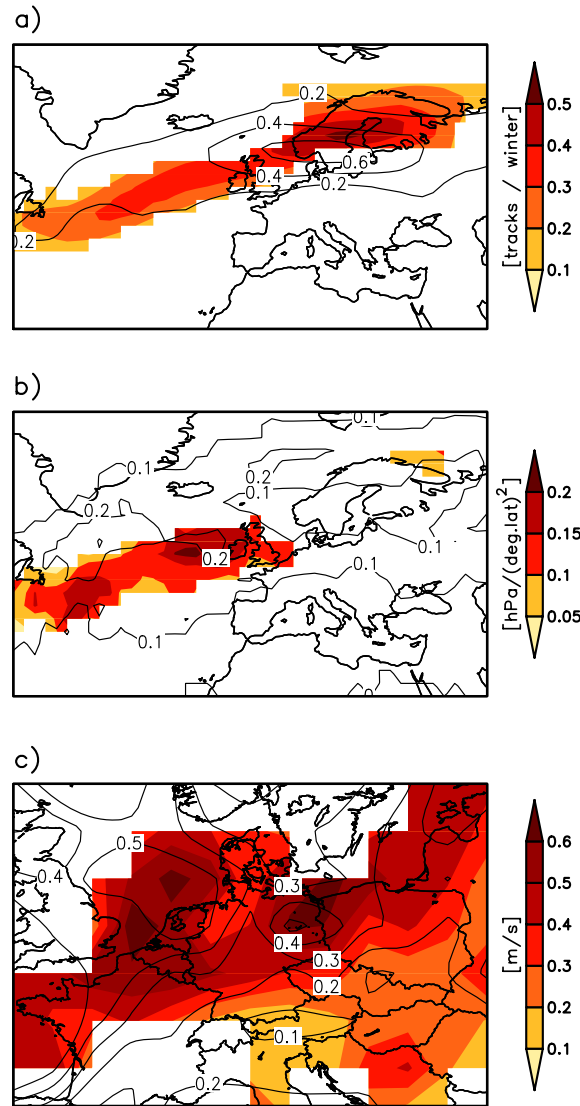


Figure 3.6: ACC signal AIB-20C for cyclones and wind speed related to JC35 gale days in the GCM ensemble. Differences are indicated by coloured areas and are only displayed for regions where the significance level is above 0.95 (according to Student t-test). The inter-model standard deviation of the change signals in the different ensemble members is shown by the contour lines.

- a) Track density of storm related cyclones (unit: tracks/winter, plotting of the change signal was omitted where track density in the 20C period is smaller than 0.3/year)
- b) Intensity (Laplacian P, unit: hPa/(deg.lat)²) of cyclones related to JC35 gale days (plotting of the change signal was omitted where track density in the 20C period is smaller than 0.3/year)
- c) Mean of daily maximum wind speed during JC35 gale days (unit: ms⁻¹)

to outlier signals (e.g. IPSL, confer to section 3.3.6). In areas with maximum magnitude of the change signal, the uncertainty between the climate signals of the individual ensemble members also shows a maximum. Taking the boundaries given by the standard deviations as a range for likely changes, the model ensemble produces a positive wind speed signal over central Europe during JC35 gale days, amounting to between 0 and 10 % (0-1 m/s). The increase of track density of cyclones associated with storm is, for example, +0.5 (± 0.6) over southern Scandinavia, i.e. between 0 and 1 tracks per year (0-40%, respectively). Similarly, the mean intensity of cyclones related to storm events in central Europe might increase between 0 and 0.2 hPa/(deg.lat²), i.e., 0-17% over the North Atlantic, British Isles and North Sea.

Consideration of ACC signals for the particular CWT classes reveals that changes for gale days with westerly flow correspond well to the presented change signals for all gale days (not shown). This is plausible, as the majority of storm days occur with flow from W and also change signals of gale frequency are strongest for those gale days with W flow (table 3.3b,d, figure 3.3b,c). Atmospheric features for storm with other CWT classes than W show largely neither relevant nor significant change signals (not shown), in line with the small changes of their frequencies. Change patterns for SP98 storm days are in general similar to those analysed for JC35 (not shown).

3.3.6. Effects of different model combinations on the ensemble mean ACC signals

Multi-model studies are unequivocally affected by the construction of the ensemble. We incorporated all available simulations from the ENSEMBLES project in the GCM ensemble, which is thus dominated by the ECHAM5 model. While different realisations with the same climate model (started from different initial conditions) are not expected to reveal significantly different climate mean states, consideration of extreme cyclones, extreme wind speeds or storminess, for example, may yield different magnitudes of the climate change signals (compare e.g. tables 3.3b, 3.3d or Pinto et al., 2007b). As the development of the different realisations is not systematically identical, it appears reasonable to consider all available simulations for this study in order to estimate the range and robustness of possible future changes. Nevertheless, we now analyse the influence of different model combinations, taking only one simulation from each GCM into account. The presented ensemble mean change signals from the previous sections are recalculated, now including only one of the ECHAM5 simulations. Thus, 4 different

ensembles of 6 different GCMs can be constructed (each containing either realisation 1, 2 or 3 of MPI-ECHAM5 or the DMI-ECHAM5 run).

Generally, when including only one ECHAM5 simulation in the ensemble, the mean change signals correspond well to the signals calculated on the basis of all 9 simulations, whereas the standard deviation of the different ensemble members is slightly increased. For example, the frequency of JC35 gale days would be increased by between 1.0 (± 2.2) up to 1.2 (± 2.2) days per winter period (i.e., between 18 and 20%), compared to an increase of 1.1 (± 1.8) days per winter if all 9 simulations are included in the ensemble (cf. table 3.3b). The increased standard deviations in the 6-model-ensembles are explained by the fact that – despite the considerable spread between the different realisations – the signals of the individual ECHAM5 simulations are all relatively close to the ensemble mean signal. This contributes to the result that the mean signals are not significantly different for the ensembles considering only one ECHAM5 simulation, whereas the inter-model uncertainty is increased.

Similar results are also found for SP98 and for the atmospheric features associated with the occurrence of wind storm days, such as track density and intensity of the related cyclones, or the composite of wind speed during storm days (compare to figure 3.6): Again, the mean change signals based on the different 6-member-ensembles considering only one realisation of ECHAM5 correspond well to the ensemble mean based on all 9 available simulations, but the significance of the signals is reduced.

Additionally, the effect of removing the IPSL-CM4 run from the ensemble was tested. Such an exclusion of a model from the ensemble could be justified by its performance in reproducing observed climate conditions and would correspond to a rather crude model-weighting approach. Also other studies identified IPSL-CM4 as a rather poorly performing GCM (e.g., Reichler and Kim, 2008; van Ulden and van Oldenborgh, 2005). Here, this GCM reveals large biases regarding MSLP pattern, CWT classes and storm day frequencies for present climate conditions. With respect to the ACC signals, it is again an outlier, showing opposite signals to most other models and to the ensemble mean. Consequently, the ensemble mean signals are higher and their uncertainty reduced if IPSL-CM4 is excluded from the ensemble. For example, the frequency of JC35 gale days would be increased by 28 (± 25) % then (compared to 19 (± 28) % if all models were considered).

3.4. Discussion

The intensification of zonal (westerly) mean flow over Europe in the future climate scenario simulations identified here is consistent with results reported by other authors. Van Ulden and van Oldenborgh (2005) computed large-scale geostrophic flow over Europe based on monthly mean MSLP from an ensemble of IPCC AR4 models. They also found a westerly bias in winter for simulations of recent climate and a tendency towards more westerly flow in the future climate simulations. Further, Stephenson et al. (2006) investigated the response of wintertime North Atlantic Oscillation (NAO) to increasing GHG concentrations in a CMIP2 multi-model ensemble. They found a positive increase of NAO index in the majority of the models. Moreover, Pinto et al. (2007b) found a shift both to more positive NAO values and to enhanced zonal flow in ECHAM5 simulations for different forcing scenarios (B1, A1B, A2).

The increased frequency of westerly flow under increased GHG forcing, together with reduced frequency of cyclonic flow (as identified in this study), are associated with changes of cyclone activity. Leckebusch et al. (2008c) investigate the changes of NH cyclone climatologies for the same GCM ensemble and show a reduced total number of cyclone tracks over large areas of NH at the end of the 21st century. Similar results were also found considering cyclone climatologies in single model studies and also smaller GCM ensembles, e.g. by Leckebusch and Ulbrich (2004), Leckebusch et al. (2006) and Pinto et al. (2007b). The reduction of cyclone tracks is, however, stronger over southern than over northern Europe. With respect to the cyclones leading to wind storms over central Europe (which are generally travelling north of the affected area), recent climate change studies also found an increased frequency of extreme cyclones and increased mean intensity of cyclones over the eastern Atlantic (Bengtsson et al, 2006; Pinto et al. 2007b, Leckebusch et al., 2008c). In particular, Pinto et al. (2009) identified an increase of explosive cyclone developments close to Europe tracking over the North Sea into the Baltic Sea (the pathway identified here as most relevant for wind storm occurrence in central Europe) in the three MPI-ECHAM5 runs also considered here. This assessment was confirmed by Della-Marta and Pinto (2009b) who used extreme value statistics to infer the changes of extreme cyclones over the North Atlantic/Europe, identifying a significant shortening of the return periods of storms over the North Sea and Baltic Sea (using Laplacian of MSLP as a measure of cyclone intensity). These results agree well with the conclusions of the present study.

Besides considering multi-model simulations, the present study adds to the above-mentioned ones (examining rather general cyclone climatologies) as it focuses on (composites of) atmospheric features (i.e., cyclone systems, wind speeds) explicitly related to storm events in central Europe. Additionally, changes of flow class and storm day frequencies are quantified. These event-specific ACC signals are of even higher significance than those found in the analyses of more general climatologies for extreme wind speeds or extreme cyclones based on the same GCM ensemble. A further important and new aspect in this study is the estimation of a range of possible future changes of storminess and their model-related uncertainties based on an MME of climate simulations. Results estimating the ACC are sensitive to the particular climate models considered and to the diagnostic methodologies applied (e.g. Christensen et al., 2007; Ulbrich et al. 2009). The ensemble of GCM simulations considered here reveals statistically significant ACC signals, in spite of a relatively large uncertainty that can be estimated by considering the inter-model standard deviations.

Ensemble mean results inherently depend on the ensemble composition. The present study considers four realisations of the ECHAM5 model (3x MPI, 1x DMI). Although the individual climate change patterns in the 4 ECHAM5 simulations are comparable, there are some considerable differences in their magnitude (e.g. tables 3.2b, 3.3c,d). We examined the impact on the ensemble results if only one of the four ECHAM5 simulations was considered, and found comparable mean signals, but increased uncertainty. This is in line with the fact that signals from all ECHAM5OM1 simulations are relatively close to the ensemble mean signal (in accordance with Ulbrich et al. 2008). Still, and for all considered ensemble mean ACC signals, the inter-model standard deviation (used here as a measure of uncertainty) is relatively large compared to the magnitude of the signal. The standard deviation is, however, strongly affected by outliers. If a rather weakly performing model in reproducing recent climate conditions (which also is an outlier with respect to ACC signals) was excluded from the ensemble, stronger signals with reduced uncertainty were obtained. While these results suggest it might be useful to exclude outliers, the inclusion of as many simulations as possible is generally recommended, as it allows for obtaining information about the possible spread of results based on state-of-the-art climate models. It might also be problematic to estimate the model performance by comparing the mean climate states of relatively short periods because of internal long-term variability. A well (weakly) performing model in a specific period might be less (more) realistic in another period (Reifen and

Toumi, 2009). Furthermore, the quality metric depends strongly on the considered variables (e.g. Reichler and Kim, 2008).

Uncertainty due to emissions scenarios was not considered in this study. Previous results, however, indicate that the intensity of the changes is in turn largely dependent on the intensity of the forcing (Leckebusch and Ulbrich, 2004; Pinto et al., 2007a/b). As the occurrence of storms is characterised by a high long-term variability, however, a direct response to a stronger GHG forcing is not necessarily detectable. This aspect leaves space for future studies. Also the detected concentration of storm-related cyclones under ACC conditions within a rather narrow “highway” remains an interesting phenomenon and requires further investigations.

A well-known weakness of current GCMs is a tendency to an overly zonal flow, related to an underestimation of anticyclonic/blocking situations (e.g. D’Andrea et al., 1998, Demuzere et al., 2008). In the present study, the largest changes were found for the westerly flow class, whose frequency was found to be overestimated for the simulations of recent climate compared to observations-based data. On the other hand, this study shows that the typical features of those cyclones and flow classes that are related to wind storms are nevertheless well reproduced by the GCMs. This suggests that the models are capable of realistically simulating the statistics of storm events and the related atmospheric features.

3.5. Summary and Conclusion

A multi-model ensemble of GCM simulations for recent and future (according to the SRES A1B scenario) climate conditions was investigated with respect to the occurrence of winter storm events over central Europe and their relation to features of large-scale atmospheric circulation. The analysed GCMs are basically capable of reproducing the observed (ERA40) circulation patterns and CWT frequencies for central Europe for the present-day period (20C). Regarding the two most frequent winter CWTs, there is a lack of anticyclonic flow (23% in GCM ensemble mean compared to 31% of all days in ERA40) and an excess of westerly flow days (29% compared to 23%). In the ensemble mean, the frequency of storm events as well as their distribution over flow classes is simulated realistically for both the CWT related criterion (JC35) and the wind speed percentile related criterion (SP98). Agreement with observational data is also found for

simulated patterns of wind speeds and for characteristics of the associated cyclones during storm days, even when considered according to the CWT during these days.

Under future climate conditions, the atmospheric circulation over Europe is characterised by an increased mean westerly flow during winter. This leads to both a higher frequency of days with westerly flow and to more frequent wind storm days (mainly in coherence with westerly flow). Furthermore, a reduced frequency of cyclonic and easterly flow is detected. The frequency of storm days is increased by 19 (± 28) % for JC35 and 33 (± 29) % for SP98, respectively. The enhanced storm day frequency is disproportionately high compared to the CWT frequency changes. Cyclones associated with the wind storms show increased mean intensity of about 10(± 10) % over the northeast Atlantic/North Sea region compared to recent climate conditions. The increased number of cyclones occurs in a rather narrow pathway along the eastern Atlantic, British Isles, North Sea to southern Scandinavia. Further, significantly higher wind speeds during storm days of 5(± 5) % are found over large parts of Europe. Even the model showing a reduced frequency of storm days under future climate conditions reveals increased intensity of cyclones and wind speeds in relation to these storm events.

The two criteria for the identification of storm days are different by definition. JC35 is based on strength and vorticity of the large-scale geostrophic flow, whereas SP98 is based on the occurrence of extreme surface-wind speeds in a central European region representative for the area of Germany. Thus, the two identification methods are applied complementarily, and similar results are found for storm days according to both of them, with respect to not only storm day frequencies, but also associated atmospheric features. Although the sets of identified events differ partly (compare D09), patterns of change signals emerging from the two methods are still comparable. The fact that the detected changes are similar although partly different events are considered indicates some robustness of the identified climate signals.

Our findings are based on a multi-model approach and corroborate recent results based on different analysis methods and mostly single-model analysis (cf. Section 3.4). Thus, there is enhanced confidence in previously identified climate change signals, indicating a more zonally large-scale flow over Europe during winter and atmospheric conditions favouring increased risk of winter storms under future climate conditions.

Acknowledgments

This work was supported by the ENSEMBLES project, funded by the European Commission's 6th Framework Program through contract number GOCE-CT-2003-505539. We kindly thank ECMWF and DWD (German Weather Service) for ERA-40 data use and availability and DKRZ (German Climate Computing Centre) for storing and providing the ENSEMBLES simulation output. We are grateful to four anonymous reviewers, whose useful and constructive comments helped to improve the clarity of the manuscript.

4. Mid-latitude Cyclones and Storms in an Ensemble of European AOGCMs under Anthropogenic Climate Change

4.1. Introduction

This study investigates the occurrence of mid-latitude cyclones and wind storms under anthropogenic climate change conditions from a multi-model perspective. It thus contributes to the work performed by the ENSEMBLES project (<http://ensembles-eu.metoffice.com/index.html>) which is supported by the European Commission's 6th Framework Programme. The main objective of ENSEMBLES is to “develop an ensemble prediction system for climate change based on the principal state-of-the-art, high resolution, global and regional Earth System models developed in Europe”. The ENSEMBLES approach is based on the assumption that “the prediction of both natural climate variability and the human impact on climate is inherently probabilistic, due to uncertainties in forecast initial conditions, representation of key processes within models, and climatic forcing factors. Hence, reliable estimates of climatic risk can only be made through ensemble integrations of Earth-System Models in which these uncertainties are explicitly incorporated.” Thus, within this framework the present study aims at a robust diagnostic of the future occurrence of extreme cyclones under anthropogenic climate change (ACC) based on an ensemble of state-of-the-art global circulation models and at deducing measures of uncertainties of these ACC signals.

Mid-latitude cyclones are a vital part of the general circulation of the atmosphere. In the Northern Hemisphere, these extratropical cyclones mostly originate at the discontinuity

Model	Institute	Resolution atmosphere	20C.	SRES A1B	No. of considered runs	References
BCCR-BCM2	Bjerkness Centre for Climate Research	T63,L45	1960-1999	2080-2099	1	Furevik et al., 2003
CNRM-CM3	Météo France/Centre National de Recherches Météorologiques	T63,L31	1981-2000	2081-2100	1	D. Salas-Mélaia et al., 2005 (personal communication)
DMI-ECHAM5	Danish Meteorological Institute	T63, L31	1961-2000	2071-2100	1	Jungclaus et al., 2006
FUB-EGMAM	Freie Universität Berlin, Institut für Meteorologie	T30, L39	1961-2000	2081-2100	1	Manzini and McFarlane, 1998 Legutke and Voss, 1999 Huebener et al., 2007
IPSL-CM4	Institut Pierre Simon Laplace	2,5°x3,75°, L19	1961-2000	2071-2100	1	Marti et al., 2005
MPI-ECHAM5	Max Planck Institute for Meteorology	T63, L31	1961-2000	2071-2100	3	Jungclaus et al., 2006
METO-HC-HadGEM1	UK Met Office, Hadley Center	1,25°x1,875°, L38	1960-1999	2070-2099	1	Johns et al., 2006 Martin et al., 2006 Ringer et al., 2006

Table 4.1: AOGCMs investigated in this study including the number of available model runs (second column), horizontal resolution, and time periods for the twentieth century (control climate) and future conditions (scenario climate).

zones in the atmosphere, the polar fronts of North Pacific and the North Atlantic, influenced by the characteristics of the Northern Hemisphere's long, planetary waves. Typically, surface cyclones travel along these zones of preferred growth conditions (e.g. Pinto et al., 2009) and are steered by the upper troposphere transient eddies of planetary (zonal) wave number 4-8. Some of the cyclones can develop to very intense systems with wind speeds of up to 250 km/h (70ms^{-1}) or more. Such developments depend on the environmental large-scale conditions, which are particularly favourable in the boreal winter half year from October to March. These winter storms are one of the most relevant meteorological-hydrological extreme events for central Europe (Cornford 2002, Ulbrich et al. 2003a, 2003b, Fink et al. 2004, Meehl and Tebaldi 2004) on which the focus of this study will be laid. Extreme meteorological conditions generate severe impacts on human facilities and infrastructure, and thus affect general socio-economic conditions (e.g. Leckebusch et al., 2007). Thus, it is necessary to increase understanding of climate change and its impact on society by generating concrete scientific information that can be used for impact studies, thus assisting a transfer of knowledge from the scientific community to decision-makers. In this context, it is of crucial importance to gain information on potential changes in central European storms and corresponding wind patterns under future climate conditions.

It is still uncertain whether the intensity or frequency of North Atlantic extra-tropical cyclones (ETC) has undergone a specific long-term trend in the recent past. There is some evidence from observational data that activity has increased since the 1960s, possibly associated with natural interdecadal variability. (e.g. Lambert 1996, Serreze et

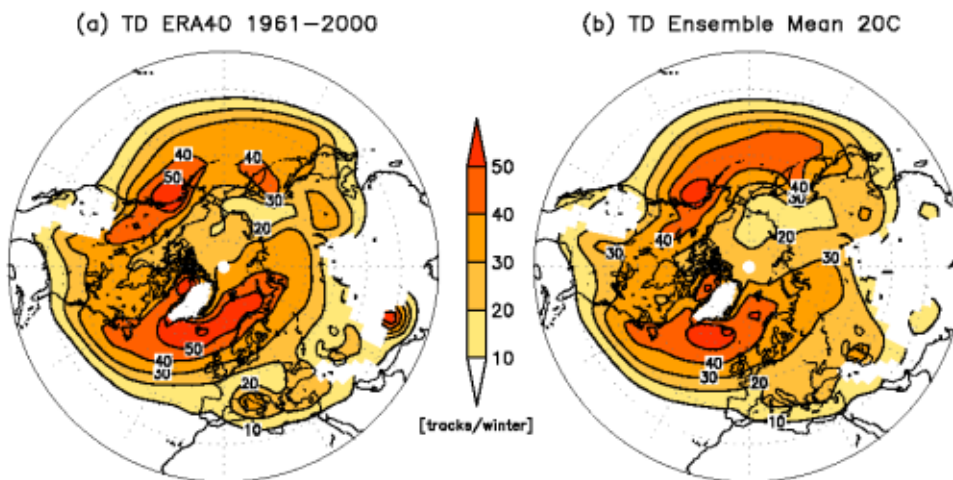


Figure 4.1: Cyclone track density for ERA40-reanalysis (left) and the Ensemble Mean (right). Unit: tracks per winter (ONDJFM). Areas with an altitude above 1500 m are eliminated (without weighting).

al. 1997, Jones et al. 1999, McCabe et al. 2001, Paciorek et al. 2002, Geng and Sugi 2003). Additionally, different trends have been suggested in the Northern and Southern Hemispheres, the latter experiencing decreasing cyclone activity since the beginning of the 1990s (e.g. Simmonds and Keay 2000). It seems reasonable to investigate the potential future occurrence of ETCs, and their related wind fields, by means of global and regional climate modelling. While most authors have concentrated their studies on the diagnosis of ETCs for one specific model (e.g. Lunkeit et al. 1996, Carnell & Senior 1998, Kharin and Zwiers 2000, Knippertz et al. 2000, Leckebusch and Ulbrich 2004, Pinto et al., 2007b), with partially different investigation methods, in this study a multi-model approach applying the same investigation method is performed. Multimodel ensemble studies investigating possible future trends in extreme cyclones were first published e.g. by Lambert and Fyfe (2006) and Leckebusch et al. (2006). A comprehensive overview of scientific results achieved so far can be found in Ulbrich et al. (2009). In order to quantify the confidence and uncertainties in future predictions, we investigated an ensemble of seven atmosphere-ocean coupled global climate models (AOGCMs). The climate change signal is identified based on the IPCC SRES A1B scenario (cf. table 4.1).

4.2. Investigation Method and Results

Extra-tropical cyclones were assessed by applying an objective identification algorithm originally published by Murray and Simmonds (1991), which is organized in 2 steps. Firstly, cyclones are identified by an algorithm based on the search for the maximum of the Laplacian of the mean sea level pressure (Δ MSLP). Under quasi-geostrophic conditions, this is equivalent to the search for extremes of relative vorticity. Secondly, a tracking algorithm is applied, which takes into account the most probable propagation of the cyclone core under the given synoptic situations. ETCs were identified for the control and scenario period of each investigated GCM for the winter half-year (ONDJFM). In order to avoid artefacts, systems localized in areas with a terrain-height above 1500 m asl are excluded (due to underground extrapolation of the MSLP). Additionally, open and closed systems are differentiated: a cyclone is determined to be closed if a true minimum of MSLP is situated in the vicinity of a maximum of Δ MSLP. Furthermore, only systems with a Laplacian above the threshold of 0.1 (0.2) hPa deg.lat.⁻². for closed (open) systems are considered. If the Laplacian exceeds 0.6 hPa

deg.lat.⁻², a system is classified as strong; otherwise it is classified as weak. Moreover, the only systems considered are at least closed and strong once in their lifetime. Details of the identification, established tracking algorithm, and current settings of the algorithm and its implications can be found in Murray & Simmonds (1991), Leckebusch and Ulbrich (2004), Pinto et al. (2005), Leckebusch et al. (2006). There is no single definition of what constitutes a wind storm event or an extreme wind speed. In accordance with previous studies we define the cyclone systems with a Laplacian of the MSLP above the long year 95th percentile (for the GCMs: of the control run) as extreme cyclones, or as severe winter storms.

The model's simulation of the recent climate is validated against ERA40-reanalysis data (1961-2000). For all cyclone systems (Figure 4.1) as well as for the extreme cyclones (not shown) a very good agreement between the ensemble mean (Figure 4.1b) and ERA40-Re-analysis (Figure 4.1a) is found respecting cyclone track density. The two well pronounced centres of activity are correctly simulated in terms of position and intensity (number of tracks per winter). It should be noted that the model-to-model variability does not emerge in this ensemble mean perspective. For single models significant deviations from the re-analysis data could be observed. For each model the level of agreement with the ERA40-Re-analysis (which is taken here as an observational data set, though the assimilation is indeed a model simulation) is estimated and used to introduce different weightings for each model for the construction of the ensemble mean climate change signals. First, the weights are constructed via the spatial correlation

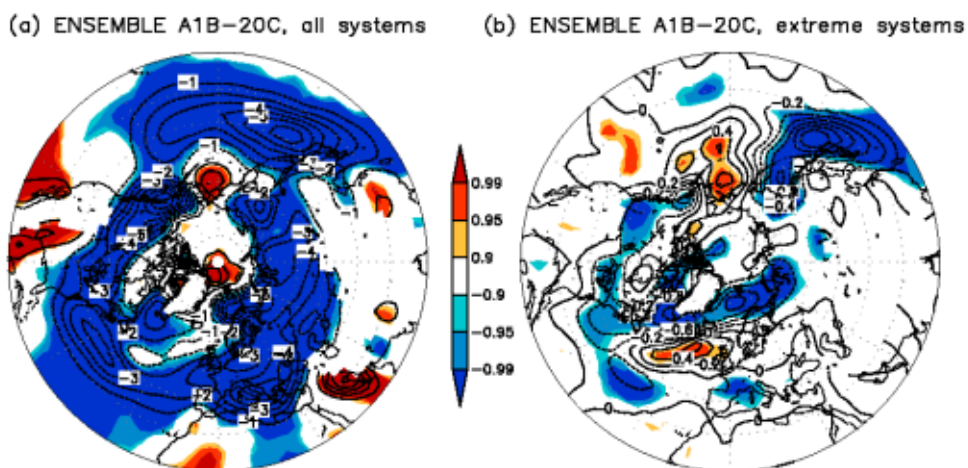


Figure 4.2: Ensemble mean climate change signal (IPCC SRES A1B) of the cyclone track density. Left a): All cyclones. Right b): Extreme cyclones. Units: systems per winter (ONDJFM). Areas with an altitude above 1500 m are eliminated. Coloured: Statistical significance above the 90/95/99% level according to a student t-test. The ACC ensemble mean signals are weighted by the quality of each model.

coefficients between the GCM's and ERA40's cyclone track densities for all recognised cyclones: both the climatological mean track density and its interannual variability pattern are correlated between GCM and ERA40 and the product of both coefficients is taken as weight (w) for each model. In order to recognise more realistic models in the ensemble mean than unrealistic ones, this weighting factor was varied, from w to $w4$. For these four different weighting factors the ensemble mean for the control period and the ACC signal were calculated. Consequently, the climate change signal is presented in terms of a weighted ensemble mean. In Figure 4.2, results for the weighting ($w4$) are presented as an example.

For all identified and tracked cyclones a decrease in the hemispheric number of tracks is found (cf. Figure 4.2a), which is in accordance to other studies (e.g. Lambert and Fyfe, 2006). For the changes of extreme cyclones (Figure 4.2b) a different pattern arises: Indeed the hemispheric total number also decreases, but the horizontal distribution clearly identifies regions of increased frequency of extreme cyclones, and thus winter storms. Two regions show increased numbers of extreme cyclone tracks: the Northeast-Pacific and the Northeast-Atlantic. In both areas the increase is between 10% and 20% compared to the control period. The spatial distribution of the anthropogenic influence is more or less independent of the strength of weighting applied. The weighting leads more to changes of magnitude and statistical significance of the identified changes, e.g. over the Northeast-Atlantic. The more the influence of unrealistic models is decreased the more the statistical significance of the ACC signal is increased.

4.3. Conclusion and Future Work

The results presented here reveal the importance of a regional perspective compared to an evaluation on hemispheric level. Although an overall decrease of the number of extreme cyclones is diagnosed, this holds not true for specific hot spots: the Northeast-Pacific and the Northeast-Atlantic affecting western Central Europe. These findings support results achieved with a simple one model-approach (e.g. Leckebusch and Ulbrich, 2004, Bengtsson et al., 2006, Pinto et al., 2007b), as well as findings from multi-model studies (e.g. Leckebusch et al., 2006). It should be noted that the model-to-model variability is high, especially for the ACC signal for the extreme cyclones. The statistical significance of the ACC signal is thus reduced, if only one realisation of one model is incorporated. Nevertheless, the overall pattern with increasing number of

extreme cyclones over the Northeast-Atlantic and the British Isles remains robust. Furthermore, from this multi-model perspective, it will be possible to deduce measures of uncertainties based on the model-to-model variability which is also assessed in this study but not presented here. Thus, it will be possible to advise the non-scientific community about the possible uncertainty of future climate developments as diagnosed from GCMs, based on the different setups of climate models. Future work will also concentrate on the identification of key reasons for the differing behaviour of “normal” vs. “extreme” cyclones. First results were published for one GCM (Pinto et al., 2009), giving hints for a broader baroclinic area during the intensification phase of extreme cyclones and a potentially increased influence of the equivalent-potential temperature on the storm development under ACC conditions.

5. Benefits and limitations of regional multi-model ensembles for storm loss estimations

Abstract

Spatial patterns of near-surface wind speeds and resulting loss potentials associated with severe winter storms are investigated in multi-model simulations with regional climate models (RCMs), driven by ERA40-reanalyses. Benefits and limitations of dynamical downscaling for windstorm loss calculations are explored, including a quantification of the performance of the multi-model ensemble as a whole and the systematic investigation of the influence of model selection on the ensemble results.

Comparison of the wind fields in the different models reveals both, systematic biases in individual RCMs and model-specific anomalies over mountainous regions. Further, a storm loss model is applied to the RCM wind fields and the calculated losses are validated against observed annual insurance loss data available for Germany. Generally a distinct profit from dynamical downscaling becomes obvious. However, all RCMs fail in realistically simulating one specific major event. Excluding this particular event from the considerations, almost all simulations reveal high correlations (above 0.8) with observed losses, comparable to losses calculated directly from the large-scale reanalysis wind field. For the best performing models considerably higher loss correlations up to 0.95 are obtained, suggesting that the high-resolution RCMs exceed the value of assimilation in the driving data for the area considered. Combining calculated losses from the individual RCMs to a multi-model ensemble, the performance of the ensemble mean is as good as the performance of the best single model. Examining all possible sub-ensembles, it is found that generally a higher minimum performance is obtained with a larger number of ensemble members, whereas the maximum performance is hardly affected by the ensemble size.

5.1. Introduction

Severe winter storms frequently cause heavy damages in Europe, in particular to infrastructure and environments (e.g. buildings, electricity supply, forests). They can also entail restrictions to traffic and might lead to injury or even loss of lives. Thus, those extreme events are of high relevance to many parts of the society. The strong wind fields generally affect large areas, contributing to high accumulated loss amounts. For example, recently storm “Kyrill” (affecting large parts of Europe between 17 and 19 January 2007, cf. Fink et al., 2009) caused estimated losses of about 4-4.5 billion Euro (Swiss Re, 2008). Series of European winter storms in December 1999 (“Anatol”, “Lothar”, “Martin”, cf. Ulbrich et al., 2001) or in early 1990 (e.g. “Daria”, “Hertha”, “Vivian”, “Wiebke”, cf. McCallum and Norris, 1990) both caused total insurance losses exceeding 10 billion Euro across Europe. Comparing to loss amounts from other natural disasters, wind storms turn out to be the most relevant cause of losses in Central Europe, e.g. in Germany accounting for 53 percent of economic losses due to natural hazards and even 64 percent of insured losses (Munich Re, 1999; Munich Re, 2007).

An estimation of storm losses is important for a multitude of applications. Examples are the assessment of changed risk under climate change conditions as well as near-term loss estimations shortly after or even before a storm occurs (e.g. in order to effectively coordinate relief operations and financial planning) or the identification of regions with particular high risk of damage. Accurate loss estimates are thus desirable not only from the insurance companies’ perspective, but also e.g. for political decision makers, emerging institutions or infrastructural planning.

For the calculation of storm losses, different loss functions can be found in literature. For example, Heneka et al. (2006) derived local empirical relations for vulnerability (i.e. the link between the storm event and the consequent damage) based on insured losses that occurred during historic storm events. Yet, insurance loss information on a high spatial and temporal resolution are usually not available for public research. Common approaches for loss calculations are based on physical assumptions, considering e.g. the kinetic energy of the wind or the wind power. Thus, in general polynomial relations (square or cubic functions) between loss and wind speed are used (Palutikof and Skellen, 1991; Dorland et al., 1999; Munich Re, 1993; Klawe and Ulbrich, 2003).

The storm loss model proposed by Klawe and Ulbrich (2003) is based on a cubic relationship between wind speed and losses. It properly calculates annual insurance

losses in Germany and Great Britain not only based on observational wind data from synoptic weather stations, but also from reanalysis data on spatial scales of about 100km (Leckebusch et al., 2007; Pinto et al., 2007a). In these studies it was also applied to global climate model data, working on spatial scales of about 200km.

Dynamical downscaling with regional climate models (RCMs) is generally applied to obtain atmospheric information at a higher spatial resolution than provided by global climate models, in particular for information on the influence of regional orographic characteristics. Additionally, physical processes acting on scales not resolved by the driving large-scale models can exert an effect on simulated regional wind patterns. The profit of dynamical downscaling with respect to wind fields over complex terrain was demonstrated e.g. by Žagar et al. (2006), obtaining wind speeds in good accordance with observations over mountainous regions. Such an improvement should in turn allow for a higher accuracy of storm loss calculations, as suggested by Heneka et al. (2006).

On the other hand, numerical climate model simulations (and thus also dynamical downscaling) are affected by different sources of uncertainty. The most important ones are uncertainties in parameterisations of physical processes and in the numerical formulation of the RCMs, sensitivity to the initial conditions, to boundary conditions and uncertainty due to internal variability generated within the model domain. Combining different models to a multi-model ensemble (MME) generally increases the skill, reliability and consistency of model projections, both in weather forecast and in seasonal prediction applications (see e.g. Hagedorn et al., 2005). Also for climate-timescale simulations a MME can be favourable compared to a single model (cf. Palmer and Räisänen, 2002; Räisänen, 2007; Collins, 2007; Ulbrich et al., 2008). MMEs primarily sample initial condition and model uncertainties (Tebaldi and Knutti, 2007). However, a quantification of the MME advantages on the climate timescale is difficult, as, for example, reliable data for verification are often missing on this timescale. Further, the way how the ensemble is constructed has influence on the ensemble performance (Weigel et al., 2008).

This study addresses added values and limitations of dynamical downscaling and of combining different models to a MME for storm loss assessment applications. RCM simulations driven by reanalysis data should reproduce the observed chronology of weather situations. This offers the opportunity of a sound validation of these climate

simulations, not only considering climate mean state and variability, but also the chronology of events. In this study we use annual accumulated insurance loss data as a proxy describing the occurrence of severe storms. Loss potentials calculated from RCM outputs are then compared with the observed loss values in order to allow for an estimation of the added value of downscaling for each RCM. In a further step the benefit from combining the different models in a multi-model ensemble (MME) of climate-scale simulations is investigated and the effect of different possible model combinations included in an ensemble is examined systematically. Again, the agreement with time series of observed loss data is used for verification.

5.2. Data and Methods

5.2.1. Data

All RCM simulations were carried out for a common domain including the whole continental European area (from approximately 10°W to 40°E and 30°N to 65°N). Overall, a set of 11 different RCMs was considered (table 5.1). All models were used for dynamical downscaling of ERA40-reanalysis data (Uppala et al., 2005). The horizontal resolution of ERA40 is approximately 1.125° (i.e. about 120 km in central Europe). Almost all RCMs were run in two different spatial resolutions of 0.44° (approximately 50km) and 0.22° (approximately 25km). Two models were run in only one resolution (GKSS: 0.44°, C4I: 0.22°). The RCM simulations were generally driven at the domain's lateral boundaries, only the GKSS-CLM simulation makes use of a spectral nudging technique (von Storch et al., 2000).

This study is based on daily maxima of simulated 10m wind speeds. This parameter is archived from all considered runs as the daily maximum speed value over all time steps. From ERA40 only 6-hourly instantaneous values of wind speed were available. Here, a daily maximum is calculated as the maximum of the 4 instantaneous wind speeds stored at 00, 06, 12 and 18 UTC. This value is expected to be slightly smaller than the maximum over all time steps (cf. Pinto et al., 2007a; Rockel and Woth, 2007), inducing a small inhomogeneity to our data basis. The daily maximum wind speed data are hereafter referred to as WIMAX.

Some of the RCMs also feature a gust parameterisation; a daily maximum 10-m gust wind speed is available for 5 models, for 4 of them (ETHZ-CLM, SMHI-RCA3, KNMI-RACMO2 and MPI-M-REMO) in both resolutions, one model with gust

parameterisation (C4I-RCA3) was only run at 25 km. Daily maxima of modelled gusts are hereafter referred to as GUST.

Also for the ERA40 dataset the 10-m wind speed (6-hourly, see above) and a 10-m wind gust is available. As in the RCMs, the latter is a model diagnostic parameter and hence its calculation is based on parameterisation. Different approaches for calculating the gust wind speeds are used in the different models. In the RCA3 models (SMHI and C4I) a wind gust estimate method based on physical considerations (Brasseur, 2001) is implemented. It assumes that surface gusts result from the deflection of air parcels from the upper boundary layer, brought down by turbulent eddies. This method takes into account the turbulence kinetic energy, the mean wind and the stability in the boundary layer. ERA40 and KNMI-RACMO2 use a scheme based on the similarity relation by Panofsky et al. (1977). Here, a standard deviation of the near-surface wind is calculated, again taking into account the static stability of the boundary layer. The maximum gust speed is then estimated by adding a term including this standard deviation to the 10m wind speed (cf. White et al., 2003). MPI-REMO and ETHZ-CLM calculate gusts based on empirical assumptions taking into account the turbulence kinetic energy in the lowest model layer (Schrodin, 1995).

RCM	Institute	Resolutions		Gust calculation	References
C4I-RCA3	Community Climate Change Consortium for Ireland	25km		X	Rummukainen et al., 2001 Jones et al., 2004
CHMI-ALADIN	Czech Hydrometeorological Institute	25km	50km		Bubnova et al., 1995
CNRM-RM4.5	Météo France/Centre National de Recherches Météorologiques	25km	50km		Gibelin & Deque, 2003
DMI-HIRHAM	Danish Meteorological Institute	25km	50km		Christensen et al., 1996
ETHZ-CLM	Swiss Federal Institute of Technology	25km	50km	X	Stappeler et al., 2003 Jaeger et al., 2008
GKSS-CLM	GKSS Forschungszentrum Geesthacht		50km		von Storch et al., 2000 Stappeler et al., 2003 Jaeger et al., 2008
HC-HadRM3	UK Met Office, Hadley Center	25km	50km		Jones et al., 1995
KNMI-RACMO2	Royal Netherlands Meteorological Institute	25km	50km	X	Lenderik et al., 2003
METNO-HIRHAM	Norwegian Meteorological Institute	25km	50km		Christensen et al., 1996
MPI-REMO	Max Planck Institute for Meteorology	25km	50km	X	Jacob & Podzun, 1997 Jacob, 2001
SMHI-RCA3	Swedish Meteorological and Hydrological Institute	25km	50km	X	Döscher et al., 2002 Jones et al., 2004

Table 5.1: RCMs included in this study (ENSEMBLES setup).

As almost all severe damage causing storm events occur during boreal winter (Klawa and Ulbrich, 2003; Munich Re, 2007), the presented analyses concern the extended winter period October to March.

Annual accumulated insurance loss data for Germany were provided by the Gesamtverband der Deutschen Versicherungswirtschaft e.V. (German Insurance Association, hereafter GDV) for the period 1970-2000. They include losses to residential buildings due to storm and hail events. The large losses are usually caused by intense winter storm events affecting a large area; losses due to convective events and hail only contribute to a small percentage to the total annual loss (Klawa and Ulbrich, 2003; GDV 2009, pers. comm.). Annual loss values are given as loss ratios, i.e. the relationship between insured claims and totally insured values. An advantage of this measure is that inflation can be neglected as it is included in both, in insured values and in the loss. The unit is given in € per 1000€ (i.e. in ‰).

5.2.2. Calculation of storm induced losses

Loss potentials for Germany are calculated using a storm loss model that was developed in Klawa and Ulbrich (2003), based on observational wind speed data from German weather stations. Recently, a version of this model was also applied to reanalysis and global climate model data (Leckebusch et al., 2007, Pinto et al., 2007a), revealing reasonable results. A detailed description of the storm loss model can be found in the previous literature; here its basic features are shortly recapitulated. Annual loss ratios (giving the ratio of insured values that is affected by storm losses) are calculated by the following equation:

$$loss = A * \sum_{area}^{Germany} pop(area) * \sum_{days}^{year} LLI + B$$

$$\text{with local loss index } LLI = \max \left[0; \left(\frac{v_{\max}(area, day)}{v_{98}(area)} - 1 \right)^3 \right]$$

In this function v_{\max} is the daily maximum wind speed (i.e. WIMAX or GUST) in a grid box and v_{98} is the local 98th percentile of daily maximum wind speeds. Thus, it is assumed that losses occur locally during the 2% of days with strongest winds. Using a

relative threshold, the loss function takes into account model biases of simulated wind speeds. A is the obtained regression coefficient from calibrating calculated losses with the insurance data and B is the axis intercept; pop(area) is the population density. Population density is regarded as a proxy for insured values, because information about spatial distribution of total insured values is not publicly available. For Central European housing, the assumption is reasonable that insured values are proportional to the population density. For the calculations in this study we use gridded population density data for the year 2000, on a 0.25x0.25 degree raster (CIESIN 2005).

The regression coefficient A could not be computed from event-based loss numbers, as the respective values are only available from a few events, at the same time being of limited reliability. Thus, we use a loss data set containing yearly accumulated loss ratios for the whole area of Germany, provided by the German Insurance Association (GDV). The annually integrated loss indices at the individual grid points in Germany are accumulated, weighted by the population density. A linear regression is then used to scale the “raw losses” as calculated by the loss function towards the GDV loss ratios (figure 5.1 exemplifies the regression for losses calculated from ERA40). The regression between calculated “raw losses” and observed loss ratios is calculated for each model individually. The ensemble mean of losses is calculated for each year by averaging the losses of the individual ensemble members for this year.

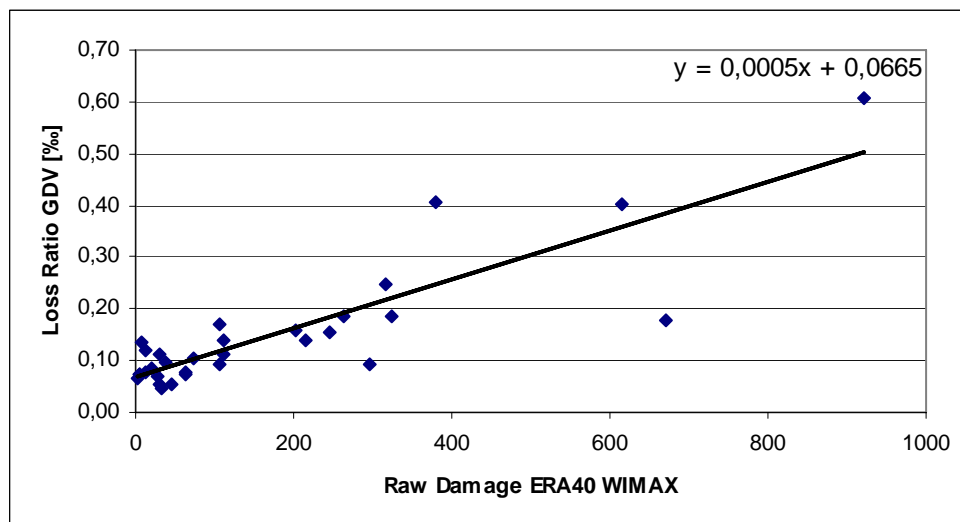


Figure 5.1: Regression of calculated raw loss data from ERA40 with annual loss ratios provided by GDV for the years 1970-2000.

5.3. Results concerning extreme wind speeds and loss estimates

5.3.1. Simulated wind fields

Even though the loss model is taking systematic biases of extreme wind speeds into account, it is worthwhile considering characteristics in the RCM (extreme) wind fields. Comparison of the 98th percentile of WIMAX in ERA40 reanalysis (figure 5.2a) and the different ERA40-driven RCM simulations in 50km and 25km resolution (figures 5.2b,c) reveals considerable differences between the individual models and to ERA40 itself. On the one hand systematic biases occur: some models simulate higher wind speeds than those in ERA40 in almost all regions (e.g. GKSS, DMI), others somewhat lower speeds values (e.g. CNRM, CHMI). On the other hand, differences in the spatial patterns, especially in regions with complex orography like the Alps or the Scandinavian Mountains are present. While some models and also ERA40 produce local minima of wind speed in these mountainous regions, other models (in particular DMI, HC and partly ETHZ) feature distinct maxima here, irrespective of the resolutions. In the simulations with higher resolution (25km) the wind maps reveal finer spatial structures and some additional models are featuring maxima over mountainous regions (in particular over the Scandinavian Mountains MPI, C4I, SMHI, METNO). This phenomenon may be influenced by different sub-gridscale roughness parameterisations in the individual models; a detailed validation of these differences is, however, beyond the scope of this study.

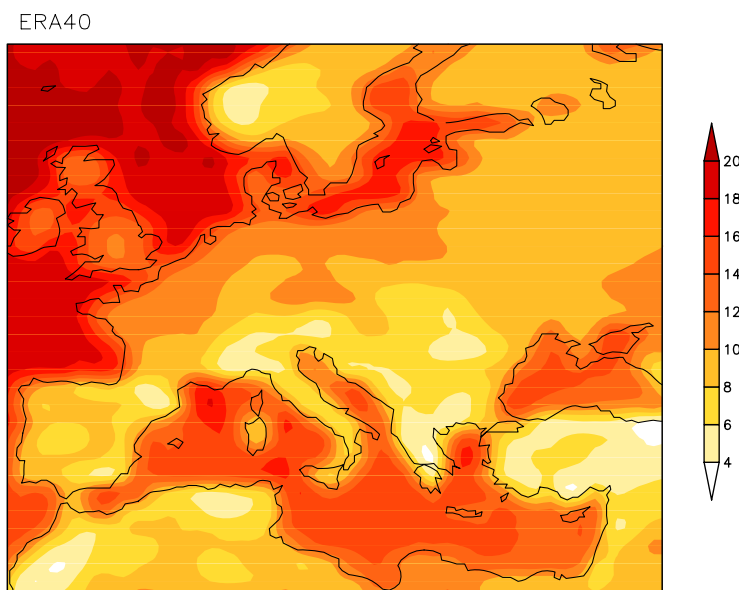


Figure 5.2: 98th percentile of WIMAX in ERA40-reanalysis (unit: m/s).
a) WIMAX in ERA40

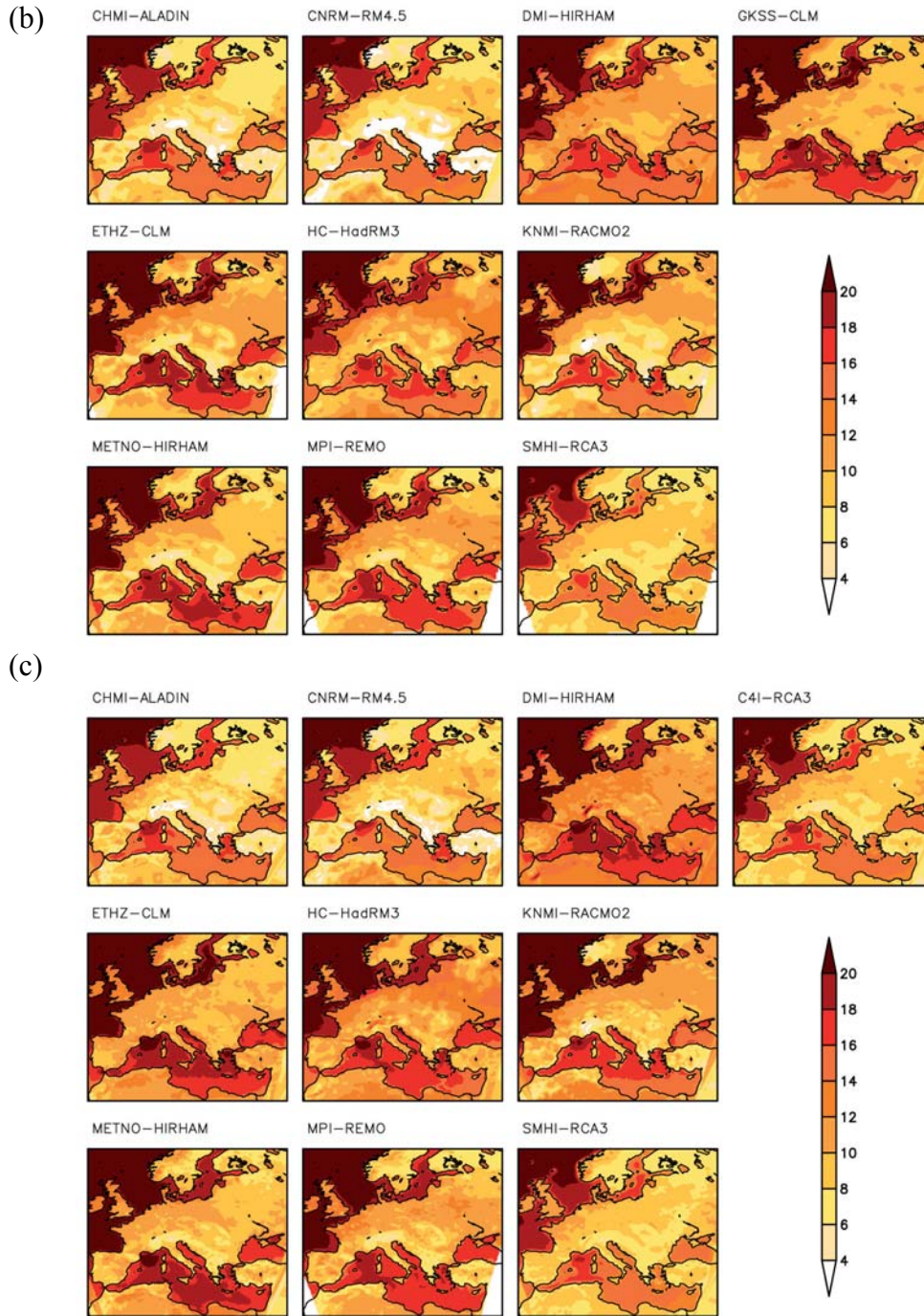


Figure 5.2: 98th percentile of WIMAX in the RCM-Simulations driven by ERA40 (unit: m/s).
 b) RCMs in 50km resolution
 c) RCMs in 25km resolution

Considering GUST, the models reproduce the typical pattern found for WIMAX, just the absolute speed values are higher (not shown). Even regarding the model-specific pattern over complex orography, characteristics described above for WIMAX can also be found for daily maximum wind gust values. For example, KNMI-RACMO2 reveals local minima over the Alps and the Scandinavian Mountains in both resolutions, whereas in other models (e.g. ETHZ, C4I, SMHI) local maxima are found here. Della-

Marta et al. (2009a) document that ERA40-reanalysis often yields unrealistic gust wind speeds over complex terrain.

The described differences in the simulation of wind speeds are incorporated by the loss model's approach, avoiding an absolute threshold. Applying a relative threshold (like the 98th percentile in this study) takes into account individual characteristics of the different models and also the local wind climatology.

5.3.2. Validation with loss data for Germany

Figure 5.3 shows the time series of annual loss ratios for GDV data and loss model results based on ERA40 and the 50km / 25km resolution ensembles of RCM simulations for the period 1970-2000. Annual accumulated loss ratios for Germany derived from ERA40 reanalysis data reveal correlations with the GDV data of 0.86 for WIMAX and 0.89 considering gust calculations, respectively. The correlations for all individual RCM simulations vs. GDV loss ratios are shown in figure 5.4. In both, the 50km and the 25km simulations, METNO-HIRHAM is the model reaching best accordance with GDV loss ratios, with correlations of 0.87 (50km) and 0.84 (25km). In the 25km simulation also SMHI-RCA3 reaches such a high correlation of 0.84. However, most of the models show reasonable agreement with observed losses in both resolutions. For the simulations in 25km (50km) resolution, for 7 (9) of the 10 models correlations are higher than 0.7. A systematic statement on a preferable resolution can not be given. There are in total 9 models that were run with both resolutions; for 2 of them the correlation is higher at 50km, for 4 models correlation is higher at 25km and for 3 models correlations at both resolutions are roughly at the same level. Weakest

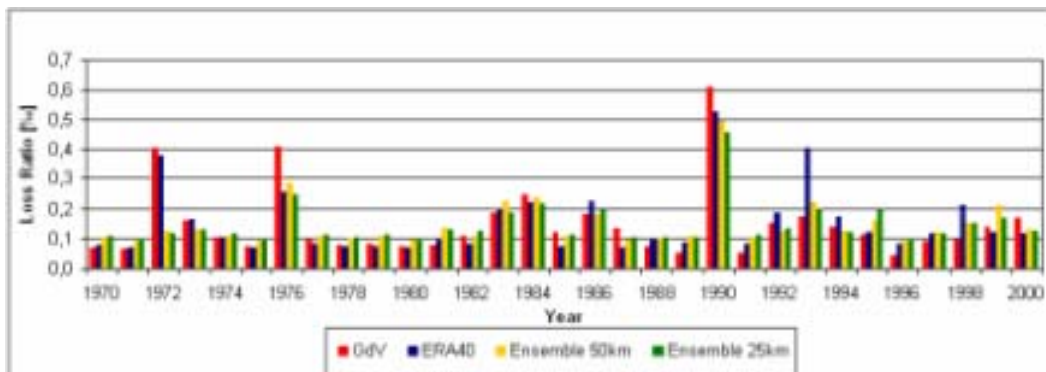


Figure 5.3: Time series of annual loss ratios for GDV data and as calculated from ERA40-reanalysis and the reanalysis-driven RCM simulations. For the RCMs the ensemble mean of the simulations in 50 km resolution (yellow bars) and 25km (green bars) are shown, respectively.

performance was found for the HC-HadRM3, revealing correlation values of 0.19 (50km) and 0.42 (25km).

Large deviations of modelled losses in comparison to observations are found for the years 1972 and 1993. The losses in 1972 were mainly caused by a strong storm event on Nov 13 in this year, the so called ‘Lower Saxony Storm’ (Cappel and Emmerich, 1975). None of the RCMs reveals intensive losses in Germany for this event, although it seems to be well captured by the ERA40-reanalysis. Thus, the correlation values of losses calculated from the RCMs are negatively affected by failing to capture the strong event in 1972 (cf. section 5.4). For 1993 losses calculated from ERA40 add up unrealistically high, while losses based on the RCMs are of the same magnitude as the observed losses. In particular, 2 days in this year show very high losses (Jan 14 (storm ‘Verena’) and Jan

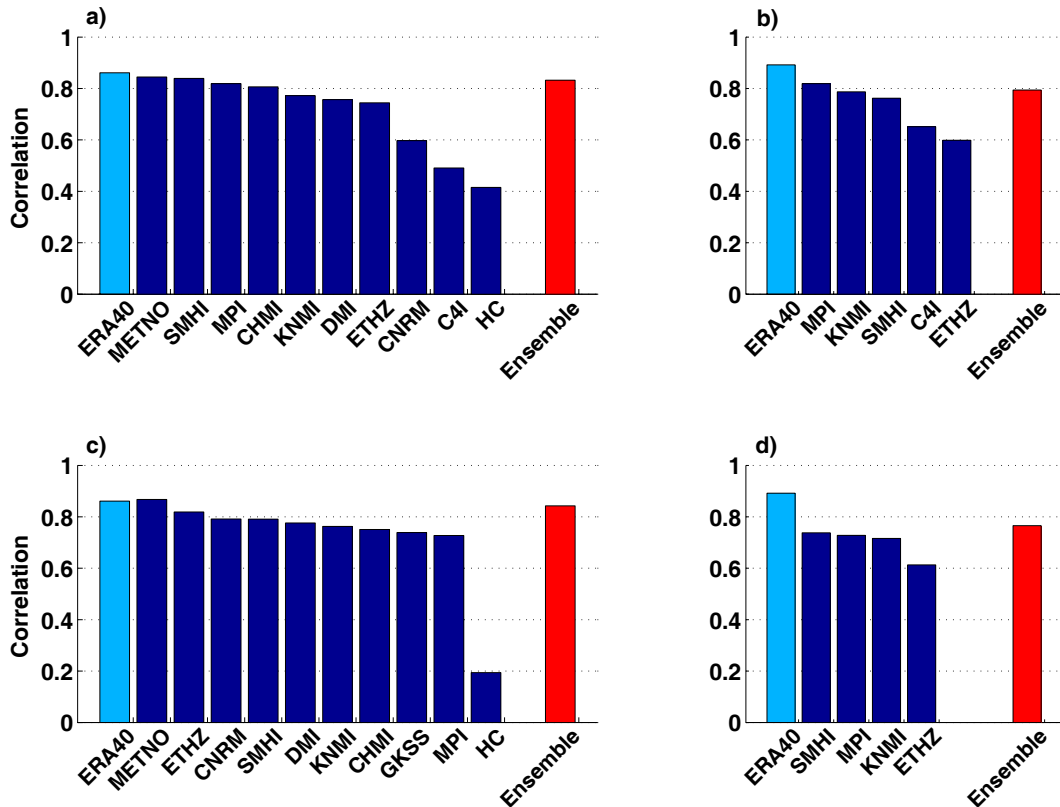


Figure 5.4: Correlations of annual loss ratios for ERA40 (light blue) and the ERA40-driven RCM simulations (dark blue) compared to GDV losses. The blue bars represent the correlations values of the individual models, in each figure the RCMs are ordered according to the correlation value, from highest values (left) to lowest (right). The red bars represent the correlations of the ensemble means of annual losses, calculated from all individual RCMs in each group.

- a) 25km WIMAX
- b) 25km GUST
- c) 50km WIMAX
- d) 50km GUST

24 ('Barbara'). In most of the RCMs the losses are by factor 2 to 3 lower for these days. Thus, the RCM-ensemble agrees considerably better with observed losses, pointing to a benefit from using the RCM ensemble. Also for the years 1976 and 1990 some larger differences are apparent. Here, however, the ERA40 and RCM-ensemble results reveal comparable magnitudes, both underestimating the losses in comparison with the insurance data. It is not obvious what causes the deviation in these particular years. There could be particular socio-economic factors leading to enhanced loss, but also an error in the reanalysis data cannot be excluded. We note that a number of RCMs reveals loss ratios which approximately agree with the insurance data. A more thorough investigation of the reasons for the deviations is necessary for these years, but is beyond the scope of the current paper.

The mean annual loss ratio for Germany is in all models around 0.15‰, like in the GDV data (table 5.2). This accordance is expected due to the fact that calculated raw losses are fitted towards observed loss ratios by linear regression specific for each model individually. The simulated inter-annual variability in terms of the standard deviation of annual loss ratios is, however, lower compared to observed loss variability in almost all models. While the standard deviation of annual losses in the GDV data is 0.12‰ and 0.10‰ in losses calculated from ERA40, it spreads between 0.02 and 0.11

	WIMAX				GUST			
	50km		25km		50km		25km	
	MEAN	STD	MEAN	STD	MEAN	STD	MEAN	STD
METNO-HIRHAM	0.14	0.10	0.14	0.10				
ETHZ-CLM	0.16	0.11	0.14	0.08	0.15	0.07	0.15	0.08
CNRM-RM4.5	0.14	0.09	0.14	0.03				
SMHI-RCA3	0.15	0.10	0.15	0.10	0.15	0.09	0.14	0.08
DMI-HIRHAM	0.15	0.10	0.15	0.10				
KNMI-RACMO2	0.15	0.10	0.15	0.09	0.14	0.08	0.15	0.10
CHMI-Aladin	0.14	0.08	0.16	0.11				
MPI-M-REMO	0.15	0.10	0.14	0.08	0.15	0.10	0.14	0.07
HC-HadRM3	0.15	0.02	0.14	0.05				
GKSS-CLM	0.15	0.10						
C4I-RCA3			0.15	0.06			0.15	0.08
Ensemble mean	0.15	0.08	0.15	0.08	0.15	0.09	0.15	0.08

	WIMAX		GUST	
	MEAN	STD	MEAN	STD
ERA40	0.15	0.11	0.14	0.10
GDV	0.15	0.12		

Table 5.2: Mean and STD of calculated loss ratios 1970-2000 for Germany in the ERA40-driven RCM simulations, ERA40-reanalysis and in the GDV data set (unit: ‰).

in the RCM simulations. Highest – and almost realistic – variability of 0.11‰ is found in losses calculated from ETHZ-CLM (50km) and CHMI-Aladin (25km); lowest variability of losses reveal CNRM-RM4.5 (25km) with 0,03‰ and HC-HadRM3 (50km) with 0,02‰. Those models revealing a low inter-annual variability of calculated losses are characterised by a relatively narrow distribution function of wind speeds, particularly in the upper tail. The magnitude of exceedances of the loss threshold is comparatively low in these models and thus the inter-annual variability of losses relatively low.

Ensemble mean loss ratios are calculated for each year as the average of the loss ratios calculated for the 10 different RCMs in each resolution, revealing correlations with GDV data of 0.84 (50km) and 0.83 (25km), respectively (figure 5.4a,b). In both resolutions this value is only slightly below the correlation of the best single model and corresponds to the correlation of losses calculated from large-scale reanalysis. In the ensemble mean of all simulations there is also a realistic mean loss amount, but the standard deviation is about 30% too low compared with observed loss data (table 5.2).

Losses calculated from GUST in the 50km-simulations (figure 5.4d) reveal generally weaker correlations with observed losses compared to losses calculated from WIMAX. Only for MPI-REMO the correlation is the same (0.73) for both wind parameters. In the 25km-simulations (figure 5.4c), there are 2 models with higher correlation compared to WIMAX (C4I-RCA3 and KNMI-RACMO2), 2 with lower correlation (SMHI-RCA3 and ETHZ-CLM) and for MPI-REMO it is again identical. These results indicate that the loss calculations are not fundamentally improved by using gust parameterisation instead of WIMAX. The 2 cases of higher correlations occur in the simulations at the finer resolution. Still, representatives of all 3 different gust parameterization schemes (MPI-REMO, KNMI-RACMO2 and SMHI-RCA3) reveal in both resolutions a good performance in reproducing observed losses (correlations higher than 0.7). Considering the MME of those RCMs with gust parameterisation (figure 5.4c,d), the ensemble mean is again close to the correlation of the best single model (for the 50km-simulations even better). In ensemble mean, the correlations with observed insurance loss data are slightly higher in the 25km-simulations compared to the simulations in coarser resolution.

5.3.3. Impact of different model combinations on the ensemble mean performance

In order to demonstrate the effect of the typically arbitrary model selection for MME studies (e.g. due to the availability of model simulations), the performance of the loss calculations is investigated with respect to which models are considered in the

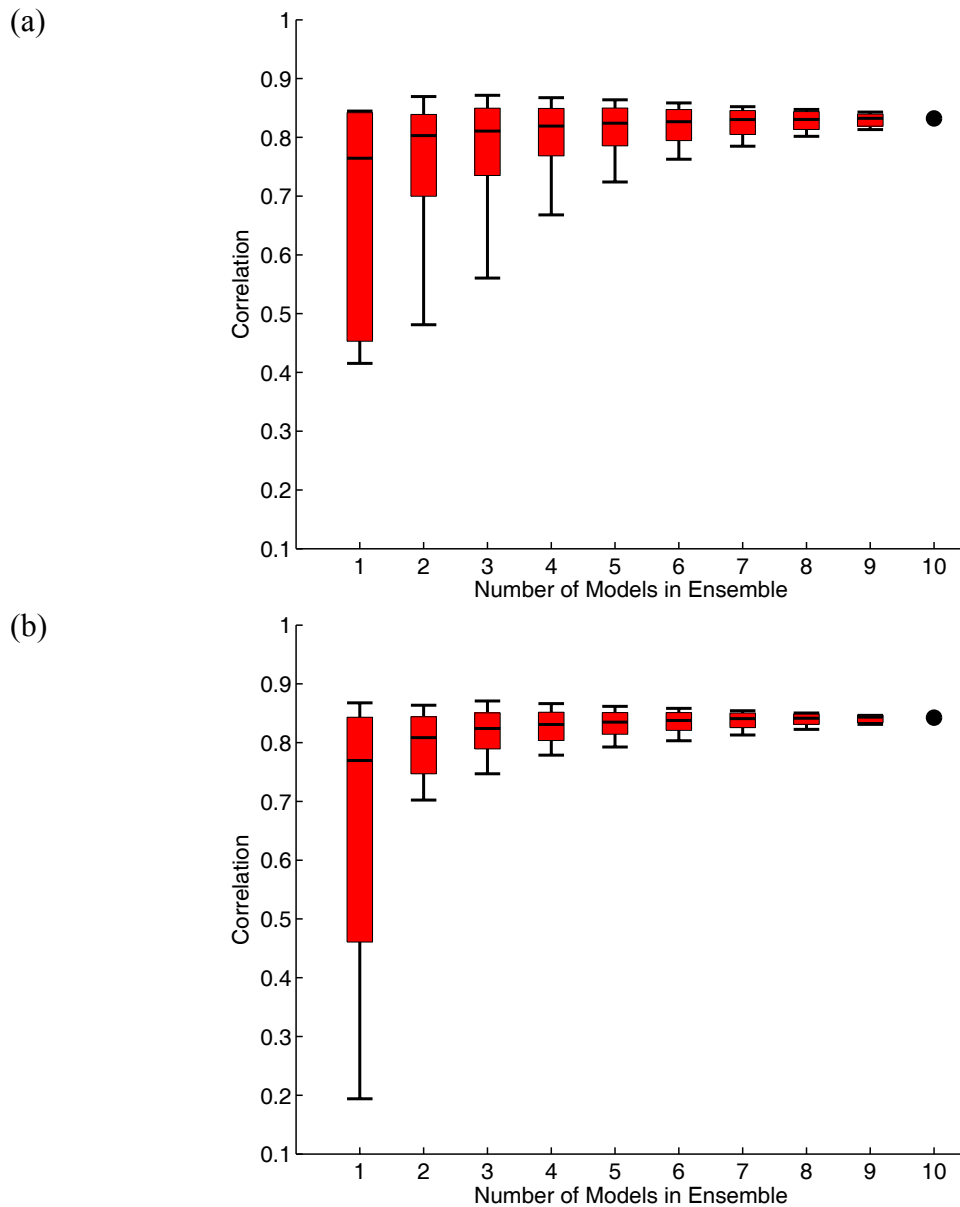


Figure 5.5: Correlations of annual losses in Germany calculated from all possible model combinations in comparison with GDV losses. For each group of sub-ensembles consisting of 1 up to 10 models (x-axis) the range of correlation values (y-axis) is indicated. The black vertical ticks at the top (bottom) of range show the highest (lowest) correlation value from all sub-ensembles in each group consisting of N models. The red boxes indicate the range between the 10th and the 90th percentile of all correlations, the black line in the center the median.

- a) 25km resolution WIMAX
- b) 50km resolution WIMAX

ensemble. Therefore, sub-ensembles were constructed, consisting only of the 2, 3, 4, ..., 9 single models with best correlations (not shown). Compared to the ensemble incorporating all models, a slightly increased correlation can be achieved, with a maximum of 0.87 in the 25km-simulations when only the best 4 models are considered and of 0.86, respectively in the 50km-simulations, considering the best 3 models. For the 25km-simulations this optimized ensemble mean is even slightly better than the best single model, although it is also obvious that the differences between the correlations are only small when leaving out the weakest models of the ensemble mean.

The topic of the different possibilities of ensemble construction and the resulting performance was examined systematically, without taking individual model performances into account for the ensemble construction. Based on 10 RCMs available in each resolution, there are in total 1023 possible combinations containing 1 to 10 models (10 single models, 45 combinations with each 2 and 8 models, 120 combinations considering 3 or 7 models, 210 considering 4 or 6 models, 252 different combinations of 5 models, 10 combinations of 9 models and 1 ensemble mean containing all 10 models). For all these combinations the correlations of the (sub-) ensemble means with GDV loss data were calculated. For each group of sub-ensembles consisting of 1 up to 10 models the spread of correlation values is presented in figure 5.5, also indicating the range between 10th and 90th percentile of all solutions, as well as the median. It becomes obvious that the more models are included in the (sub-) ensemble, the higher is the minimum correlation, whereas the maximum correlation is for all (sub-) ensemble sizes slightly above the correlation of the complete ensemble with all 10 models included. Best correlation values between 0.85 and 0.87 are reached. The absolutely best performance ($r=0.872$) is obtained in the 25km-simulations for the ensemble of 3 models (METNO-HIRHAM, MPI-REMO, CHMI-ALADIN, i.e. the single models with best, 3rd and 4th best correlations); also in the 50km-simulations the highest correlation ($r=0.871$) is found for the combination of 3 models (METNO-HIRHAM, CNRM-RM4.5, DMI-HIRHAM, again the models with best, 3rd and 4th best correlations). Please note that these maximum correlations not necessarily consist of the 3 best single models (compare figure 5.4). Nevertheless, regarding the best each 10 correlations for each group of sub-ensembles according to the number of included models (not shown), it becomes obvious that the best 4 single models (METNO-HIRHAM, SMHI-RCA3, MPI-REMO, CHMI-ALADIN for 25km; METNO-HIRHAM, ETHZ-CLM, CNRM-RM4.5, DMI-HIRHAM for 50km) are most often among the

“best ensembles”. Vice versa, for each weakest 10 correlations the 4 weakest single models (ETHZ-CLM, CNRM-RM4.5, C4I-RCA3, HC-HadRM3 for 25km; MPI-REMO, SMHI-RCA3, HC-HadRM3, GKSS-CLM for 50km) are found to be included most often. Considering for example the best 10 sub-ensembles of the 25km simulations consisting of 5 models, the best performing single models are included in most of these (METNO in 9 sub-ensembles, SMHI in 7, MPI in 9 and CHMI in 10). However, there are also some combinations among these best sub-ensembles where the weakest models are included (ETHZ in 4, CNRM in 6 and C4I in 2). On the other hand, the weakest individual models are included in most of the 10 weakest sub-ensembles consisting of e.g. 5 models (ETHZ in 7, CNRM in 8, C4I and HC in all 10 model combinations). Still, also the best individual models can be found as members of some of the weakest sub-ensembles (METNO in 1, SMHI in 2 and MPI in 3).

In summary, these results illustrate how multi-model ensembles might reveal a high performance, even if weak models are included; they hence support the use of large ensembles. The spread between the best and weakest performing model combinations is found considerably reduced if more models are included in the ensemble (Fig 5.5). The performance can only slightly be increased using an optimal choice of model combinations containing a subset of the whole ensemble.

5.4. Specific considerations of the storm on 13 November 1972 and impacts on the RCM performance measure

On 13 November 1972 Europe was hit by one of the most devastating storm events during the 20th century, leading to immense losses, several fatalities and dozens affected by injuries. In Germany this storm was named the ‘Lower Saxony Storm’, as the state of Lower Saxony was hit particularly strong. The synoptic situation was characterised by a fast moving, explosively developing secondary depression on the southern flank of a strong steering cyclone west of Norway. The secondary low travelled fast from the North Atlantic eastwards, crossing the British Isles and the northern part of Germany where it reached its maximum intensity with a core pressure below 960 hPa. Several weather stations in Central Europe registered extraordinary high wind speeds exceeding 40 m/s. On the Brocken (mountain station at 1142 m asl.) wind gusts even reached 68 m/s.

All RCMs fail in realistically simulating the explosive development of the small depression inside the European model domain. Although most simulations show a strong wind field in relation with a (not sufficiently strong) secondary cyclone, none of the simulations reveal significant exceedances of the loss threshold (98th percentile of daily maximum wind speeds). In contrast, the explosive development seems to be well contained in the ERA40-reanalysis and thus extreme wind speeds are obtained, contributing to high simulated losses. For illustration, the MSLP field and extreme wind field caused by this storm are shown in figure 5.6 for ERA40 and the MPI-REMO simulation in 25km resolution as a representative for the RCMs. In this exemplary RCM the position of the cyclone seems to be simulated realistically, however the core

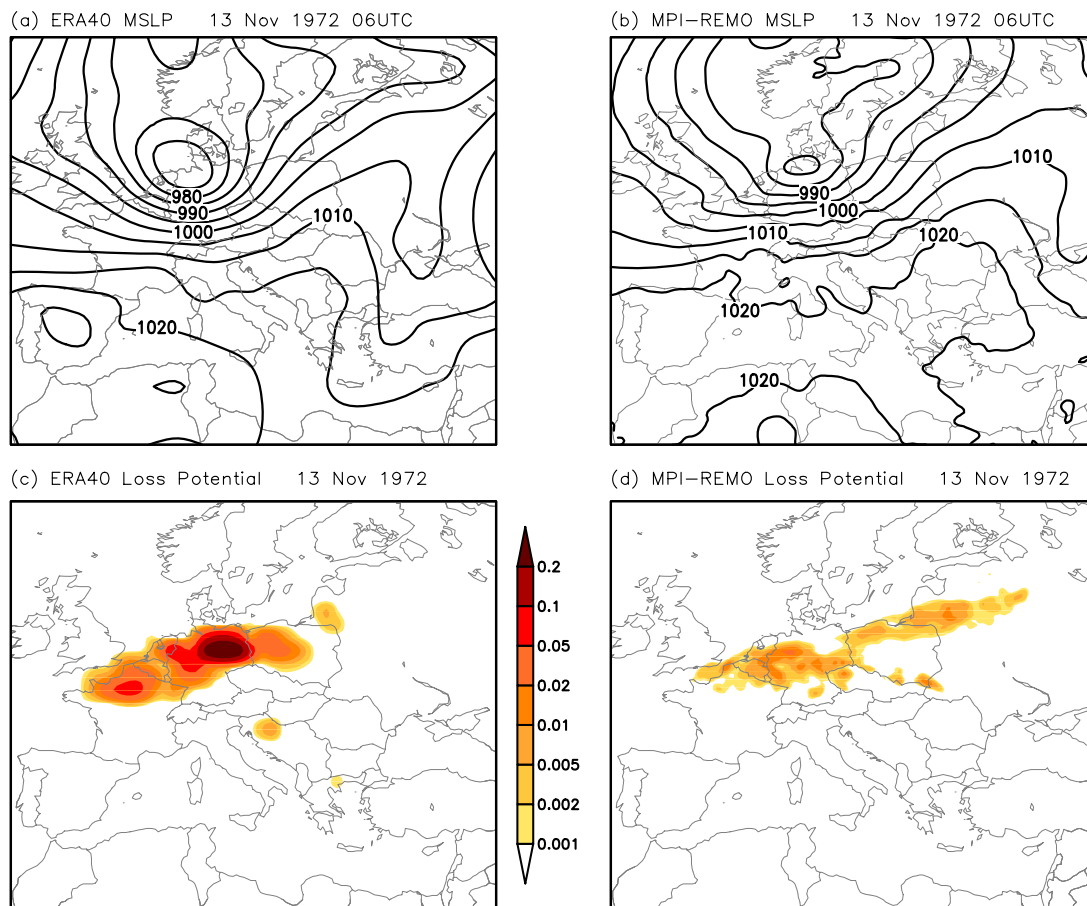


Figure 5.6: Situation of the storm on 13 November 1972 as depicted by ERA40 (left) and the MPI-REMO simulation in 25km resolution (right, exemplary for the reanalysis-driven RCM simulations).

- a) MSLP field for 06UTC on 13 Nov 1972 in ERA40 (unit: hPa)
- b) Same as 6a), but for MPI-REMO
- c) Maximum wind speed on 13 Nov 1972 in ERA40, displayed as the normalised cubic

$$\text{exceedance of the } 98^{\text{th}} \text{ percentile of daily maximum wind speeds } \left(\frac{v - v_{98}}{v_{98}} \right)^3$$

- d) Same as 6c), but for MPI-REMO

pressure is more than 10hPa higher compared to ERA40 and thus, the pressure gradient and maximum wind speeds are considerably lower.

The failure of all RCMs to realistically simulate this particular storm event seems to document a limitation of dynamical downscaling. We assume that the explosive development of the small cyclone inside the domain can obviously not be triggered from the domain's lateral boundaries. Though, also the model with spectral nudging does not reproduce the observed development and thus also fails in simulating high losses in Central Europe. In some simulations extreme loss potentials are found, affecting, however, rather Eastern Europe (KNMI-RACMO2 in 25km resolution) or Scandinavia (CNRM-RM4.5 in both resolutions), respectively. Also the DMI-HIRHAM run in 50km resolution reveals a region with wind speeds strongly exceeding the loss threshold which is, however, shifted northwards, over the North Sea. Thus, explosive development takes place in some realisations, despite differences from observations are obvious with respect to the affected region. In line with the failure of all RCMs to simulate this specific event it should also be considered that for the early 1970's the

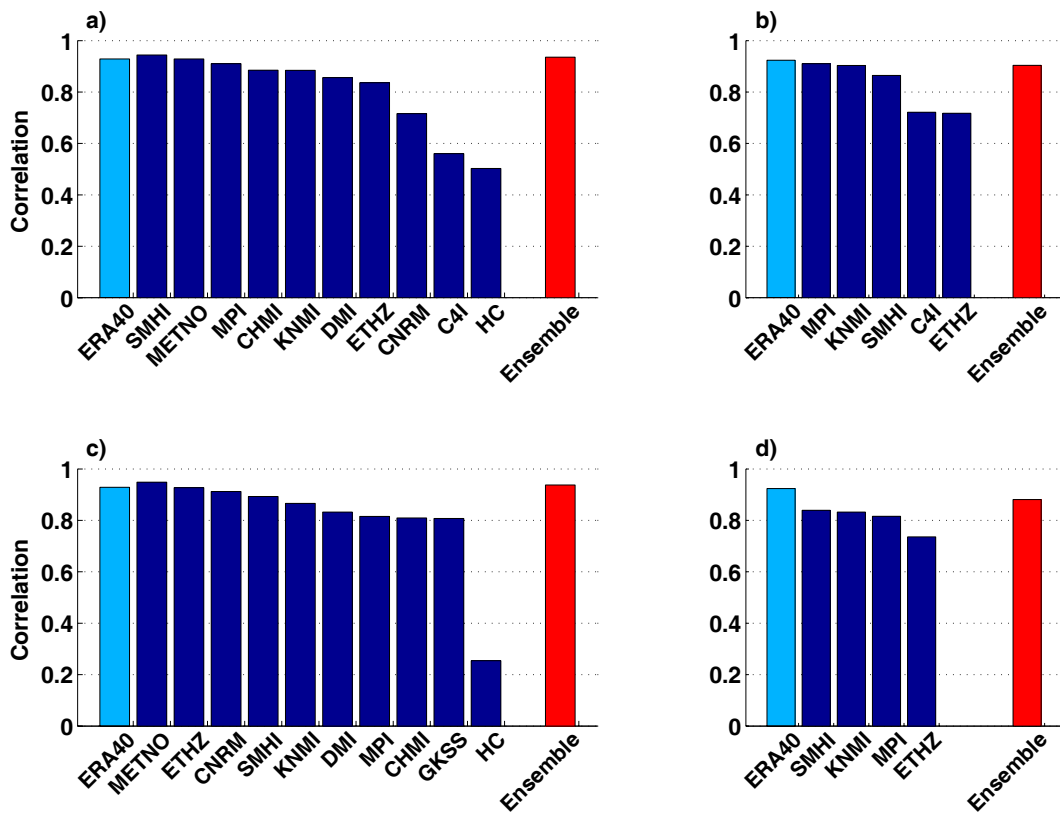


Figure 5.7: Same as figure 5.4, but correlations were recalculated excluding the losses of the year 1972.

uncertainty in the ERA40 upper troposphere is still relatively large, as e.g. only a few satellite observations are assimilated for this early period (Uppala et al., 2005). It is thus possible that atmospheric conditions favouring the explosive development of this storm are not sufficiently included in the reanalysis data used for driving the RCMs at the lateral boundaries. Analysis of the forecast runs of the ERA40 model started on 12 Nov 1972 00UTC and 12UTC (i.e. 18 and 30 hours prior to the maximum intensity in the reanalysis data) also reveals less intensive developments (minimum core pressure +9 and +15 hPa, respectively), suggesting that the extreme growth conditions related with the explosive development are not sufficiently captured in the large-scale data. Due to ongoing assimilation of observations, the extremely deep pressure values are finally included in the reanalysis data. Hence, the failure of the RCMs related with this particular storm should not necessarily be seen as a shortcoming of the RCMs but possibly as a shortcoming of the driving data. Later, a similar situation of an explosively developing secondary depression south of a strong steering cyclone on 25 and 26 December 1999 (storm 'Lothar', cf. Ulbrich et al., 2001) is well simulated by most RCMs.

In order to assess potential benefits of using RCMs for loss calculations apart from the obvious failure for one event, the model performance measure (i.e. correlation of simulated losses with insurance records) was recalculated excluding the year 1972 from the considerations (figure 5.7). Although only a few days would have to be excluded, due to the annual resolution of the insurance loss data the complete year 1972 has to be removed here. This leads to considerably higher correlations with observed losses in all simulations and a clear benefit from dynamical downscaling becomes obvious: while the correlations for losses based on ERA40 remain on the same level (0.84 for WIMAX and 0.89 for GUST), the best 3 RCMs in both resolutions reveal correlations higher than 0.9, while the best correlations based on single models are 0.95 (0.94) in 50km (25km) resolution. For 9 (7) out of the 10 simulations in 50km (25km) resolution the correlation is above 0.8 then. The ensemble mean of all 10 RCMs reveals a correlation of 0.94 in both resolutions and performs thus considerably better than losses calculated based on the large-scale reanalysis wind field. Hence, aside from one event not realistically simulated by all RCMs, a clear improvement of the loss estimates can be obtained by dynamical downscaling.

5.5. Summary, Discussion and Conclusion

Spatial patterns of extreme wind speeds and related loss potentials due to severe wind storms are validated in a multi-model ensemble of reanalysis-driven RCM simulations. The typical regional distribution of wind speeds is reproduced by all models, although considerable biases of the simulated speed values were identified for some models. Specific anomalies of the wind fields were found particularly over complex terrain, where some models reveal local minima and others local maxima of simulated wind speeds. For some models a dependence of this phenomenon on the spatial resolution was found, suggesting that part of this effect might be caused by the sub-orography in the grid boxes which are representative for larger areas, including mountains as well as valleys. Even if the grid box size can be considerably reduced by dynamical downscaling, it still covers an area of about 625km² in the finest resolution considered here. In contrast, observational data for comparison are strongly influenced by the location of the station which might be close to mountain tops or in valleys and thus affected by accelerating or decelerating effects. Thus, a sound validation of the wind speeds over complex orography requires a further systematic investigation and is beyond the scope of this study.

The applied loss model provides reasonable results (as also proven in previous studies, cf. Leckebusch et al., 2007; Pinto et al., 2007a). High correlations of 0.86 (using WIMAX) and 0.89 (using GUST) between observed annual losses for Germany and calculated losses based on ERA40-reanalysis are obtained. All RCMs fail to realistically simulate one of the most loss-intensive storm events occurring in November 1972. Excluding this particular event from the considerations, for most of the reanalysis-driven RCM simulations loss correlation values above 0.8 are found. For the best performing models a considerable improvement of loss calculations by dynamical downscaling is documented in comparison to losses calculated based on the large-scale reanalysis data: correlations of annual losses increase even up to 0.95. Thus, in most cases a distinct profit of applying RCMs becomes obvious. Considering the complete time series (i.e. including the 1972 event), the RCM benefits are masked by the failure with this specific event. The performance of losses calculated from the RCM simulations is consequently on average 0.1 points lower and thus slightly below the performance of losses calculated based on the reanalysis dataset. The deficiencies in realistically simulating the explosive development related with the 1972 event seem to

be due to shortcomings in the large-scale driving data: atmospheric conditions favouring an explosive cyclone development might not be sufficiently captured by the reanalysis data, as e.g. for this early period only a few satellite observations are available for assimilation. It should, however, be noted that the ERA40-reanalysis is subject to data assimilation and thus regularly “corrected” towards observations. Obviously, this accounts for its better performance. In contrast, the RCMs are generally driven at the domain boundaries only and develop their specific dynamics inside the domain. Thus, a better matching with observed losses would not directly be expected if the driving data are erroneous. Though, most of the RCMs simulate the majority of the storm events realistically and feature thus reasonable results in terms of loss calculations. Calculated losses for 1993 are unrealistically high based on ERA40, but more realistic for the RCM-ensemble, pointing to a profit from downscaling. The RCM using spectral nudging does not reveal a better performance than those without. Additionally, the considered loss measure is integrated with respect to sampling of different events and regions. Thus, the possible profit from a more realistic representation of regional wind features might be cancelled out. Availability of event-based and regionalised insurance data seems to be desirable for a specific examination of the added value of dynamical downscaling for loss calculations in comparison with observed losses in a higher temporal and spatial resolution, which is ongoing research.

Considering RCM simulations in two different horizontal resolutions, we could not find any evidence for better results with a finer resolution. However, a resolution of 25km might still not be fine enough to obtain a significant improvement. Still, it should not be excluded that positive effects might come from simulations in considerably finer resolutions, resolving meso-scale processes.

This study is to our knowledge the first investigating the benefits of dynamical downscaling for storm loss estimations. Previous studies have presented reasonable estimates of insured losses for Germany and Great Britain based on reanalysis data on a spatial scale of about 100-200km (Leckebusch et al., 2007; Pinto et al., 2007a). Benefits of dynamical downscaling with respect to a more realistic representation of winds over complex terrain were documented e.g. by Žagar et al. (2006). However, only a relatively short period of 2 months has been considered there. In the present study a period of about 3 decades is investigated, using an independent proxy for the occurrence of severe storms for validation. Another study analysing partly the same reanalysis-driven RCM simulations also reveals a large spread of skill, comparing simulated monthly

precipitation with observations (Sánchez et al., 2009). Further, Christensen et al. (2008) document considerable biases in the ENSEMBLES RCMs compared to observational data with respect to temperature and precipitation. None of these studies investigates if there is benefit from dynamical downscaling in comparison to the skill of the large-scale driving data, as presented here.

The most serious damages are generally assumed to be caused by severe gusts. Consequently, the assumption that gust wind speeds should be more suitable for the calculation of storm losses than maximum wind speeds without gusts is often found. The results presented here, however, indicate that correlations of annual losses are generally not higher when simulated gusts are considered for the loss calculations (with ERA40 being a major exception). This might on the one hand reveal deficits with the gust parameterisations; on the other hand it supports the approach of using a relative threshold for the calculation of losses, such as the 98th percentile. With this approach, calculations are independent from the absolute simulated speed values and the loss model is applicable to different climate models, although biases compared to observed absolute values of wind speed may exist. Please note that the loss correlations based on daily maximum gusts tend to reveal minimally higher correlations in the finer resolution. This can be found in three out of four models with gust parameterisation that are available in both resolutions and also in the ensemble mean. Three different gust parameterisation schemes are used in the considered RCMs. Although they are of different complexity and partly rather based on more empirical or more physical assumptions, a favourable scheme could not be identified. Representatives of all 3 schemes reveal a good performance in reproducing observed losses. Still, a considerable improvement could not be achieved in comparison to loss estimates based on daily maximum wind speeds without gust parameterisations.

The reanalysis-driven RCM simulations offer a chance to demonstrate the profit of combining different models to a MME also for climate simulations. On shorter timescales (such as weather and seasonal prediction), the superiority of MMEs compared to single models was demonstrated by different studies (compare e.g. Hagedorn et al., 2005), whereas on climate-timescales a verification and quantification of the MME advantages is less straight forward, as skill measures are generally not applicable and appropriate data for comparison are often missing. Here, due to the

large-scale forcing which depicts observed atmospheric developments, also the RCMs are expected to reproduce a realistic chronology of events and the results can be compared with observations time series. We use insurance loss data as an independent proxy for the occurrence of severe storms. Despite identical large-scale forcing, losses calculated from the reanalysis-driven RCMs reveal a large spread regarding their ability to reproduce observed annual losses. Combining the different RCM simulations leads to good correlations with observed losses, comparable to the best single model. Thus, again excluding (including) the 1972 storm event, high correlation values of about 0.94 (0.85) are obtained, although models with weak correlations smaller than 0.3 (0.2) are included. Sub-ensembles leaving out the weaker models might lead to slightly increased correlation values, in some cases higher than for the best single model. A systematic investigation of the influence of the MME construction on the performance demonstrates a lower spread of results for large ensembles, mainly caused by an increased minimum performance.

Though the multi-model performance turns out not to be significantly better than the best single model, the largest benefit can be seen in the consistently better performance of the multi-model ensemble, even if weak performing models are included. This is particularly important as considering climate simulations, it is generally difficult to measure the performance of the individual models (which would be necessary for obtaining objective quality measures, serving as a criterion for which models to include into the MME). Further, the best models identified for a specific application or time period not necessarily have to be the best for a different application or time period (cf. Reichler and Kim, 2008). Not only is it difficult to identify one best model. The results further demonstrate that it might also be difficult to identify a best sub-ensemble as some of the models are included in both, the best and the weakest model combinations. Thus, the findings of this study suggest that a MME consisting of all available models should lead to reasonable results. Weighting of models or use of sub-ensembles might still improve the performance. However, in the presented cases a selection of the best models yields only a marginal improvement compared to the inclusion of all models, supporting the use of large ensembles. The results suggest that the more models are included in the ensemble, the higher is the obtained consistency of performance: for larger ensemble sizes the spread between the best and the weakest performing model combination becomes considerably lower. The use of a large MME should be a good

choice for obtaining stable and reliable results and at the same time also allows for an estimation of the (model-) uncertainty.

Loss calculations based on RCM simulations for future climate scenarios, driven by global climate models will be considered in subsequent studies. An interesting question will be how the change signals from the RCMs compare to the change signals in the driving large-scale model.

Acknowledgements

This study was supported by the ENSEMBLES project, funded by the European Commission's 6th Framework Programme through contract GOCE-CT-2003-505539. We particularly thank the modelling groups for performing the simulations and DMI (Danish Meteorological Institute) for archiving the model results. We further kindly thank ECMWF, DWD (German Weather Service) and DKRZ (German Climate Computing Centre) for ERA40-data use and availability. We are much obliged to Philip Lorenz (Max Planck Institute for Meteorology, Hamburg) for fruitful discussions and are also grateful to three anonymous reviewers whose constructive comments helped to focus this paper.

6. Future changes of European winter storm losses and extreme wind speeds in multi-model GCM and RCM simulations

Abstract

Extreme wind speeds and related storm loss potentials in Europe are investigated based on multi-model simulations with global (GCM) and regional (RCM) climate models. Potential future changes due to anthropogenic climate change are analysed from simulations according to the IPCC SRES A1B scenario. The large number of considered simulations allows for an estimation of the robustness of the identified climate change signals.

All models in general reproduce the observed spatial patterns of wind speeds, although partly systematic biases are found for some models. A storm loss model is applied to the GCM and RCM simulations. It is found that the resulting mean loss amounts calculated based on the 20th century climate simulations are realistic, whereas the inter-annual variability of losses is generally underestimated. For the future scenario, most simulations as well as the ensemble mean generate enhanced extreme wind speed values (up to 5% in the ensemble mean) over northern parts of Central and Western Europe. As a consequence, also loss potentials are increased in these regions, particularly in Central Europe. For Southern Europe decreased extreme wind speeds and loss potentials are analysed. There is, however, a considerable spread between the change signals of the individual ensemble members, with signatures opposite to the ensemble mean signal analysed in some models. The downscaling of the large-scale simulations with RCMs increases the range of computed change signals. Even RCMs with identical large-scale driving show partly different change signals. The robustness of the change signals is estimated by two different measures: First, the inter-model standard deviation is considered which is, however, sensitive to outliers and thus reveals large uncertainty ranges. Second, robustness is estimated by means of multi-model combinatorics, considering all possible sub-ensembles from GCMs and RCMs and hence taking into account the arbitrariness of model selection for multi-model studies. Based on all available GCM and RCM simulations, e.g. for Germany an ensemble mean increase of loss potentials by +25% is analysed for the end of the 21st century, and 90% of the possible results show increased loss potentials in a range between +15% and +35%.

6.1. Introduction

Mid-latitude winter storms frequently hit Europe. Barring the risk of injury or even loss of lives those events cause heavy damages, in particular to infrastructure. The related losses often amount to several millions of Euros for single events and thus wind storms are the most loss-intensive natural hazards in Central Europe. For example in Germany 53 percent of economic losses due to natural hazards and even 64 percent of insured losses are caused by winter storms (Munich Re, 1999; Munich Re, 2007). It is thus important for different institutions involved in planning, rescue and insurance to gain information on how the risk of those extreme events might change under anthropogenic climate change (ACC) conditions.

Considering changes of storminess during the recent past, a high inter-decadal variability becomes obvious and often no clear trends can be identified during the last century (Barring and von Storch, 2004; Matulla et al., 2008). On the other hand, studies focussing on storms during the winter season presented upward trends towards the end of the 20th century (Leckebusch et al., 2008b; Wang et al., 2009). Time series of monetary storm losses show clear upward trends during the recent decades. Barredo (2009) associates this trend, however, mainly with societal factors, in particular with increasing values. For normalised losses no clear trend is found. A number of studies have recently dealt with changes of storminess in ACC scenario simulations using global climate models (GCMs) and found indication for more frequent occurrence of intensive cyclones over eastern North-Atlantic (Bengtsson et al., 2006; Lambert and Fyfe 2006, Leckebusch et al., 2006) and an eastward extension of the North Atlantic storm track (Ulbrich et al., 2008). This is in line with findings of higher extreme wind speeds over parts of Western and Central Europe (Knippertz et al., 2000, Leckebusch and Ulbrich, 2004, Pinto et al., 2007a; Gastineau and Soden, 2009). Based on multi-model GCM simulations, Donat et al. (2010a) found increased frequencies of storm days under future climate conditions as well as increased wind speeds during storm events. Studies estimating changes of storm losses under ACC conditions found increased risk of losses particularly in Western and Central Europe if no adaptation of buildings to higher wind speeds takes place (Leckebusch et al., 2007; Pinto et al., 2007a).

Such investigations based on GCMs can be complemented by applying dynamical downscaling with regional climate models (RCMs). This way, atmospheric information

at a higher spatial resolution is obtained, in particular providing information on the influence of regional orographic characteristics. Additionally, physical processes acting on scales resolved by the RCMs (but not by the GCMs) might affect the simulated regional wind patterns. The profit of dynamical downscaling with respect to wind fields over complex terrain was demonstrated e.g. by Žagar et al. (2006), obtaining wind speeds in better accordance with observations for mountainous regions compared to the driving large-scale reanalysis. An improved representation of local wind speeds should allow for a higher accuracy of storm loss calculations. The benefit of dynamical downscaling for storm loss calculations was documented in a recent study using loss data for Germany (Donat et al., 2010b). Future changes of extreme wind speeds in multi-model RCM simulations (all driven by the same GCM) have been explored by Rockel and Woth (2007), finding increased speed values in Central and Western Europe during winter. ACC signals of wind speed patterns in RCM simulations driven by different GCMs were previously investigated in comparison to the large-scale GCM signals e.g. by Leckebusch et al. (2006).

It is well known that results from numerical climate model simulations are affected by different sources of uncertainty. The most important ones are sensitivity to the initial conditions, to boundary conditions, model uncertainties and uncertainty due to internal variability. Due to non-linear processes in the climate system, small variations in the initial conditions of the simulations might lead to different solutions for the simulated state of the atmosphere. This source is most relevant for shorter time scales like weather and seasonal prediction applications, while climatological means computed from long-term climate projections are largely insensitive to small variations in the initial state (cf. Tebaldi and Knutti, 2007). However, recent studies (Pinto et al., 2007a) showed that with respect to ACC signals of extreme wind speeds over Europe, runs of the same model under the same climate scenario, but started from different initial conditions, can produce a rather large range of signals. Further, the climate system features a natural (internal) variability with periods from a few years up to decades and climate models generally do not reproduce the observed chronology of events. Thus, a sampling uncertainty is introduced by the fact that model climate states are estimated from a finite number of years. The occurrence of wind storms is of particularly high variability (Barring and von Storch, 2004, Matulla et al., 2008), so for a reliable estimation of trends large samples are desirable (which can also be produced by ensemble simulations, see e.g. Della-Marta et al., 2009c). Boundary condition uncertainty

includes the different possible future greenhouse gas (GHG) emission scenarios, based on hypotheses about future developments which include assumptions about possible societal changes, use of resources, global vs. regional development, etc. (e.g. Nakićenović et al., 2000). Model uncertainty is due to inaccuracy arising from the computational representation of the dynamic equations and the different parameterization of sub-grid processes. It is generally larger than the other sources (Déqué et al., 2007) and thus, results of ACC studies might be fundamentally dependent on the particular climate models taken into account.

Combining different models to a multi-model ensemble (MME) generally increases the skill, reliability and consistency of model projections. The superiority of MMEs for weather and seasonal prediction applications could be widely shown (see e.g. Hagedorn et al., 2005) and a verification and quantification is relatively straight-forward e.g. by skill measures. Also for climate-timescale simulations a MME can be favourable compared to a single model (cf. Palmer and Räisänen, 2002; Räisänen, 2007, Collins, 2007). MMEs primarily sample initial condition and model uncertainties (Tebaldi and Knutti, 2007) and by increasing the sample of considered years also the uncertainty due to internal variability should be reduced. Donat et al. (2010b) demonstrated the profit of MMEs for storm loss calculations, showing the ensemble mean performance to be close to the best single model and an increased agreement of the results for the more models are included in the ensemble.

Aim of this study is to estimate a range of possible future changes of extreme wind speeds and related storm loss potentials, as well as the robustness of the change signals based on a multi-model ensemble of GCM and RCM simulations. Further, the change signals in the RCMs are compared to the signals in the driving GCM. The robustness of the change signals can be estimated based on the differences between the signals from the different ensemble members. The availability of a large ensemble of (GCM and RCM) simulations conduces to an estimation of a possible range of change signals as well as of the signal (un-) certainties. We follow two different approaches for estimating this uncertainty: In addition to considering the inter-model standard deviation, the effect of different ensemble configurations on the loss signals is examined systematically for all possible combinations of subsets of available models. This allows for giving probabilistic information about the magnitude of possible changes.

This work is part of the ENSEMBLES project (<http://ensembles->

eu.metoffice.com/index.html, cf. Hewitt, 2005), where multi-model simulations with state-of-the-art global and regional climate models are produced and investigated with respect to the assessment of uncertainties in future climate projections.

6.2. Data and Methods

6.2.1. Meteorological Data

In total, 9 GCM simulations from 6 different GCMs are considered (ENSEMBLES project setup, see table 6.1. From each simulation, a period representing recent greenhouse gas forcing conditions during the last decades of the 20th century (20C) and a projection of future climate for the 21st century (21C) according to the SRES A1B scenario (A1B) are analysed. Two future periods are regarded: one for the middle (2021-2050) and one for the end of 21C (2071-2100 of most models).

All RCM simulations were carried out for a common domain including the whole continental European area (from approximately 10°W to 40°E and 30°N to 65°N). Overall, a set of 14 RCM simulations was considered (table 6.2), downscaling 7 different GCM runs. Most of them are carried out at a resolution of 0.22° (approximately 25km), 2 simulations (KNMI-RACMO2_E5_1/2; for an explanation of the nomenclature of the RCM run-labels please cf. table 6.2) were performed in a coarser resolution of 0.44° (approximately 50km). All scenario simulations follow the SRES A1B scenario and are integrated until at least year 2050. A smaller set of simulations continues until year 2100. Thus, we examine climate change signals for the

Model	Resolution atmosphere	20C.	A1B (mid 21C)	A1B (end 21C)	No. of considered runs	References
BCCR-BCM2	T63,L45	1960-1999	2021-2050	2080-2099	1	Furevik et al., 2003
CNRM-CM3	T63,L31	1981-2000	2021-2050	2081-2100	1	D. Salas-Méllia et al., 2005 (personal communication)
DMI-ECHAM5	T63, L31	1961-2000	2021-2050	2071-2100	1	Jungclaus et al., 2006
FUB-EGMAM	T30, L39	1961-2000	2021-2050	2081-2100	1	Manzini and McFarlane, 1998 Legutke and Voss, 1999 Huebener et al., 2007
IPSL-CM4	2,5°x3,75°, L19	1961-2000	2021-2050	2071-2100	1	Marti et al., 2005
MPI-ECHAM5	T63, L31	1961-2000	2021-2050	2071-2100	3	Jungclaus et al., 2006
METO-HC-HadGEM1	1,25°x1,875°, L38	1960-1999	2021-2050	2070-2099	1	Johns et al., 2006 Martin et al., 2006 Ringer et al., 2006

Table 6.1: Climate models included in this study (ENSEMBLES setup), GCM simulations

middle (of all models) as well as for the end (of the subset of models integrating until 2100) of the 21st century. For the 4 HadCM3-driven simulations (C4I-RCA3_HCh, HC-HadRM3_HCn, ETHZ-CLM_HCn and METNO-HIRHAM_HCn) different realisations from a perturbed parameter GCM-ensemble have been used for boundary forcing. Due to their different sensitivities (detailed description in Collins et al., 2009) they must be considered as simulations with different models. Unfortunately no daily maximum wind speeds were available from these HadCM3 runs that would allow for an interpretation of the RCM signals in context with the large-scale forcing. This is, however, possible for the remaining 10 RCM simulations, driven by GCMs also analysed in this study (cf. section 6.3.1): each 2 driven by CNRM-CM3 and BCCR-BCM2, in total 4 driven by MPI-ECHAM5_run3 and each 1 driven by MPI-ECHAM5 run 1 and 2, respectively (cf. table 6.2).

The investigated ensemble of GCM simulations is obviously dominated by the ECHAM5 model (in total 4 of the 9 simulations are based on this model), and the presented results could thus potentially be biased due to the dominance of this particular

RCM	Driving GCM	RCM Run-Label	Resolution	A1B (2021-2050)	A1B (2071-2100)	References
C4I-RCA3	HadCM3-Q16 (high sensitivity)	C4I-RCA3_HCh	25km	X	X	Rummukainen et al., 2001 Jones et al., 2004
HC-HadRM3	HadCM3Q0 (normal sensitivity)	HC-HadRM3_HCn	25km	X	X	Jones et al., 1995
ETHZ-CLM	HadCM3Q0 (normal sensitivity)	ETHZ-CLM_HCn	25km	X	X	Stappeler et al., 2003 Jaeger et al., 2008
CNRM-RM4.5	CNRM-CM3	CNRM-RM4.5_C	25km	X		Gibelin & Deque, 2003
DMI-HIRHAM	CNRM-CM3	DMI-HIRHAM_C	25km	X	X	Christensen et al., 1996
DMI-HIRHAM	ECHAM5_run3	DMI-HIRHAM_E5_3	25km	X	X	Christensen et al., 1996
METNO-HIRHAM	BCCR-BCM2	METNO-HIRHAM_B	25km	X		Christensen et al., 1996
METNO-HIRHAM	HadCM3Q0 (normal sensitivity)	METNO-HIRHAM_HCn	25km	X		Christensen et al., 1996
KNMI-RACMO2	ECHAM5_run1	KNMI-RACMO2_E5_1	50km	X	X	Lenderik et al., 2003
KNMI-RACMO2	ECHAM5_run2	KNMI-RACMO2_E5_2	50km	X	X	Lenderik et al., 2003
KNMI-RACMO2	ECHAM5_run3	KNMI-RACMO2_E5_3	25km	X	X	Lenderik et al., 2003
MPI-REMO	ECHAM5_run3	MPI-REMO_E5_3	25km	X	X	Jacob & Podzun, 1997 Jacob, 2001
SMHI-RCA	ECHAM5_run3	SMHI-RCA_E5_3	25km	X	X	Döscher et al., 2002 Jones et al., 2004
SMHI-RCA	BCCR-BCM2	SMHI-RCA_B	25km	X	X	Döscher et al., 2002 Jones et al., 2004

Table 6.2: Climate models included in this study (ENSEMBLES setup), RCM scenario simulations; the RCM run-labels (as referenced in the text) consist of the abbreviations for the modelling institution, the particular RCM and a code for the driving GCM.

model. As we prefer to include as many simulations as possible in our ensemble, we generally considered all 9 available simulations to compute the GCM ensemble mean. This approach also seems to be reasonable as the change signals from the individual realisations with ECHAM5 reveal a considerable spread. Nevertheless, the results will also be discussed for the case that only one of the ECHAM5 simulations contributes to the ensemble. Similarly, the RCM ensemble consists of different models downscaling the same GCM simulation. As even RCMs with identical large-scale forcing reveal considerably different results (cf. section 6.3.2) and given the aim of this study to incorporate as many models as available, generally all simulations are included in the ensemble mean calculations. Nevertheless, the impacts of alternative ensemble constructions will be discussed. ERA40-reanalysis (Uppala et al., 2005) is used for validation of the GCM and RCM 20C climate period simulations. Further, these data are used for calibration of the loss model; the obtained loss regression function is also used for loss calculations based on the GCM simulations (see methods section 6.2.2).

Our analyses concentrate on the daily maximum 10-m wind speeds from all data sets. This parameter is recorded as the daily maximum speed value, based on all time steps within a 24 h period. It was derived for almost all GCMs and for all RCMs. Only 6-hourly instantaneous values of wind speed were available for ERA40 and the GCM simulations with BCCR-BCM2, CNRM-CM3 and DMI-ECHAM5. Hence, a daily maximum is calculated as the maximum of the 4 instantaneous wind speeds stored at 00, 06, 12 and 18 UTC. This value is expected to be slightly smaller than the maximum over all time steps (cf. Pinto et al., 2007a, their figure 3b,c), inducing a small inhomogeneity to our data basis. The daily maximum wind speed data are hereafter referred to as WIMAX.

Five of the RCMs (used for in total 8 simulations) also feature a gust parameterisation: C4I-RCA3_HCh, ETHZ-CLM_HCn, SMHI-RCA_B, MPI-REMO_E5_3, KNMI-RACMO2_E5_1,2,3 and SMHI-RCA_E5_3. The respective daily maximum 10-m gust wind speeds are hereafter referred to as GUST. For the ERA40 dataset the 10-m wind speed (6-hourly, see above) and a 10-m wind gust is available. As in the RCMs, the latter is a model diagnostic and hence calculated based on a parameterization. Note that different approaches for calculating the gust wind speeds are used in the different models. The method used in the RCA models (SMHI and C4I) assumes that surface gusts result from the deflection of air parcels from the upper boundary layer, mixed down by turbulent eddies (Brasseur, 2001). This method takes into account turbulent

kinetic energy, the mean wind and the static stability in the boundary layer. ERA40 and KNMI-RACMO2 make use of a scheme based on the similarity relation by Panofsky et al. (1977). Here, a standard deviation of the near-surface wind is calculated, again taking into account the static stability of the boundary layer. The maximum gust speed is then estimated by adding a term including this standard deviation to the 10m wind speed (cf. White et al., 2003). MPI-REMO and ETHZ-CLM calculate gusts based on empirical assumptions taking into account the turbulent kinetic energy in the lowest model layer (Schrodin, 1995).

Almost all severe damage causing storm events occur during boreal winter (Klawa and Ulbrich, 2003; Munich Re, 2007). Hence, the analyses presented here focus on the extended winter period October to March.

6.2.2. Calculation of storm induced losses

Storm losses are calculated by applying a linear regression model developed by Klawa and Ulbrich (2003). In recent studies this model was applied to reanalysis and GCM data (Leckebusch et al., 2007, Pinto et al., 2007a) as well as to (reanalysis-driven) RCM simulations (Donat et al., 2010b), revealing reasonable results. Annual loss ratios (giving the ratio of insured values that is affected by storm losses) are calculated by the equation

$$loss = A * \sum_{area}^{Germany} pop(area) * \sum_{Tage}^{Jahr} LLI + B$$

$$\text{with local loss index } LLI = \left(\frac{v_{max}(area, day)}{v_{98}(area)} - 1 \right)^3 \text{ (for } v_{max} > v_{98}, \text{ else } LLI=0)$$

In this function v_{max} is the daily maximum wind speed (i.e. WIMAX or GUST) in a grid box and v_{98} is the local 98th percentile of daily maximum wind speeds. Thus, it is assumed that losses occur locally during the 2% of days with strongest winds. Using a relative threshold, the loss function takes into account model biases of simulated wind speeds. A is the obtained regression coefficient from calibrating calculated losses with the insurance data and B is the axis intercept; pop(area) is the population density. Population density is regarded as a proxy for insured values, because information about spatial distribution of total insured values are highly sensitive for insurance companies and thus difficult to assess. Particularly for Central and Western Europe the assumption

is reasonable that insured values are proportional to population density. For the calculations in this study we use gridded population density data for the year 2000, on a 0.25x0.25 degree raster (CIESIN 2005).

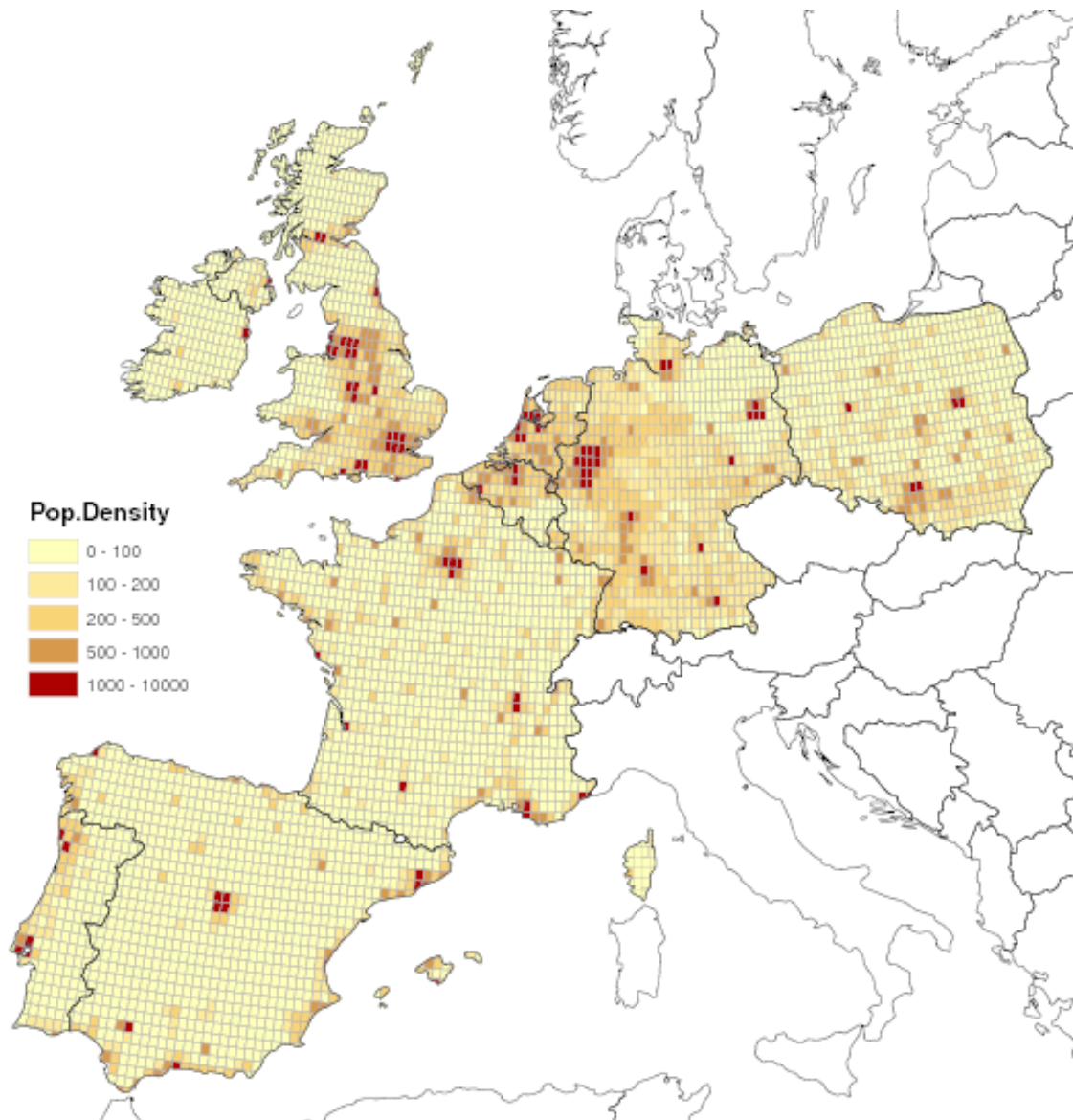


Figure 6.1: Population density on a 0.25°x0.25° grid is used as a proxy for insured values in the considered regions for which loss calculations were performed (unit: inhabitants per km²).

The loss index (calculated at each grid point) has to be calibrated with loss data from historical storms. Therefore, annually accumulated loss data (including losses to residential buildings due to storm and hail events) for Germany were provided by the Gesamtverband der Deutschen Versicherungswirtschaft e.V. (German Insurance Association, hereafter GDV) for the period 1970-2000. The large losses are usually caused by intense winter storm events affecting a large area; losses due to hail can generally be neglected, as their percentage in the total annual loss is small (Klawnski and

Ulbrich, 2003; pers comm. GDV, 2009). Annual loss values are given as loss ratios, i.e. the ratio between insured claims and totally insured values (unit: € per 1000€, i.e. in ‰). An advantage of this measure is that inflation can be neglected as it is included in both, in insured values and in the loss. A linear regression is used to calibrate “raw losses” as calculated by the loss function with the GDV loss ratios. We used the regression derived for Germany also for the other considered countries. Leckebusch et al. (2007) showed that similar results are obtained if damage data from the UK were used to calibrate the calculated loss values. Thus, the calculated loss ratios for other countries than Germany might not be fully realistic in terms of their absolute value, but estimates of future changes will still be possible. Besides for Germany, in this study storm losses are estimated for Poland, France, Belgium, Netherlands and Luxembourg (together “BeNeLux”), United Kingdom and Ireland (together “UK+IRE”) and Spain and Portugal (together “IBERIA”). This selection is motivated by former results with respect to future changes of loss potentials and cyclone tracks (e.g. Leckebusch et al., 2006; 2007; Donat et al., 2010a) Population densities used for the loss calculations for these considered regions are presented in figure 6.1.

For the calculation of losses from the GCM simulations the regression of “raw losses” and insurance data determined for losses calculated from the ERA40-reanalysis is used. Because the models simulate a specific realisation of climate and generally do not reproduce the observed chronology of events, model years can not be assigned to observed annual loss data. GCM wind biases against ERA40 are less relevant, as normalised wind speeds rather than absolute model output values are used. For the RCM simulations model-specific regressions were determined from simulations driven by ERA40-reanalysis, which are expected to depict the observed chronology of storm events and related losses (cf. Donat et al., 2010b). Again, deviations of a RCM wind climatology arising from driving the model with GCM data other than ERA40 are largely removed by the percentile approach.

Loss potentials for the future climate periods are calculated in two ways: in the first, the local 98th percentile of daily maximum wind speeds calculated for the 20C period is maintained as the threshold for the occurrence of losses also for the future climate simulations; in the second approach the percentile of the future simulation is used as the loss threshold. The first approach means that damage should occur at the same wind speed as presently. Thus, damage to buildings occurs without adaptation to a new wind climatology. The second approach takes adaptation into account. This means that e.g.

the architecture of houses is adapted to higher or lower local wind speeds, so that losses again occur only during the 2% of days with highest wind speeds (also refer to Leckebusch et al., 2007; Pinto et al., 2007a).

6.3. Extreme wind speeds and related losses estimated from GCM and RCM scenario simulations

6.3.1. Analysis of the GCM simulations

6.3.1.1. Extreme wind speeds

Regarding the ensemble average of all GCMs, there is a general agreement with the ERA40 reanalysis for both spatial patterns and absolute speed values (figure 6.3a/b), although peculiarities are found in some individual models. The GCM ensemble reveals systematically higher speed values in comparison to ERA40 over the Atlantic and the Mediterranean (approximately 5%), whereas over land and parts of the Baltic region lower speed values are found (up to 10%). Still, the typical patterns of extreme wind speeds (here: 98th percentile of WIMAX) in the European region with maximum values over sea areas and lower values over continental areas are also reproduced by all GCMs (figure 6.2a). Over land areas, highest wind speeds are found over northern parts of Western (British Isles, northern France) and Central Europe (Benelux, Denmark, northern Germany and northern Poland) and also over parts of Scandinavia. Minimum speed values are over terrain with complex orography. FUB-EGMAM reveals relatively high speed values also in the area of the Iberian Peninsula. Note that this is the model with the coarsest spatial resolution and uses sea grid boxes in this area to keep the Strait of Gibraltar opened. Thus, lower roughness allows for higher near-surface wind speeds, disagreeing with the observation-based (reanalysis) data set.

Although the speed values in the individual models are in a similar scale, there are some specific differences. For example, wind speeds in FUB-EGMAM are systematically higher compared to ERA40 and the other models, while IPSL-CM4 and CNRM-CM3 reveal largely lower speed values. These differences can only partly be assigned to the different calculation of daily maxima. Remember that for some models daily maxima were calculated as maxima of 6-hourly instantaneous values (ERA40, CNRM-CM3, BCCR-BCM2, DMI-ECHAM5, cf. Section 6.2). The model-to-model differences of absolute wind speeds can be largely resolved by the use of relative thresholds for loss calculations in subsequent parts of this paper.

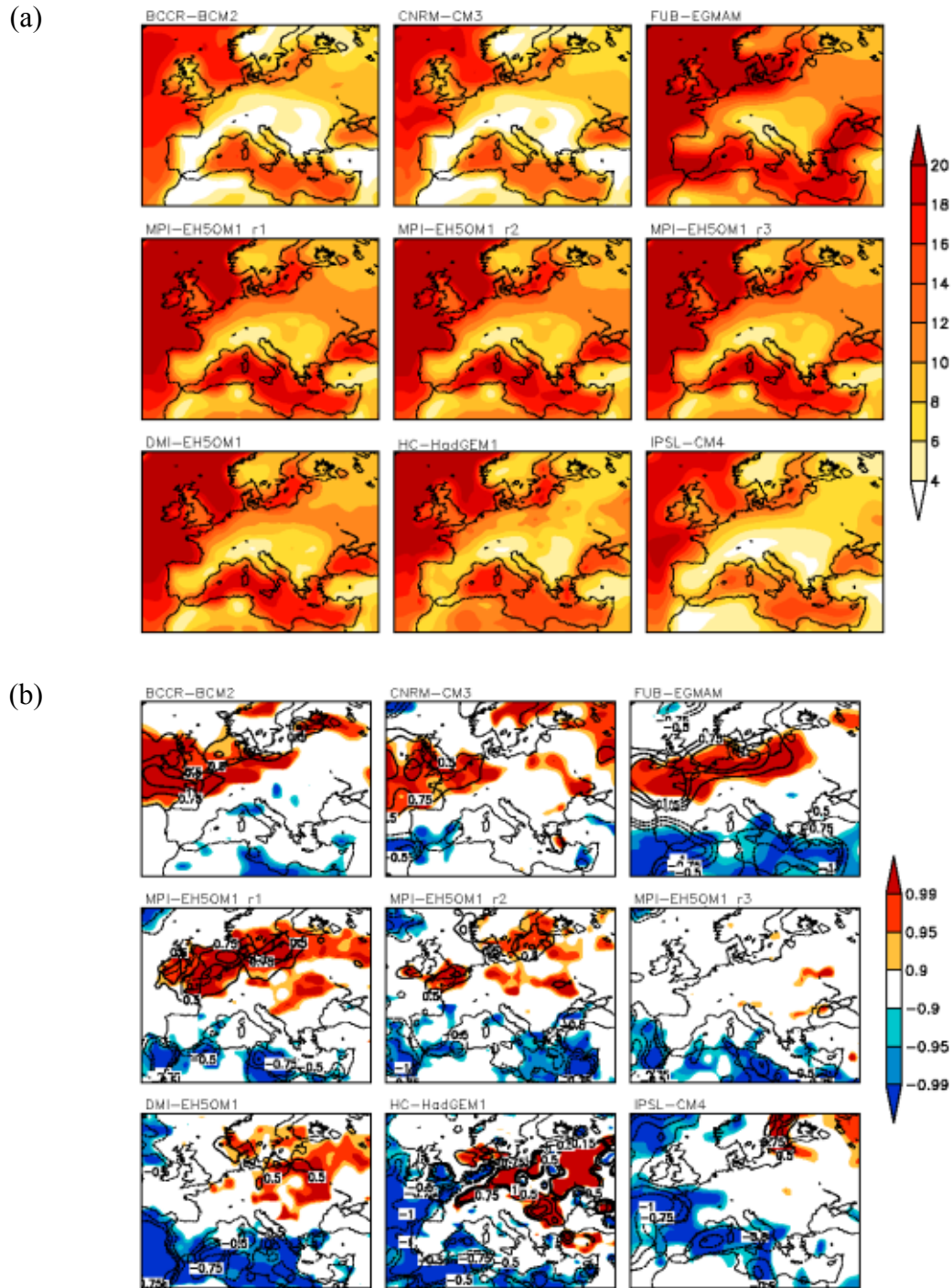


Figure 6.2: Daily maximum wind speed (*WIMAX*), 98th percentile in the GCM simulations

- a) absolute values for 20C (unit: m/s)
- b) ACC signals A1B-20C: magnitude of changes is displayed by black iso-lines (unit: m/s), coloured areas indicate statistical significance above 0.9 (Student-T-test).

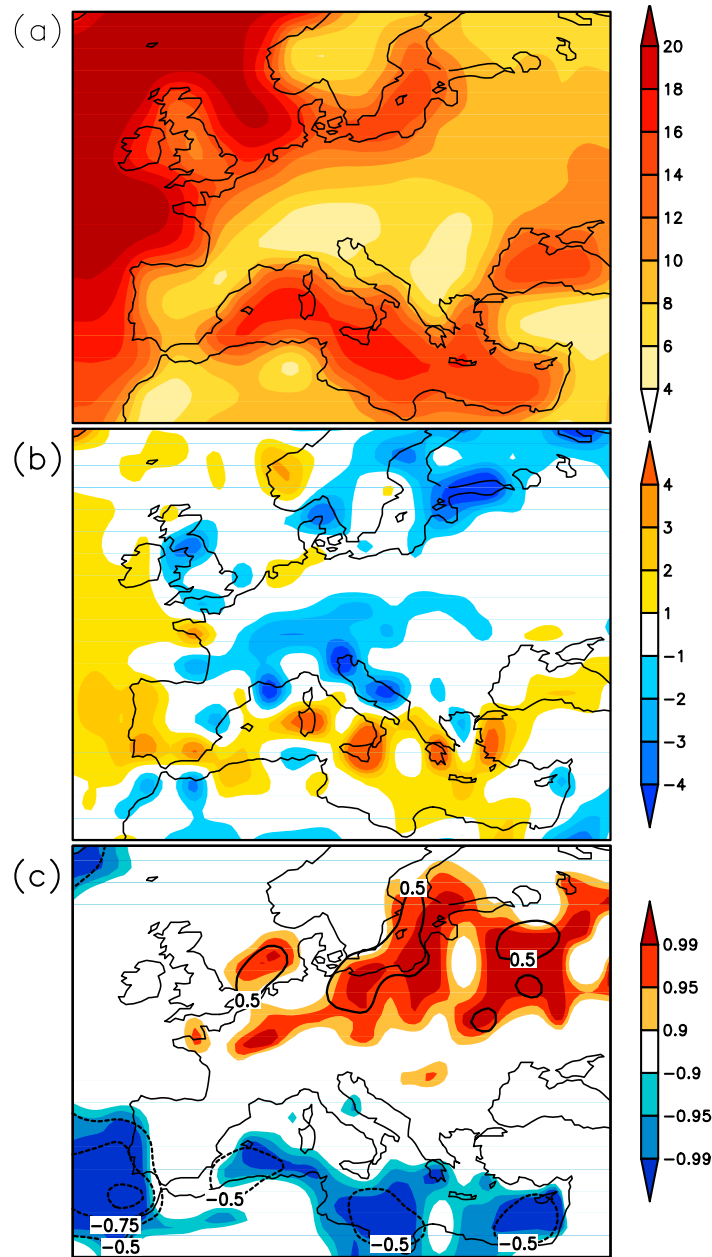


Figure 6.3: Ensemble Mean of 98th percentile of WIMAX in the GCM simulations

- a) absolute values for 20C (unit: m/s)
- b) anomaly GCM ensemble (20C) relative to ERA40 (unit: m/s)
- c) ACC signal A1B-20C: magnitude of changes is displayed by black iso-lines (unit: m/s), coloured areas indicate statistical significance above 0.9 (Student-T-test)

The ensemble mean A1B scenario signal for the end of the 21st century (figure 6.3b) features a significant increase of extreme wind speeds over northern parts of Central and Eastern Europe and a decrease over the Mediterranean. Similar results are found in most of the individual GCMs (figure 6.2b), whereas the exact position of the maximum change is shifted somewhat east- or westwards in the individual ensemble members.

The most different signal is found in the IPSL-CM4 simulation: here, the zone of significantly increased wind speeds is shifted north-eastwards towards the northern Baltic region, whereas over Western Europe a decrease of extreme wind speeds is analysed. A decrease over Western Europe is similarly found in the HadGEM1 simulation. At the same time, this simulation also reveals a particularly strong increase of the 98th percentile of daily maximum wind speeds over Eastern Europe, up to nearly a doubling. The third run of MPI-ECHAM5 produces the smallest signal of all simulations; in particular the increase of extreme wind speed over Central Europe is not significant in this realisation.

The characteristics of the ACC signals for the first half of the 21st century are similar as those for the end of the 21st century in all individual models, though magnitude and significance are mostly lower (not shown). In the ensemble mean there is even a small (non-significant) decrease over the North Sea region for this early period which is mainly caused by the signals from IPSL and HadGEM1.

6.3.1.2. Loss potentials

Insurance companies have to pay on average about 900 million € per year only in Germany as a consequence of storm losses to residential buildings (GDV 2006; 2009). On the basis of the German insurance data, for the recent decades a mean annual loss ratio of approximately 0.15‰ (± 0.12 ‰ inter-annual standard deviation) is assumed (compare also Leckebusch et al., 2007; Pinto et al., 2007a; Donat et al., 2010b). Despite model-specific differences in the wind climatologies and also specific decadal variabilities, realistic annual mean losses are simulated on the basis of output from the 20C runs (cf. table 6.3), supporting the applicability of the GCMs for loss estimates. From the simulations with ECHAM5 and HadGEM1, mean loss ratios are closest to the insurance data (between 0.14 and 0.16‰); somewhat lower values are obtained from the other models (e.g. 0.11‰ from CNRM-CM3). The inter-annual standard deviation of annual losses is too low in all models except for DMI-ECHAM5. Based on this model, the mean loss ratio as well as the standard deviation is closest to the insurance data. Losses calculated from the other models reveal a too low inter-annual variability compared to the observed insurance loss data.

Examining the storm losses in the ACC simulations for the end of the 21st century, considerable differences between the individual ensemble members are apparent, particularly for the case of no adaptation (Appendix table AT6.1a). Considering area

averages for individual countries, largest changes are found for Germany, with 8 out of 9 ensemble members showing enhanced risk of mean loss, up to +87.1% (HadGEM1). Only losses calculated from the DMI-ECHAM5 simulation show slightly decreased values (-6.2%). In the ensemble average (figure 6.4, upper row), the annual mean loss ratio for Germany is increased by 37.7 (± 31.0)%. This increase goes along with an increased standard deviation of the annual losses in 7 of the 9 simulations and also in the ensemble mean. The increase of inter-annual variability is primarily caused by the occurrence of individual years with extremely high losses, partly occurring during single exceptionally strong events (Leckebusch et al., 2008b), which do not occur in the GCM control periods. Thus, the increase of the inter-annual standard deviation might be even more relevant for impact assessments than changes in mean losses.

In the future climate simulations, France is affected by higher extreme wind speeds in its northern parts and lower extreme wind speeds in the Mediterranean region (cf. figure 6.3b), partly compensating each other in the country mean. Consequently the change signals for France are relatively small. In the average of all simulations risk is increased by 9.0 (± 13.2)%, with slightly increased inter-annual variability (measured in terms of standard deviation of annual loss values). 7 out of the 9 ensemble members reveal increased risk by up to +36.5% (FUB-EGMAM), and in 2 ensemble members storm losses are slightly decreased (up to -7.6% in HadGEM1).

For the BeNeLux area 7 of the 9 ensemble members reveal increased loss potential of up to +50,4% (CNRM-CM3) and in the other 2 GCM simulations a slightly decrease of

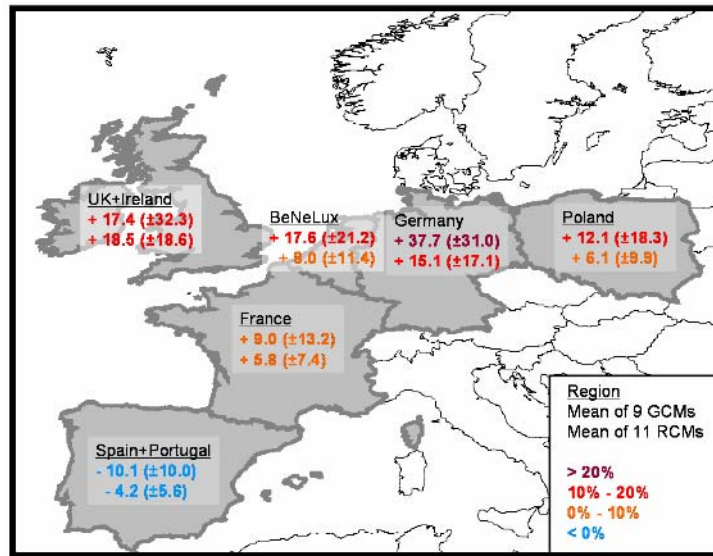
	MEAN	STD
GDV	0.15	0.12
ERA40 WIMAX	0.15	0.10
ERA40 GUST	0.14	0.10
BCCR-BCM2	0.12	0.08
CNRM-CM3	0.11	0.04
DMI-ECHAM5	0.15	0.12
FUB-EGMAM	0.12	0.06
IPSL-CM4	0.12	0.07
MPI-ECHAM5 run1	0.15	0.09
MPI-ECHAM5 run2	0.16	0.10
MPI-ECHAM5 run3	0.14	0.09
METO-HC-HadGEM1	0.14	0.09
GCM-Ensemble mean	0,13 \pm 0,02	0,08 \pm 0,02

Table 6.3: Mean and Standard deviation of annual loss ratios for Germany as provided by the German Insurance Association GDV and calculated from the ERA40 reanalysis and the 20C GCM simulations (unit: %). The ensemble mean is calculated as the average \pm inter-model standard deviation of the 9 GCM simulations.

about -4% is analysed. The ensemble mean indicates increased values of mean annual losses by +17.6 (± 21.2) %. Also the inter-annual variability of loss is significantly increased in this area.

Cumulated losses of the United Kingdom and Ireland increase in 7 of the 9 ensemble members (up to 67.6% in FUB-EGMAM). The 2 models revealing reduced extreme wind speeds over Western Europe (cf. Fig. 6.2b) also feature considerably lower loss values (HadGEM1: -22.1%, IPSL-CM4: -16.5%). In the ensemble average, mean

(a)



(b)

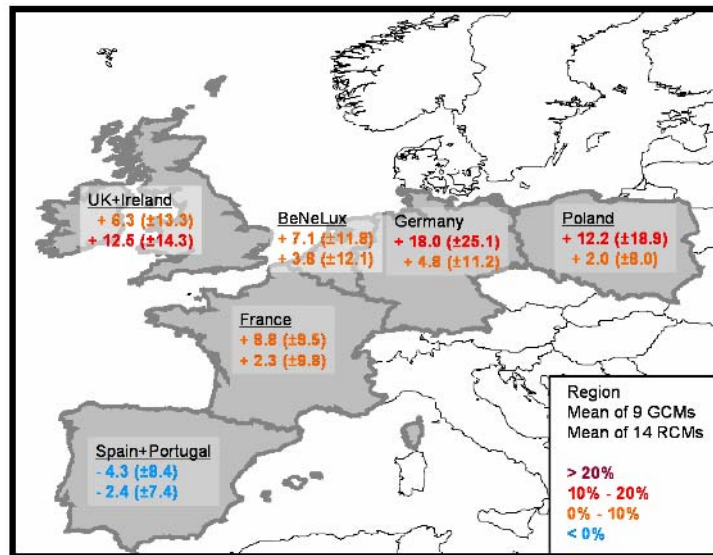


Figure 6.4: Relative changes (unit: %) of mean annual storm loss potential based on the GCM (upper row) and RCM (bottom row) simulations for the end (a) and middle (b) of the 21st century compared to recent climate conditions (20C, 1961-2000). Values in parentheses are inter-model standard deviations.

a) end of 21C (2071-2100), based on 9 GCM and 11 RCM simulations

b) middle of 21C (2021-2050), based on 9 GCM and 14 RCM simulations

annual losses are enhanced by +17.4 (± 32.3) %. Also the standard deviation of annual losses is considerably enhanced (+27.8% in ensemble mean), although only 5 ensemble members feature increased inter-annual variability, in the other 4 it is reduced.

For the Iberian Peninsula (where reduced extreme wind speeds were analysed) 7 ensemble members reveal also decreased losses (HadGEM1 up to -24.2%). In 2 ensemble members a light increase is found (BCCR up to +8.4%). The ensemble average of mean annual losses is reduced by -10.1 (± 10.0) % in this area.

A significant increase of extreme wind speed values was found over eastern Central Europe in the ACC simulations (Fig 6.3b). Regarding now the change signals of loss potentials in Poland, the majority of 7 ensemble members features enhanced risk of loss (HadGEM1 up to +52.8%); 2 realisations feature small decreases (MPI-ECHAM5 run1 up to -7.6%). Consequently, in ensemble mean an increase of mean annual losses by +12.1 (± 18.3)% is found.

The 4 simulations with the ECHAM5 model reveal considerably different loss changes (cf. table AT6.1a). Although comparing the individual ECHAM5 signals with the other models does not suggest any suspect that the ensemble results could be biased due to including multiple runs of this particular model, we recalculated the ensemble mean loss changes including only 1 simulation of each GCM. Thus, 4 different ensembles of 6 different GCMs can be constructed (each containing either realisation 1, 2 or 3 of MPI-ECHAM5 or the DMI-ECHAM5 run). Indeed, considering only 1 of these simulations for the ensemble mean calculation, the presented results remain largely valid, though there are some modifications with respect to the ensemble mean signals' magnitudes. For example, the modified ensemble mean change signals for losses in Germany range between +41.4 % (including the DMI run) and +51.2 % (including MPI run1). For UK and Ireland increased losses between 14.3 % (including MPI run2) and 23.2 % (including MPI run1) are found; or e.g. for the BeNeLux region the different ensemble mean signals range between +14.9 % (including MPI run3) and +22.3 % (including MPI run1). Thus, the large spread of possible signals between the different realisations of this particular model, comparable to the spread of signals based on the different GCMs, justifies the inclusion of all available simulations. We find no evidence for a bias due to including different realisations of the same model. Hence, including all simulations enlarges the ensemble size and allows for a sound estimation of the change signal's robustness.

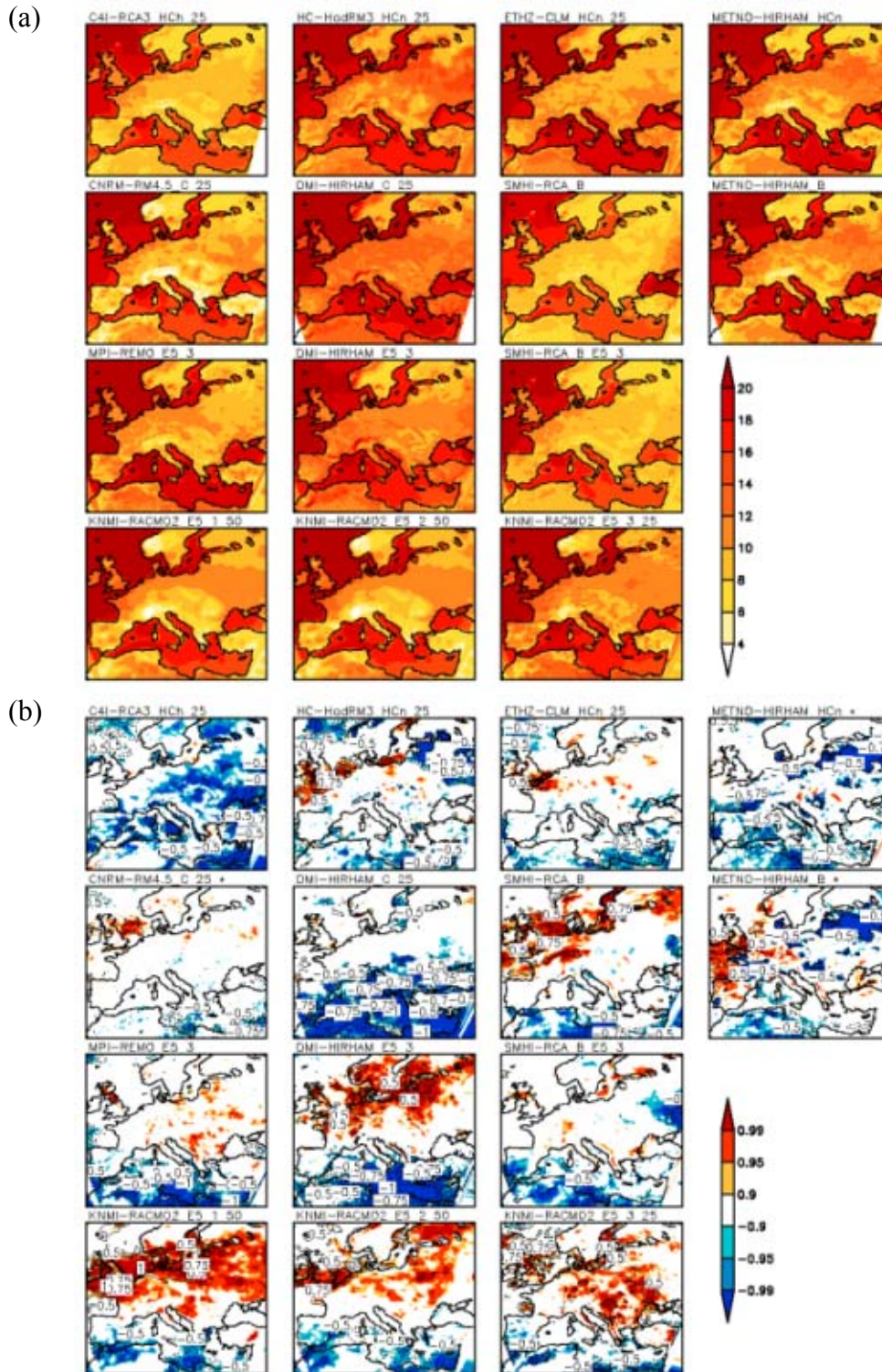


Figure 6.5: Daily maximum wind speed (*WIMAX*), 98th percentile in the RCM simulations. 1st line: driven by the (different) *HadCM3* simulations, 2nd line: driven by *CNRM-CM3* or *BCCR-BCM2*, 3rd line and 4th line: driven by *MPI-ECHAM5* (run 1,2 or 3)

- a) absolute values for the 20C period (1961-2000)
- b) ACC signals for 98th percentile of *WIMAX* in the RCM simulations, all results are for the future period 2071-2100, except for *METNO_HIRHAM_HCn**, *METNO-HIRHAM_B** and *CNRM-RM4.5_C** (only integrated until 2050) signals for the period 2021-2050 are presented. Magnitude of changes is displayed by black iso-lines (unit: m/s), coloured areas indicate statistical significance above 0.9 (Student-T-test).

Future loss calculations for the case that adaptation takes place (i.e. the threshold for occurrence of losses is adapted to future wind climate so that at each grid point again the 2% strongest wind events cause losses) reveal distinctly smaller changes (Appendix table AT6.1b). For example for Germany, the spread of changes in the different ensemble members is between +16.8% (IPSL-CM4) and -22.6% (DMI-ECHAM5). In ensemble mean, change signals for Germany, France, BeNeLux and UK with Ireland are small (up to 2%), though increased inter-annual variability of losses is still found for Germany. For the Iberian Peninsula and Poland changes of mean losses are about 6.5% increase (IBERIA) or decrease (Poland), respectively. Increased losses for the Iberian Peninsula are also found in 8 of the 9 ensemble members. Please note that due to the reduction of extreme wind speed in this region also the threshold for loss is reduced. Thus, the adaptation approach would correspond to an adaptation to weaker structures of buildings here.

Change signals for the first half of the 21st century (considered 2021-2050) mostly show the same characteristics as the signals for the end for the 21s century (upper row in figure 6.4b for loss changes without adaptation), but largely a lower magnitude, although still a large variability between the ensemble members is apparent (Appendix table AT6.1c). In ensemble mean the magnitude of changes for Germany in the middle of the 21st century is about 50% compared to the change signal at the end of the 21st century. For France and Poland the difference between the two forcing periods is small; for United Kingdom and Ireland the mean signal is about 33%, for the Iberian Peninsula 50% and for BeNeLux 40% of the mean signal for the end of the 21st century. Regarding the ratio of change signals between the earlier and the later future climate period in the individual ensemble members discloses a large variability between the different realisations. Whereas in some cases even contrary signals are found for the two periods (e.g. for Germany: IPSL-CM4, DMI-ECHAM5, MPI-ECHAM5_run3; for France: FUB-EGMAM, HadGEM1, MPI-ECHAM5_run2; for Poland: MPI-ECHAM5_run1), also examples with double or even higher magnitude of change in the earlier period can be found.

These results demonstrate the high variability on a decadal scale in the occurrence of severe wind storms in the different realisations. The analysed loss potential change signals partly do not seem to scale proportional with the GHG forcing, as the identified signals include both, internal variability and response to ACC. In the ensemble mean the pattern of the change signals is comparable for both future periods, demonstrating the

value of an ensemble by enlarging the sample size and thus reducing the uncertainty due to internal variability. In the case of adaptation of the loss threshold to the changed wind climate again only small changes are found (not shown).

6.3.2. Analysis of the RCM scenario simulations

6.3.2.1. Extreme wind speeds

Patterns of the 98th percentile of WIMAX as produced by the GCM-driven RCM simulations for the 20C period do not show major deviations from the reanalysis-driven runs (figure 6.5a, compare to Donat et al., 2010b). The model-specific characteristics (such as systematic biases in absolute speed values and anomalies over mountainous regions) discussed in the previous study for the ERA40-driven simulations are almost identical with those originating from the (GCM-driven) 20C scenario simulations.

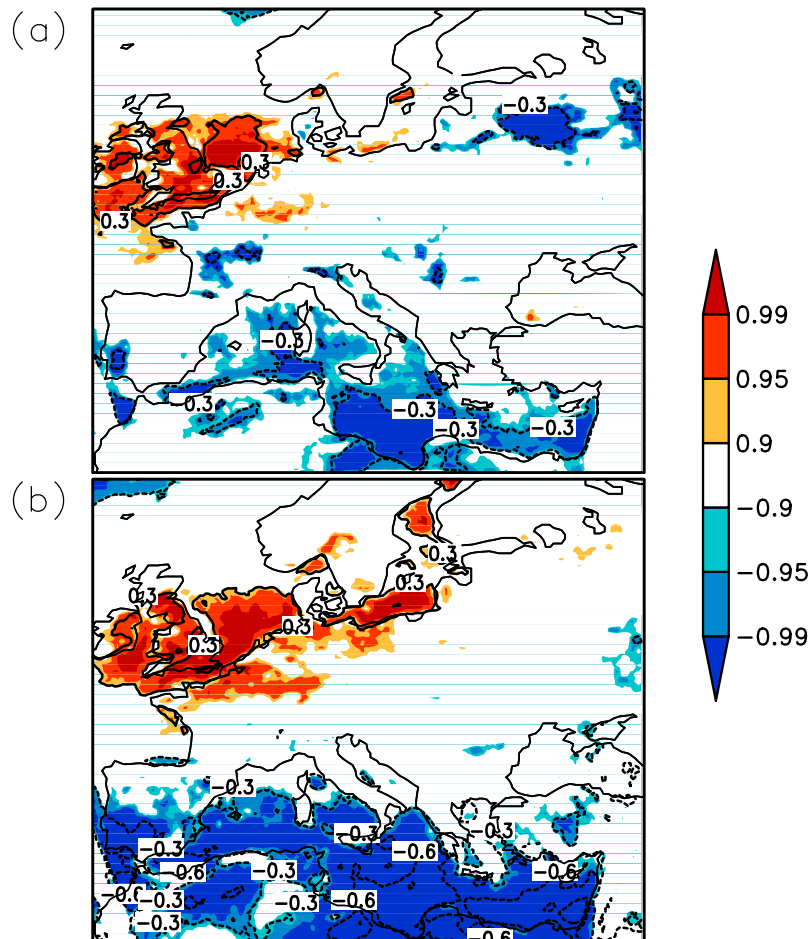


Figure 6.6: RCM-Ensemble Mean of ACC signal for 98th percentile of WIMAX in the future scenario simulations. Magnitude of changes is displayed by black iso-lines (unit: m/s), coloured areas indicate statistical significance above 0.9 (Student-T-test).

a) A1B (2021-2050) – 20C

b) A1B (2071-2100) – 20C

For the RCM future scenario simulations (figures 6.5b and figure 6.6a,b), significantly increased extreme wind speeds are found in the ensemble mean particularly over Western Europe and in the North Sea and Baltic Sea regions; over the Mediterranean reduced wind speeds are analysed. These are common features also in the majority of the RCMs. The C4I-RCA3_HCh simulation (driven by HadCM3-Q16, i.e. high sensitivity) is the only one showing largely decreased wind speed values also in the Central European region. Whereas relatively smooth signals are found in the GCM simulations (cf. section 6.3.1), the signals in most individual RCMs noticeably appear somewhat spotty over continental areas. Consequently they partly seem to compensate in the ensemble mean and thus, the changes over Central Europe are comparatively lower than in most of the individual models and also than in the GCM ensemble. Although patterns of the change signals are similar when driven by the same GCM, with respect to the signals' magnitudes a considerable spread becomes obvious. Note e.g. the differences between the 4 simulations driven by ECHAM5_run3 and also remember that the driving run reveals only marginal change signals (cf. figure 6.2b).

The ensemble mean patterns of the change signals for the middle of the 21st century (figure 6.6a) correspond again well to the patterns for the end of 21C (figure 6.6b), whereas the significance of the signals is considerably higher for the later period. Please note that in the ensemble for the earlier period there are 3 more simulations included than in the ensemble mean for the end of 21C, because CNRM-RM4.5_C, METNO-HIRHAM_B and METNO-HIRHAM_HCn were only integrated until 2050. The picture is, however, similar if the ensemble mean for the earlier period is calculated only from the 11 simulations which are also available for the later period. Also regarding the individual ensemble members, for those simulations integrated until 2100 generally the decrease over Mediterranean is more significant for the latter period. Particularly the DMI-HIRHAM_E5_3 and KNMI-RACMO2_E5_1/2/3 simulations reveal a considerably stronger increase over Western and Central Europe for the later period, whereas for the other simulations signals in this region are similar for both periods.

6.3.2.2. Loss potentials calculated from the RCM simulations

Regarding the RCM storm loss potentials, the change signals correspond in general to the signals found from the GCM simulations, although for most regions the mean relative changes are slightly smaller in the RCM ensemble (figure 6.4, bottom row, compare with top row). Again there are considerable differences between the individual

ensemble members (Appendix table AT6.2). In the following paragraph the ensemble mean changes (\pm standard deviation between the different simulations) and additionally the maximum spread (i.e. the most extreme signals) are discussed.

Following the no-adaptation approach, storm losses in Germany could increase by +15.1 (\pm 17.1) % in ensemble mean for the end of 21C (spread between +54.9 % (KNMI-RACMO2_E5_3) and -4.5 % (SMHI-RCA_E5_3)). For France, the ensemble mean change signal is +5.8 (\pm 7.4) %, for UK together with Ireland +18.5 (\pm 18.6) %, for BeNeLux +8.0 (\pm 11.4) %, for Poland +6.1 (\pm 9.9) % and for the Iberian Peninsula by -4.2 (\pm 5.6) % decreased losses are analysed. Again a noticeable increase of inter-annual variability of losses is diagnosed, particularly for Germany, Poland, BeNeLux and UK+IRE.

Analysis of different RCMs driven by the same GCM simulation reveals that despite identical large-scale driving, dynamical downscaling might increase the spread of possible results considerably. Regarding e.g. the 4 RCM simulations driven by ECHAM5_run3, change signals between +33.6% and -4.5% are obtained, whereas the change signal of the driving ECHAM5_run3 is +17.0%: 1 RCM simulation reveals a considerably stronger change signal (KNMI-RACMO2_E5_3), 2 realisations (MPI-REMO_E5_3 and SMHI-RCA_E5_3) show only small changes of loss, and in the DMI-HIRHAM-E5_3 run the change signal is almost identical with the GCM signal. Thus, with respect to the large spread, the average signal of the 4 RCM runs is similar (+12.4%) to the GCM signal, but still about 30% too low. Further analysis of the impact of regional downscaling related to the spread of climate change signals seems thus to be motivated and of additional need, but is behind the scope of this study.

Note that the magnitude of mean change signals in the RCM ensemble is for all regions except for UK and Ireland considerably smaller compared to the signal's magnitude in the GCM ensemble. This might partly be explained by the model setup, as e.g. the GCM simulations showing the largest change signals were not used to drive RCM simulations (cf. tables 6.1, 6.2 and section 6.2). Further, 4 RCM scenario simulations were driven by different perturbed-parameter experiments with the HadCM3 model; daily maximum wind speeds from these experiments were not available for this study and could thus not be included in the GCM ensemble. Nevertheless, the phenomenon of comparatively smaller signals in the RCM ensemble is still present if only those GCM simulations that were used for downscaling are considered in the GCM ensemble mean and only those

RCM simulations where the driving GCM simulation is available are considered in the RCM ensemble. However, in some cases (e.g. KNMI_RACMO2_E5_3) also stronger RCM signals are found in comparison to the driving GCM. Understanding the differences between the signals from the large-scale and regional models makes further studies necessary.

Ensemble mean change signals for the first half of 21C (figure 6.4b, bottom row) are small (below 5%) for most of the considered regions, only for UK+IRE a considerable signal is found (+12.5 (\pm 14.3) %). As already found for the GCM simulations, change signals are small in the case that adaptation of the loss threshold to the future climate is taken into account (not shown), demonstrating the value of in time initiation of adaptation strategies.

6.3.2.3. Does the use of RCM gust wind speeds modify the results?

From a subset of the RCM simulations also gust wind speeds estimations (as a model diagnostic) are available. The heavy damages in the “real world” are generally caused by severe wind gusts; Rockel and Woth (2007) documented that wind speeds exceeding 20m/s (8Bft.) are in general not produced by RCMs without a gust parameterisation. However, as the loss model applied here uses a relative threshold for the occurrence of losses, exceedance of a specific absolute wind speed should not be necessary for a realistic calculation of losses, assuming a correspondence of extreme sustained winds and gusts. With respect to the reproduction of observed losses, Donat et al. (2010b) demonstrated that the temporal correlation of losses calculated based on GUST is generally not higher than for losses calculated based on WIMAX.

Also regarding the change signals of extreme wind speeds and loss potentials, the results presented in the sections above remain largely valid when considering GUST. The patterns of the ACC signals for the 98th percentile of GUST correspond well to the change patterns for WIMAX, whereas the change magnitudes and significance levels tend to be stronger for some simulations (C4I-RCA3_HCh, ETHZ-CLM_HCn and SMHI-RCA_B, not shown) when regarding GUST. For the other 5 simulations providing GUST (KNMI-RACMO2_E5_1,2,3, MPI-REMO_E5_3 and SMHI-RCA_E5_3) the change patterns and magnitudes for GUST are very similar to WIMAX.

Also considering the losses calculated based on GUST, the changes of loss potentials

are in general comparable to loss changes calculated based on WIMAX. Again, C4I-RCA3_HCh and ETHZ-CLM_HCn reveal somewhat larger signals for most regions compared to WIMAX, whereas the signals of the other simulations are mostly similar to (or partly even slightly smaller than) the corresponding WIMAX signals. It is remarkable that for MPI-REMO_E5_3 the loss changes based on GUST are for all regions almost equal to the results based on WIMAX. For all regions except for IBERIA this was also found for the SMHI-RCA_E5_3 run. The ensemble mean loss changes are for most regions comparable to the RCM mean signals based on WIMAX (compare figure 6.4). Non-negligible deviations are, however, found for France and IBERIA. For France, the mean loss change for the end of 21C is approximately twice (+10.4%) compared to the RCM signal based on WIMAX. For IBERIA the decrease is by factor 4 smaller (-0.9%).

In summary, we find no systematically altered results if losses are calculated on the basis of wind gusts instead of WIMAX.

6.3.3. Multi-model combinatorics: Uncertainty of ACC loss potentials considering all possible model combinations

MME studies are affected by a certain level of arbitrariness. The construction of an ensemble is for example determined by the availability of model simulations. As the individual simulations produce ACC signals with different magnitudes and even different sign (cf. chapters 6.3.1 and 6.3.2), the MME change signals will depend on the models included. Here, the influence of different model combinations on the loss potential change signal is for the first time investigated systematically by considering all possible model combinations in a multi-model combinatorics approach. The range of the resulting ACC signals allows for an estimation of the signal's (un-) certainty. The idea of this approach is to use all information that are included in the MME. For this study, the composition of the MME was defined by the models included in the ENSEMBLES project (tables 6.1, 6.2).

Based on the 9 available GCM simulations, there are in total 511 different possibilities of calculating (sub-) ensembles including 1 up to 9 individual ensemble members (9 single models, 36 combinations with each 2 and 7 models, 84 combinations considering 3 or 6 models, 126 considering each 4 or 5 models, 9 combinations of 8 models and exactly 1 ensemble containing all 9 simulations). Additionally, 14 RCM scenario simulations are available until 2050 (and 11 until 2100), allowing for 16,383 (or

respectively 2,047) different RCM combinations. Thus, in total 23 individual (GCM or RCM) ACC signals for the first half of 21C and 20 for the end of 21C are available, enabling 8,388,607 different model combinations for the earlier period and 1,048,575 for the latter. The consideration all different possible model combinations can be seen as an “ensemble of (sub-) ensembles”. In basic, this idea of assessing the uncertainty of the ACC signals is related to the principle of bootstrapping (Efron, 1979), which is applied to gain information about characteristics (e.g. quantiles) of an unknown theoretical distribution. However, whereas bootstrapping generally considers different limited samples to assess the characteristic of a basic population, the approach presented here accounts for all possible solutions that can be constructed from the ensemble of models. A limitation might arise from the fact that the different (sub-) ensembles are not necessarily independent from each other. On the one hand, signals from each simulation are included in several (sub-) ensembles and on the other hand some of the GCM simulations are used for driving the RCM simulations (and are thus included in the RCM results). Further, even different models are not completely independent, as they partly share common components or modules. This all contributes to difficulties in a sound estimation e.g. of the degrees of freedom of the sample of possible change signals. Nevertheless, these all are possible results if only different subsets of simulations were available for this study and thus have to be included into the considerations. Further, even different realisations with the same model reveal different change signals (cf. section 6.3.1) and the RCMs have been shown to increase the spread of possible results and reveal partly fundamentally different results, even compared to their driving GCMs (cf. section 6.3.2). Still, following the suggested approach, a complete sample based on the different sub-ensembles is gained, making use of all information included in the ensemble of models. Assuming that the sample of signals constructed from the available models that are included in the study is representative for a sample based on all existing climate models, this methodology allows for an estimation of a range of ACC signals that might be expected.

We focus on the ACC signals without adaptation of the loss threshold (cf. Appendix tables AT6.1, AT6.2). The range of possible change signals on the basis of the GCM and RCM simulations for the end of 21C is presented in figure 6.7 for the different regions. The signals of the different sub-ensembles were counted for different ACC signal magnitudes (in 2%-steps) and the relative frequency of the different magnitudes is displayed. Here, the green curve summarizes the results of the 511 GCM

combinations (of 9 GCM simulations), the blue curve represents the 2,047 RCM sub-ensembles (of 11 RCM simulations integrated until 2100), and the red curve comprises the results from the 1,048,575 combinations of all available GCM or RCM simulations. For each region, the red shaded area indicates a confidence interval where the inner 90% of the signals between the 5th and the 95th percentile are found. As each individual simulation is included in the same number of model combinations, the average of the ensemble of possible (sub-) ensembles is exactly the same value as for the simple ensemble mean of all available models (compare also figure 6.4).

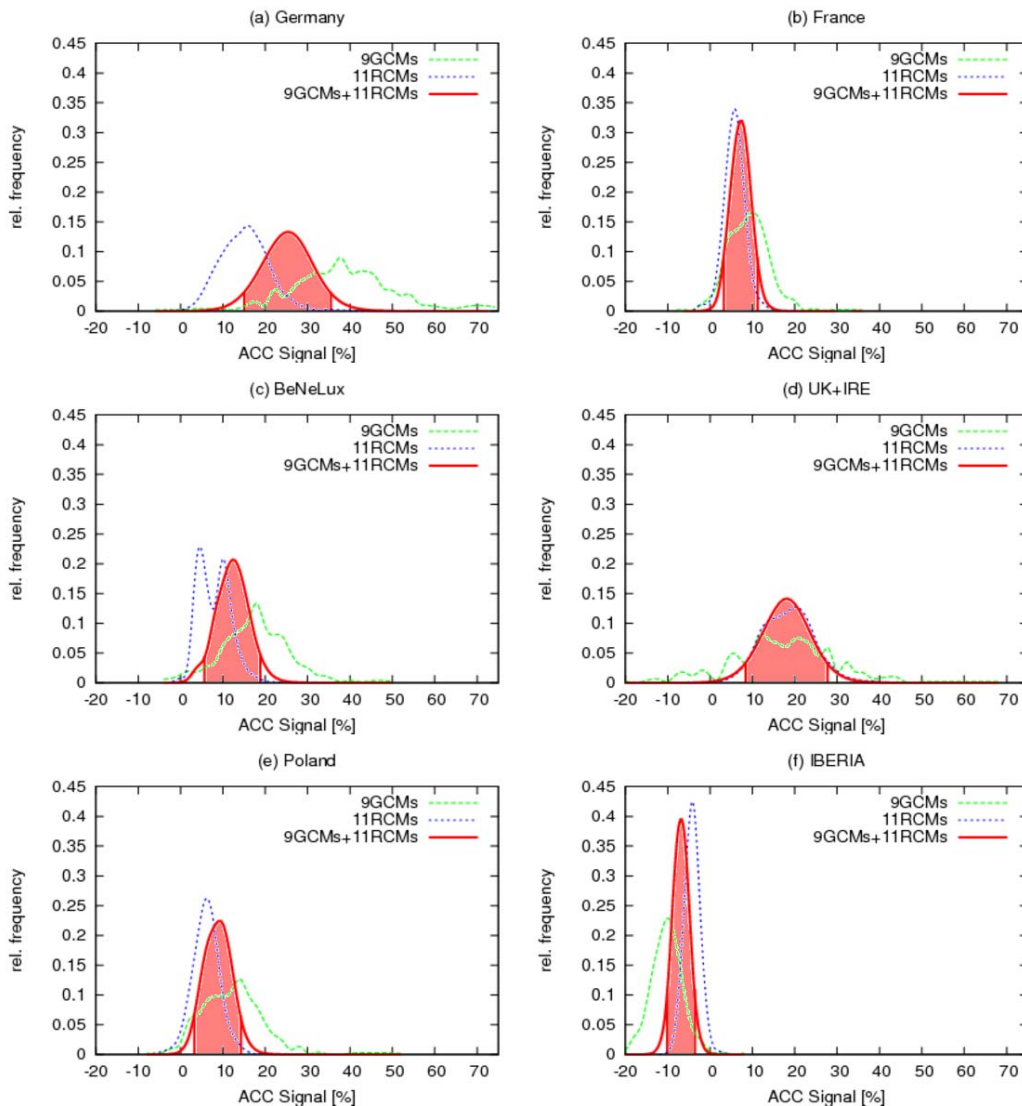


Figure 6.7: Probability of loss potential changes for the future climate period end of 21C (2071-2100) compared to 20C (1961-2000) without adaptation of the loss threshold, based on all possible model combinations of GCMs (green curve), RCMs (blue curve) and all available GCM and RCM scenario (red curve) simulations. The red shaded areas mark the range where 90% of the change signals (between 5th and 95th percentile) based on all model combinations are found.

It becomes obvious that the largest spread of ACC signals is found for Germany and the UK+IRE region. For Germany, the red curve comprising all combinations of available simulations indicates a mean increase of loss potential of about 25.2%, with the confidence interval of 90% of the possible solutions between +15.1% and +35.4%. Regarding again all possible combinations of the GCM and RCM scenario simulations for UK+IRE, loss potentials for the end of 21C show an increase of 18.1%, with 90% of the possible signals between +8.4% (5th percentile) and +27.6% (95th percentile). Accordingly, for the BeNeLux countries a mean increase of 12.3% (confidence interval between 5.7% and 18.8%) is analysed and for Poland an increase of 8.8% (confidence interval between 3.4% and 14.2%). The sharpest ranges of possible signals are found for France and the Iberian Peninsula. For France, a mean increase of 7.2 (± 3.9)% is found, and for IBERIA decreased risk of loss by 6.9 (± 3.2)%. As already discussed in section 6.3.2, for most regions (except for UK+IRE) the magnitude of the signals on the basis of the GCM ensemble (green curves in figure 6.7) is larger than the RCM ensemble signal (blue curve). Furthermore, generally also the GCM spread is larger compared to the spread of RCM simulations, resulting in a broader distribution of possible results. Remember, though, that those GCMs revealing outlier signals (and thus contributing to a large spread) were not used to drive RCMs. The phenomenon that the mean magnitude of change signals for the GCM simulations is considerably larger than for the RCM simulations is not only found when all available models are considered. If the ensembles are restricted to those GCMs used for downscaling (and available for this study: CNRM-CM3, BCCR-BCM2, ECHAM5) in comparison to the connected RCM runs, different magnitudes are still obvious for the (reduced) GCM- and RCM-ensembles (not shown). The uncertainty range of the GCM signals is, however, considerably reduced (and similar to the RCM range) if only those GCMs used for driving the RCMs are considered.

The uncertainty range estimated from all model combinations is considerably smaller compared to the inter-model standard deviation (compare figure 6.4), which is more affected by outlier models. For example, considering only the change signals from the GCM simulations and the respective confidence interval from the range covering 90% of all 511 possible results, the mean change signal for Germany is 37.7 (± 19.7)%. For comparison, using the inter-model standard deviation as uncertainty measure (cf. section 6.3.1.2), the signal was 37.7 (± 31.0)%. Accordingly, also for the other regions sharpened confidence intervals are obtained: mean GCM signal for BeNeLux is +17.6

(±14.4)%, for France +9.0 (±8.1)%, for Poland +12.1 (±11.5)%, for UK+IRE +14.4 (±21.6)% and for IBERIA -10.1 (±6.3)%.

Mean change signals for the period 2021 to 2050 are generally smaller compared to signals for the end of 21C (Appendix figure AF6.1, in accordance with tables AT6.1c, AT6.2b). For this earlier period, considering the 8,388,607 possible model combinations of all 23 ACC simulations, the widest spreads are again found for Germany and UK+IRE, whereas the change signals for France and IBERIA reveal the sharpest distributions. The magnitudes of the mean change signals for this earlier period constitute between 40% (Germany, BeNeLux) and 70% (France, Poland) compared to the signals for the end of 21C.

6.4. Summary, Discussion and Conclusion

Patterns of extreme wind speeds and related loss potentials due to severe wind storms are investigated based on multi-model simulations with global and regional climate models. Potential future changes are analysed for different European regions according to the IPCC SRES A1B emission scenario. The considered GCMs and RCMs reproduce well the typical spatial patterns of extreme wind speeds (98th percentile) over the European region in the simulations of recent climate, even though some of the models reveal biases in the absolute speed values. Considering loss potential calculations based on the 20C simulations, realistic mean losses are obtained; the inter-annual variability of simulated losses is in ensemble mean about 30% lower than that of observed insurance loss data for Germany. In the future climate simulations most models and also the ensemble mean commonly feature an increase of extreme wind speeds over northern Central Europe and a decrease over the Mediterranean region. Assuming that no adaptation takes place (and the loss-wind relation remains thus unaltered in a changing climate), also the mean loss ratios increase in the Western and Central European regions. In ensemble mean, loss potentials in Germany at the end of 21C are increased by 37.7% (15.1%) based on the considered GCM (RCM) simulations. Also over eastern Central Europe (e.g. over the area of Poland) simulated losses increase significantly by 12.1% (6.1%). Mean losses for UK+IRE are increased by 17.4% (18.5%) and respectively for France by 9.0% (5.8%) and by 17.6% (8.0%) in the BeNeLux countries. Over Southern Europe, in accordance with the reduction of extreme wind speeds, reduced risk of storm losses is found (e.g. for the Iberian Peninsula -10.1% (-4.2%) in

the GCM (RCM) ensemble).

There is, however, a large spread between the signals from the individual ensemble members, pointing at the large variability in severe storm occurrence, even for different realisations with the same climate model. The characteristic of the mean signals for the first half of 21C corresponds in general to the signals found for the end of 21C, though in the individual simulations again a large variability is obvious, revealing partly larger changes for the earlier period than for the latter. Particularly for Central Europe also increased inter-annual variability of losses is found, caused by single years with exceptionally high losses (cf. Pinto et al., 2007a); this phenomenon has to be investigated in future studies.

Concerning dynamical downscaling, Leckebusch et al. (2006) showed that the spatial patterns of the extreme wind speeds change signal are close to the change pattern of the driving GCM. The same behaviour is found in this study. However, with respect to the change signal magnitudes, dynamical downscaling using RCMs is shown to increase the spread of possible results compared to the signal from the driving GCM. For different RCMs driven by the same GCM simulation, comparable spatial change patterns of extreme wind speeds are found, though the magnitudes differ considerably. Consequently the changes of loss potentials reveal strongly different magnitudes despite identical large-scale forcing. From an ensemble mean perspective, for most regions the RCM ensemble loss signals are smaller than those from the GCM ensemble. This effect might partly be explained by the rather spotty change signals of extreme wind speed patterns in the individual RCMs: Hence, a smaller area is affected by changed loss potentials in comparison to the relatively smooth change patterns of the GCM wind fields. Further, the spotty RCM wind changes partly compensate each other in the ensemble average. In detail, effects related with the RCM signals in comparison with the large-scale results still have to be understood from future studies.

The most serious damages are generally caused by severe gusts. Consequently, the assumption that gust wind speeds should be more suitable for the calculation of storm losses than maximum wind speeds without gusts is often found. In a recent study using the same loss function as applied here, however, no evidence could be found that losses calculated based on GUST agree better with observed losses than losses calculated based on WIMAX (Donat et al., 2010b). Considering now the climate change signals of loss potentials, there is a tendency towards stronger changes using GUST in some

models, whereas it is of a comparable magnitude with WIMAX in others and also in ensemble mean.

The identified changes in the pattern of extreme wind speeds correspond to results from previous studies where also significantly increased values over northern parts of Central and Western Europe and decreased values over Southern Europe were found (Leckebusch and Ulbrich 2004; Leckebusch et al., 2006; Pinto et al., 2007a; Gastineau and Soden, 2009). The increase of extreme wind speed values over Western and Central Europe is consistent with the increased activity of extreme cyclones identified over the eastern Atlantic/western European region in the future climate simulations with the considered GCM ensemble (Leckebusch et al., 2008c).

The magnitude of the identified change signals of loss potentials is similar to results in recent studies based on smaller MMEs (Leckebusch et al., 2007) or single model ensembles (Pinto et al., 2007a). They further also identified a large spread between the different GCMs or even different realisations with the same GCM. Whereas the previous studies focus on loss changes in Germany and partly in UK, here change of loss potentials is estimated for in total six regions in Central and Western Europe. Further, compared to the previous studies, this study is based on a relatively large MME, allowing for a more detailed estimation of the uncertainties of expected change signals. Please note that the slightly different signals for the 3 ECHAM5 simulations in this study compared to Pinto et al. (2007a) are due to different population density datasets applied. In contrast to them, we used population data in a finer resolution, also applicable for loss estimates based on RCMs.

Barredo (2009) suggests that observed recent upward trends of storm loss amounts are mainly driven by societal factors and can thus be explained by increasing values. For the analysis of future loss potentials in this study, societal factors on the change signal were explicitly excluded by maintaining today's population data (as a proxy for insured values) also for the future periods. Further, the considered loss measure takes into account the ratio between insured claims and totally insured values and thus inflation is normalised. Consequently, assuming continuously increasing values for the next century, total monetary loss amounts might increase considerably stronger than those analysed here. In this study only the "pure" meteorological effect of anthropogenic induced climate changes are analysed, which has to be recognised additionally to any societal trend. Considering only Germany, given today's mean annual loss amounts to

residential buildings of about 900 million €, a meteorologically induced increase of loss potentials of about 25% (as derived from the model combinations in section 6.3.3) would account for additional 225 million € costs per year, approximately. Increases in societal factors might lead to further considerably increased loss amounts.

Within the discussion of climate change impacts, this study further demonstrates that relatively small changes of a meteorological parameter might cause considerably increases of risk. For storm losses an exponential relationship between wind speeds and losses is assumed, contributing to the partly significantly changed loss estimates: While the increase of the absolute wind speed values is relatively low (e.g. up to 5% in the GCM ensemble for Central Europe), conspicuously increased losses are expected (e.g. approximately 37% for Germany in the GCM ensemble).

The magnitude of potential future changes in losses differs strongly between the different ensemble members, even for different realisations with the same GCM. Further, comparing the change signals for the first half and the end of the 21st century reveals for some ensemble members fundamental differences. Both phenomena, the large spread of ACC signals in the different simulations as well as the differences for the 2 future periods in some simulations indicate the large long-term variability in severe storm occurrence, which is partly related to decadal-scale atmospheric variabilities. Thus, ACC signals from individual models might be influenced by effects connected to this high variability. This demonstrates that ACC studies based on single models might be misleading. The increased sample size by using multi-model simulations leads to considerably increased stability of the results. Uncertainties due to internal variability but also due to individual model formulations should be cancelled out.

Regarding an ensemble of simulations further provides information allowing for an estimation of the uncertainty of the results. The uncertainty range of loss potential change signals is regarded by two different measures. On the one hand, the standard deviations between the change signals in the different simulations are calculated (cf. figure 6.4), revealing values of the same order as the mean changes for most considered regions. The standard deviation as uncertainty measure is, however, strongly influenced by outliers. Thus, the fact that some individual models reveal fundamentally different signals compared to most of the other models (cf. Appendix Tables AT6.1, AT6.2) contributes to the large uncertainty ranges measured in terms of standard deviation.

Alternatively, the range (and the probability) of possible signals is calculated by considering the signals from all sub-ensembles that can be constructed from the available climate simulations. This results in a relatively symmetric distribution of possible change signals around the ensemble mean and further allows for giving probabilistic information about the range of expected changes. For example, combining the loss potential change signals from all available GCM and RCM simulations for the end of 21C for Germany, a mean increase of +25% is analysed, with a 90% confidence to be between +15% and +35%.

Acknowledgements

This study was supported by the ENSEMBLES project, funded by the European Commission's 6th Framework Programme through contract GOCE-CT-2003-505539. We particularly thank the modelling groups for performing the simulations, DMI (Danish Meteorological Institute) for archiving the RCM results and DKRZ (German Climate Computing Centre) for archiving the GCM results. We further kindly thank ECMWF, DWD (German Weather Service) and DKRZ for ERA40-data use and availability.

6.5. Appendix Chapter 6: Supplementary Material

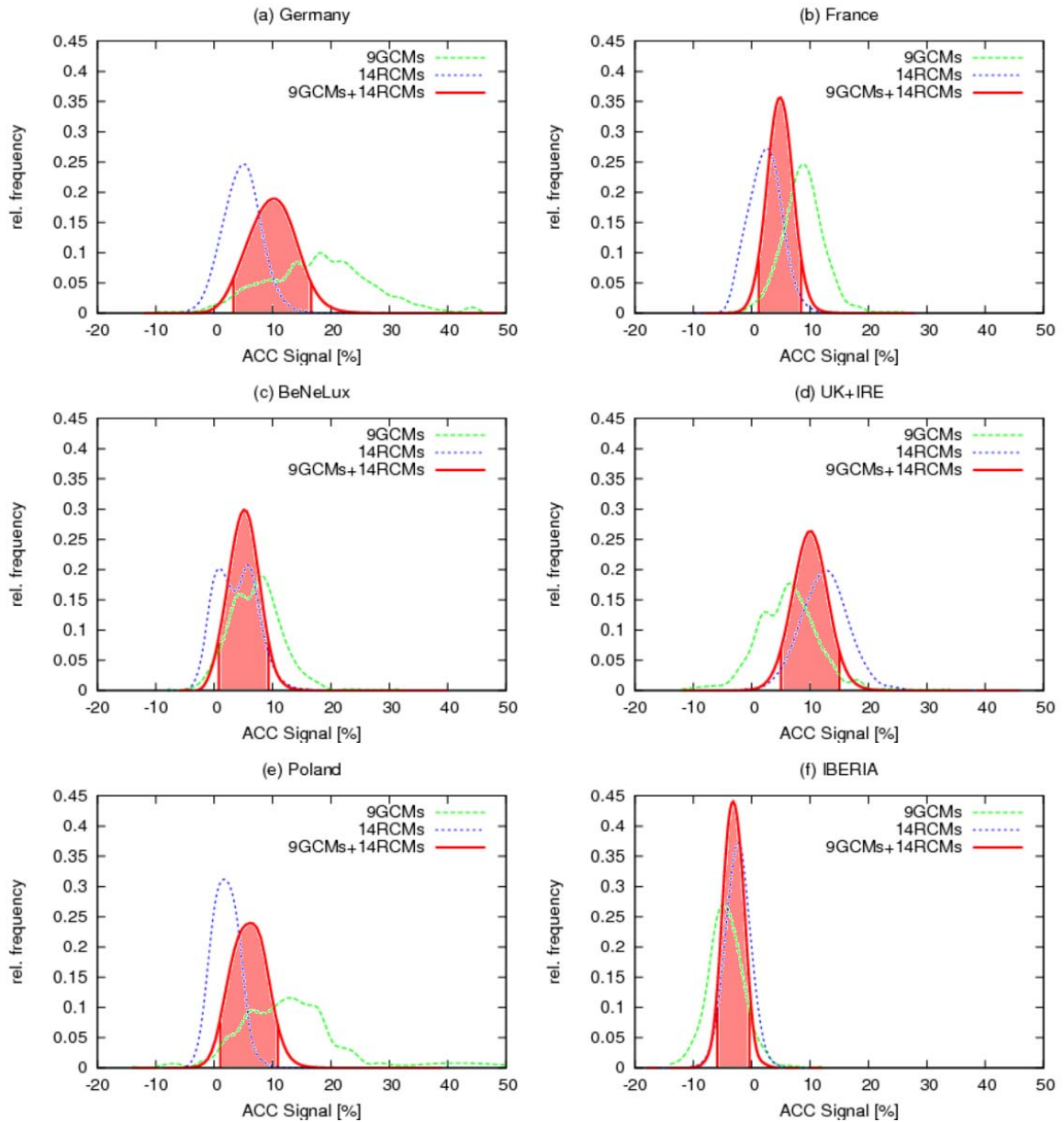


Figure AF6.1: Probability of loss potential changes for the future climate period in the middle of 21C (2021-2050) compared to 20C (1961-2000) without adaptation of the loss threshold, based on all possible model combinations of GCMs (green curve), RCMs (blue curve) and all available GCM and RCM scenario (red curve) simulations. The red shaded areas mark the range where 90% of the change signals (between 5th and 95th percentile) based on all model combinations are found.

Table AT6.1: ACC signal of simulated loss ratios in the individual GCMs. Relative changes for the considered future climate periods compared to the 20C simulations are presented (unit: percent). MEAN=signal of mean annual loss; STD=signal of interannual standard deviation of loss
a) 2071-2100 without adaptation

	Germany		France		UK		Iberia		Poland		Benelux	
	MEAN	STD	MEAN	STD	MEAN	STD	MEAN	STD	MEAN	STD	MEAN	STD
BCCR-BCM2	51,5%	26,6%	19,7%	1,6%	4,6%	-31,5%	8,4%	46,3%	14,3%	78,3%	4,5%	-3,0%
CNRM-CM3	43,1%	127,6%	5,0%	-58,7%	50,9%	134,3%	-5,1%	-43,1%	-0,9%	-39,0%	50,4%	280,7%
FUB-EGMAM	69,4%	261,6%	36,5%	49,0%	67,6%	119,5%	-17,5%	-54,5%	27,4%	91,2%	41,4%	172,5%
MPI-EH5OM1 r1	52,8%	215,3%	14,0%	21,4%	54,6%	152,3%	-10,5%	-18,2%	-7,6%	-43,0%	40,2%	560,5%
MPI-EH5OM1 r2	21,6%	50,9%	-3,0%	-10,3%	1,5%	15,9%	-12,5%	-15,7%	12,6%	-9,7%	18,8%	88,5%
MPI-EH5OM1 r3	17,0%	63,5%	9,8%	107,3%	4,5%	6,2%	0,8%	103,2%	4,8%	51,4%	-4,1%	-44,6%
DMI-EH5OM1	-6,2%	-47,1%	3,2%	13,4%	11,7%	-4,4%	-16,8%	-17,6%	3,9%	-50,0%	10,2%	47,7%
HC-HadGEM1	87,1%	99,9%	-7,6%	-53,2%	-22,1%	-76,3%	-24,2%	-28,0%	52,8%	37,2%	-4,3%	-33,5%
IPSL-CM4	3,4%	-11,7%	3,7%	17,8%	-16,5%	-56,0%	-13,3%	-27,5%	1,6%	-9,5%	1,3%	19,9%
Ensemble-Mean	37,7%	87,4%	9,0%	9,8%	17,4%	28,9%	-10,1%	-6,1%	12,1%	11,9%	17,6%	121,0%
\pm inter-model STD	\pm 31,0%	\pm 101,2%	\pm 13,2%	\pm 50,5%	\pm 32,3%	\pm 85,3%	\pm 10,0%	\pm 49,6%	\pm 18,3%	\pm 53,9%	\pm 21,2%	\pm 195,1%

b) 2071-2100 with adaptation

	Germany		France		UK		Iberia		Poland		Benelux	
	MEAN	STD	MEAN	STD	MEAN	STD	MEAN	STD	MEAN	STD	MEAN	STD
BCCR-BCM2	-6,5%	-42,4%	-12,3%	-48,7%	-21,6%	-66,8%	11,3%	75,2%	-2,0%	10,1%	-12,9%	-59,4%
CNRM-CM3	-10,8%	-9,6%	-15,2%	-76,1%	-3,7%	-8,1%	11,8%	-9,9%	-15,4%	-69,2%	4,8%	36,5%
FUB-EGMAM	12,5%	117,1%	7,0%	-1,7%	21,6%	35,8%	3,7%	-27,1%	1,1%	3,9%	9,1%	52,6%
MPI-EH5OM1 r1	7,0%	102,6%	-3,9%	-26,7%	6,3%	40,0%	0,7%	6,9%	-23,0%	-65,3%	15,3%	321,0%
MPI-EH5OM1 r2	-1,8%	12,1%	-7,8%	-16,1%	-16,1%	-17,0%	0,5%	13,2%	-3,9%	-33,0%	5,2%	28,2%
MPI-EH5OM1 r3	9,5%	54,4%	2,3%	84,3%	-2,9%	-11,7%	12,4%	120,4%	-1,2%	32,8%	-7,1%	-53,7%
DMI-EH5OM1	-22,6%	-61,2%	-5,3%	-7,9%	7,5%	-10,5%	0,4%	24,7%	-14,4%	-68,9%	-6,3%	-46,1%
HC-HadGEM1	-15,3%	-33,4%	-15,4%	-62,2%	1,1%	-24,2%	-5,2%	29,8%	2,9%	-23,7%	2,5%	52,9%
IPSL-CM4	16,8%	7,5%	30,8%	101,6%	-9,2%	-42,4%	25,1%	52,3%	-2,3%	-23,0%	8,3%	54,3%
Ensemble-Mean	-1,2%	16,3%	-2,2%	-5,9%	-1,9%	-11,7%	6,8%	31,7%	-6,5%	-26,2%	2,1%	42,9%
\pm inter-model STD	\pm 13,6%	\pm 63,0%	\pm 14,5%	\pm 61,4%	\pm 13,1%	\pm 33,7%	\pm 9,2%	\pm 45,2%	\pm 8,9%	\pm 37,0%	\pm 9,1%	\pm 114,9%

c) 2021-2050 without adaptation

	Germany		France		UK		Iberia		Poland		Benelux	
	MEAN	STD	MEAN	STD	MEAN	STD	MEAN	STD	MEAN	STD	MEAN	STD
BCCR-BCM2	14,5%	-10,1%	10,8%	10,0%	-0,8%	-35,7%	11,4%	69,9%	-13,4%	-68,3%	-0,9%	-9,9%
CNRM-CM3	19,8%	55,9%	3,1%	-51,8%	8,3%	17,8%	1,0%	-5,4%	-5,9%	-55,2%	16,9%	120,6%
FUB-EGMAM	7,1%	14,1%	-3,4%	-30,7%	19,6%	119,5%	-6,5%	-17,9%	17,4%	157,5%	5,3%	26,1%
MPI-EH5OM1 r1	45,5%	103,4%	26,5%	3,4%	33,7%	77,7%	-13,5%	-29,6%	17,3%	-16,6%	32,4%	254,6%
MPI-EH5OM1 r2	4,5%	7,1%	14,4%	119,7%	2,0%	31,6%	-6,9%	0,8%	10,1%	13,3%	9,7%	30,8%
MPI-EH5OM1 r3	-9,6%	-16,3%	2,5%	71,9%	1,6%	7,5%	-13,6%	-37,0%	11,1%	22,3%	-8,7%	-55,8%
DMI-EH5OM1	16,8%	-13,5%	6,6%	-7,6%	1,9%	-14,8%	3,7%	41,9%	53,3%	85,3%	1,4%	-9,3%
HC-HadGEM1	69,2%	156,8%	18,0%	36,0%	-12,7%	-61,6%	-11,2%	-27,6%	17,5%	-23,9%	4,8%	80,8%
IPSL-CM4	-6,1%	-10,5%	0,7%	-5,0%	3,0%	3,8%	-3,5%	-16,6%	2,2%	-15,4%	3,2%	62,9%
Ensemble-Mean	17,9%	31,9%	8,8%	16,2%	6,3%	16,2%	-4,3%	-2,4%	12,2%	11,0%	7,1%	55,6%
± inter-model STD	± 25,1%	± 61,4%	± 9,5%	± 52,7%	± 13,3%	± 55,5%	± 8,4%	± 35,7%	± 18,9%	± 71,1%	± 11,8%	± 91,5%

Table AT6.2: ACC signal of losses calculated in the individual RCM scenario simulations. Change signals AIB-20C without adaptation of the loss threshold for the 2 future periods in the middle (2021-2050) and at the end of 21C (2071-2100).
a) 2071-2100 without adaptation

	Germany		France		UK		Iberia		Poland		Benelux	
	MEAN	STD	MEAN	STD	MEAN	STD	MEAN	STD	MEAN	STD	MEAN	STD
C4I-RCA3_HCh	-2,8%	3,6%	-0,4%	-19,2%	7,3%	50,7%	-6,1%	-59,2%	-8,6%	-83,0%	3,7%	109,4%
HC-HadRM3_HCn	10,5%	78,1%	10,5%	109,7%	12,3%	99,6%	0,8%	45,4%	9,4%	82,9%	8,2%	281,4%
ETHZ-CLM_HCn	19,0%	65,6%	9,3%	16,7%	27,1%	202,3%	0,6%	32,3%	8,0%	101,5%	10,8%	93,6%
DMI-HIRHAM_C	2,5%	-22,2%	-2,1%	-21,5%	15,8%	84,9%	-7,8%	-25,7%	10,4%	67,2%	-1,7%	-23,4%
SMHI-RCA_B	17,6%	-6,2%	15,9%	99,1%	23,0%	57,3%	7,9%	125,7%	-1,7%	-24,0%	4,4%	10,6%
MPI-REMO_E5_3	5,3%	55,7%	0,0%	67,8%	0,9%	-24,1%	-3,5%	-34,4%	2,8%	13,2%	1,8%	81,2%
DMI-HIRHAM_E5_3	15,2%	34,1%	12,1%	39,0%	12,7%	-31,8%	-3,5%	-14,5%	19,6%	351,7%	9,1%	72,3%
KNMI-RACMO2_E5_1	54,8%	114,0%	8,7%	6,2%	63,6%	288,0%	-11,8%	8,3%	20,4%	20,0%	39,6%	252,2%
KNMI-RACMO2_E5_2	14,3%	26,7%	14,8%	37,8%	35,4%	10,2%	-5,1%	60,0%	-3,7%	-40,3%	9,9%	10,2%
KNMI-RACMO2_E5_3	33,6%	274,6%	-1,7%	-13,4%	8,5%	36,7%	-7,9%	-0,9%	14,1%	128,7%	4,3%	35,1%
SMHI-RCA_E5_3	-4,5%	-9,9%	-3,9%	-38,4%	-2,6%	-17,3%	-9,8%	-30,5%	-4,3%	-11,2%	-2,6%	-14,2%
Ensemble-Mean	15,1%	55,8%	5,7%	25,8%	18,5%	68,8%	-4,2%	9,7%	6,1%	55,2%	8,0%	82,6%
± inter-model STD	± 17,1%	± 83,8%	± 7,4%	± 49,9%	± 18,6%	± 99,1%	± 5,6%	± 53,0%	± 9,9%	± 117,6%	± 11,4%	± 101,2%

b) 2021-2050 without adaptation

	Germany		France		UK		Iberia		Poland		Benelux	
	MEAN	STD	MEAN	STD	MEAN	STD	MEAN	STD	MEAN	STD	MEAN	STD
C4I-RCA3_HCh	-1,7%	-32,1%	-1,8%	-30,6%	8,4%	41,4%	4,3%	-31,4%	-5,8%	-70,4%	1,9%	22,6%
HC-HadRM3_HCh	6,6%	26,5%	0,0%	-4,4%	9,0%	81,8%	-3,5%	-29,6%	6,7%	87,0%	5,7%	92,4%
METNO- HIRHAM_HCh	-11,7%	-57,9%	-10,4%	-39,5%	9,2%	79,9%	-7,6%	-15,1%	-4,5%	-47,8%	0,3%	31,2%
ETHZ-CLM_HCh	0,0%	-14,0%	1,4%	-7,1%	21,1%	122,0%	-4,5%	-23,9%	2,1%	7,1%	1,8%	6,4%
CNRM-RM4.5_C	1,9%	42,3%	0,4%	27,0%	1,8%	11,5%	1,1%	35,7%	2,2%	96,7%	0,4%	50,6%
DMI-HIRHAM_C	3,9%	-32,5%	0,8%	-3,1%	25,3%	49,3%	-2,0%	-13,1%	-0,9%	-16,7%	-0,9%	-10,4%
METNO-HIRHAM_B	-4,4%	-47,4%	-3,0%	-14,2%	15,5%	-3,6%	6,0%	24,5%	3,1%	44,8%	-3,8%	-62,7%
SMHI-RCA_B	19,9%	29,7%	16,8%	201,5%	25,1%	83,6%	12,7%	240,9%	-5,7%	-48,0%	5,0%	-15,7%
MPI-REMO_E5_3	0,1%	12,1%	-3,3%	4,4%	0,6%	-1,9%	-1,7%	-11,5%	5,5%	83,3%	-2,8%	-53,7%
DMI-HIRHAM_E5_3	11,9%	34,3%	-0,8%	-7,9%	2,6%	-37,3%	-3,7%	-13,2%	1,9%	39,3%	2,8%	74,8%
KNMI- RACMO2_E5_1	32,1%	5,0%	9,4%	-1,7%	45,5%	154,3%	-18,0%	-45,1%	24,1%	89,0%	40,7%	167,3%
KNMI- RACMO2_E5_2	2,3%	-8,1%	28,2%	151,0%	21,9%	7,4%	0,5%	22,4%	-8,3%	-46,9%	15,4%	45,5%
KNMI- RACMO2_E5_3	11,4%	150,3%	-0,9%	23,6%	-0,5%	1,3%	-8,1%	-27,6%	6,6%	56,1%	-4,9%	-13,0%
SMHI-RCA_E5_3	-5,5%	-11,0%	-4,4%	-14,2%	-10,4%	-29,0%	-8,5%	-28,1%	0,4%	-8,0%	-8,9%	-43,4%
Ensemble-Mean ± inter-model STD	± 4,8%	± 6,9%	± 2,3%	± 20,3%	± 12,5%	± 40,0%	± -2,3%	± 6,1%	± 2,0%	± 19,0%	± 3,8%	± 20,8%
	± 11,2%	± 51,7%	± 9,8%	± 69,0%	± 14,3%	± 57,4%	± 7,4%	± 71,6%	± 8,0%	± 59,2%	± 12,1%	± 62,9%

7. Conclusions and Outlook

The thesis is concluded by briefly answering the set of *research questions* raised in the introduction. Moreover, some general points are discussed regarding the range of results based on multi-model studies and the representation of wind storms in climate model simulations, leading to an outlook on unresolved issues which may be interesting topics for future research. The specific results of the individual studies are discussed in their own context within each chapter (i.e. journal paper).

7.1. Conclusions

What are preferred atmospheric conditions for the occurrence of (Central) European winter storms? Do state-of-the-art climate models have the capacity to reproduce observed atmospheric characteristics relating to storms?

Examinations based on ERA40-reanalysis data reveal that the majority of storm days in Central Europe are associated with westerly flow regimes (about 80%) and with a positive NAO phase (about 60%), the latter being computed on a daily basis. Strong positive NAO phases (daily NAO index greater than 1.5) occur relatively seldom (only 6.4% of all days), but have a share of more than 20% of the storms. While storm days with W flow are of highest relevance in terms of their frequency, storm days with NW flow seem to be of highest relevance in terms of their intensity: highest wind speeds during storm days over (Central European) inland areas and also over the North Sea occur for storm days in this class. The most frequent pathway of cyclone systems associated with storms over Central Europe leads from the North Atlantic over the British Isles, North Sea and southern Scandinavia into the Baltic Sea. The mean intensity of the systems typically reaches its maximum near the British Isles.

The GCM simulations for the present-day period (20C) are basically capable of reproducing the observed (ERA40) circulation patterns and CWT frequencies for central Europe during the extended winter season. A typical limitation of most models, however, is an excess of zonal (westerly) flow situations and an underestimation of anticyclonic flow. Although peculiarities are found for some models, in ensemble mean the frequency of storm events as well as their distribution over flow classes is simulated realistically. Agreement with observational data is also found for simulated patterns of wind speeds and characteristics of the associated cyclones during storm days.

How do atmospheric features related to wind storms respond to increased GHG concentrations in the climate model simulations?

This question is investigated on the basis of future scenario (SRES A1B) simulations with GCMs, regarding changes in large-scale flow (circulation weather types, CWTs) as well as focussing on the frequency and intensity of extra-tropical cyclones. In the majority of considered models, and also in ensemble mean, an enhanced frequency of westerly flow over Central Europe is found during winter. The number of extratropical cyclone tracks is largely reduced under future climate conditions in the northern hemisphere, whereas with regard to extreme cyclones (here: the strongest 5 % of systems), a hotspot showing increased frequency of these strong systems is found over the eastern North Atlantic.

Focussing on Central Europe, there is an increase in the frequency of storm days in future scenario simulations for the end of the 21st century. Applying two different criteria of storm days, the ensemble mean increase is between 19 and 33 %. Looking at cyclones associated with storm days in Central Europe, an accentuation on the pathway from the North Atlantic over the British Isles, North Sea and to Scandinavia is found, and their intensity is increased by about 10 % in ensemble mean in the Eastern Atlantic, near the British Isles and in the North Sea. The mean wind speeds during storm events increase significantly over large parts of Central Europe by about 5%. Increased wind speeds associated with storm events are even found for the one outlier model showing reduced frequency of storm days.

The detected increased frequency of storm days is disproportionately high compared to the related CWT changes and is thus only partly explained by the changed frequency of flow classes. Another contribution comes from a higher ratio of storm days during days with westerly flow.

What is the consequence of increased GHG forcing on the occurrence of extreme wind speeds in Europe?

As a measure of extreme wind speeds, the local 98th percentile of simulated daily maximum wind speeds during the extended winter period ONDJFM was considered. At each grid box, this wind speed value is exceeded on average during about 4 days per winter half year. It thus marks the windiest 2% of days at each location. In line with the signals described above (increased cyclone intensity and occurrence of extreme cyclones over northwest Europe, and increased number of gale days in Central Europe),

extreme wind speed values are also increased over northern parts of western, central and eastern Europe in the future scenario simulations of most models and in ensemble mean (up to 5%). Over southern Europe and the Mediterranean region, extreme wind speed values are generally reduced. These change patterns are basically found for most of the considered models. With respect to the location of the strongest and most significant signals, and signals magnitudes, considerable inter-model differences are apparent.

How do loss potentials due to severe wind storms change under future ACC conditions?

Consistent with the wind speed signals, increased storm loss potentials are found over the northern parts of western, central and eastern Europe for the case where no adaptation to a changed wind climate is taken into account (i.e. the 98th percentile of the recent climate simulations is also used as the loss threshold for future scenario simulations). Owing to the cubic relation between losses and wind speeds, the magnitude of the loss signals is considerably greater than that of the wind signals. Applying a loss regression model, storm losses are calculated for different European countries. In ensemble mean, loss potentials towards the end of the 21st century are increased by 37.7% (15.1%) in Germany based on the considered GCM (RCM) simulations. Mean losses for UK and Ireland are found to increase by 17.4% (18.5%), by 9.0% (5.8%) for France, by 17.6% (8.0%) in the Benelux countries and by 12.1% (6.1%) over the area of Poland. Representatively for southern Europe, losses were calculated for the Iberian Peninsula (i.e. Spain and Portugal). Here, in accordance with the reduction in extreme wind speeds, reduced risk of storm losses by -10.1% (-4.2%) is found in the GCM (RCM) ensemble. Taking adaptation into account (i.e. using the 98th percentile from the future simulations as the threshold for future loss calculations), the change signals are generally small.

How robust are the identified ACC signals concerning the changes in the different individual simulations? What are suitable measures of uncertainty? How large is the uncertainty of the signals?

With regard to the change signals in the different analyses (large-scale flow, storm days, extreme cyclones, extreme wind speeds, storm loss potentials), a large spread between the individual ensemble members is apparent. Considerable differences are found not only with respect to the signal magnitudes, partly even signals of contrary sign are analysed. Further, in addition to the inter-model differences, the results reveal a

considerable spread even for different realisations with the same climate model, highlighting the large long-term variability in severe storm occurrence. The characteristic of the change signals described above is similar for the majority of considered model simulations (in total 9 GCM and 14 RCM simulations); generally only one or two outliers reveal contrary signals.

Two different measures are applied to provide an estimation of the uncertainty of the ACC signals. First, uncertainty ranges are calculated by considering the standard deviations between the change signals in the different simulations. Secondly, applying multi-model combinatorics, a new measure has been developed which takes into account the signals from all possible model combinations that can be constructed from the available climate simulations. Thus, a large number of sub-ensembles is obtained (e.g. 9 individual simulations allow for 511 different sub-ensembles), resulting in a relatively symmetric distribution of possible change signals around the ensemble mean, and further enabling the provision of probabilistic information about the range of expected changes.

Uncertainty measured in terms of the inter-model standard deviation is strongly influenced by outlier signals. Thus, the fact that some individual models reveal fundamentally different signals compared to most of the other models leads to the large uncertainty ranges according to the first measure, generally in a magnitude similar to that of the signal itself. The uncertainty range estimated based on the multi-model combinatorics approach is considerably smaller, as the outlier signals of individual models affect only a few sub-ensembles and are compensated in the majority of the model combinations. For example, considering the storm loss potential ACC signal for Germany based on the 9 GCM simulations, mean annual losses at the end of the 21st century are found to have increased by 37.7 (± 31.0) % using the inter-model standard deviation as an uncertainty measure. In comparison, the respective confidence interval from the range covering 90% of all 511 possible results is considerably sharper; the mean change signal for Germany is 37.7 (± 19.7) %.

What is the benefit of combining different climate simulations into a MME?

MMEs sample different types of uncertainties (in particular model uncertainties and uncertainties due to internal variability). With respect to the performance in reproducing observed storm losses, this thesis demonstrates that the performance of the ensemble mean is comparable to the best single model, even if weak performing models are

included. Thus, the largest benefit of MMEs can be seen in their consistently high performance. This is particularly important as with regard to climate simulations, in many cases it is difficult to measure the performance of the individual models. Hence, the results presented suggest that large MMEs consisting of as many available models as possible should be used in order to obtain the best results.

With respect to an estimation of climate change signals, the spread of signals from the different ensemble members allows for an estimation of the robustness of the identified signal.

What influence do different ways of constructing the ensemble (e.g. model selection, weighting) have on MME performance, and on possible change signals?

With regard to the MME performance, it was documented that sub-ensembles leaving out the weaker models (i.e. corresponding to a strong weighting of the better models) might lead to a slightly improved quality of the results, in some cases better than the performance of the best single model. As demonstrated on the example of storm loss calculations, however, such a weighting approach yields only a marginal improvement compared to the inclusion of all models, rather supporting the use of large (unweighted) ensembles. The results presented suggest that the more models are included in the ensemble, the higher is the obtained consistency of performance: for larger ensemble sizes the spread between the best and the weakest performing model combinations becomes considerably lower. Thus, the use of a large MME should be a good choice for obtaining stable and reliable results.

For the estimation of change signals in future scenario simulations, in the cases considered, weighting approaches favouring the models which more accurately reproduce observed climate conditions (or excluding the weakest model) lead to similar ensemble mean signals, but also to a higher significance (i.e. reduced uncertainty) in climate change signals. This result is explained by the fact that for the specific applications considered, the outlier model with respect to the climate change signal is generally a rather weak performing model in terms of reproducing the recent climate. While it is generally recommended to include as many models as possible, this finding suggests that for some applications it might be beneficial to exclude models if they reveal obvious deficiencies. In most cases it is, however, difficult to derive reliable performance measures for the models, as generally the quality metric depends strongly

on the considered variables (Reichler and Kim, 2008) and time periods (Reifen and Toumi, 2009).

What are the benefits and shortcomings of using regional climate models (RCMs) for extreme wind analysis and storm loss calculations?

This question is dealt with on the basis of reanalysis-driven RCM simulations, enabling a comparison with observed storm losses. Dynamical downscaling with regional climate models (RCMs) is generally applied to obtain atmospheric information at high spatial resolution. In particular, physical processes acting on scales not resolved by the driving large-scale models can influence simulated regional wind patterns, and the influence of regional orographic characteristics is also taken into account.

Analysis of RCM wind fields reveals model-specific structures particularly over mountainous regions: some models show local wind speed maxima over complex terrain, others local minima, whereas the large-scale driving reanalysis data systematically show local wind speed minima in these regions. A sound validation against wind speed measurements is difficult, because speed values in the climate models are representative for the whole grid box, including e.g. valleys and crests, whereas mountain weather stations are often located on mountain peaks.

With respect to storm loss calculations in comparison to observed loss data, a distinct benefit from dynamical downscaling could be shown. For both the best performing models (driven by reanalysis data) and the RCM ensemble mean, it was possible to obtain considerably higher correlations with observed losses than for losses calculated on the basis of large-scale reanalysis data directly. This finding suggests that the high-resolution RCMs seem to exceed the value of assimilation in the driving data for the area considered. All considered RCMs fail in realistically simulating one particular major event. This failure, however, seems to be due to the inaccurate capture of tropospheric conditions in the reanalysis data for the early 1970's, and hence points more to a limitation of the large-scale driving data, rather than a limitation of the RCMs. The benefits of dynamical downscaling are thus partly masked by the failure with regard to this specific event, and become more obvious, if this event is excluded from the considerations.

Does dynamical downscaling provide any additional information about ACC signals?

The spatial patterns of the extreme wind speeds change signal are generally close to the change pattern of the driving GCM. When looking at the change signal magnitudes, however, dynamical downscaling using RCMs is shown to increase the range of computed change signals compared to the large-scale results. Different RCMs with identical large-scale driving show comparable spatial change patterns of extreme wind speeds, though the magnitudes differ considerably. Consequently, even changes to loss potential reveal substantially different magnitudes.

From an ensemble mean perspective, for most regions the RCM ensemble signals are smaller than those from the GCM ensemble. This effect is apparent regarding both, extreme wind speeds as well as calculated losses. Excluding contributions coming from different ensemble constructions (owing to model output availability, for example), this effect might partly be explained by the rather spotty change signals of extreme wind speed patterns in the individual RCMs. At the same time, the magnitude of the (spotty) RCM signals is generally not greater than the magnitude of the (smooth) GCM signals and consequently the different RCM signals affect partly different regions and may therefore partially compensate in the ensemble mean. This may contribute to the finding that the RCM ensemble changes over Central Europe are comparatively lower than in most of the individual models, and also in the GCM ensemble. Further, with respect to loss potentials, due to the spotty RCM wind changes, a smaller area is affected by changed loss potentials in comparison to the relatively smooth change patterns of the GCM wind fields. The differences between the RCM and GCM signals should, however, be investigated more detailed in future studies.

Thus, for all considered regions the RCM ensemble signals generally correspond to the GCM signals, although for most regions the signal magnitudes are somewhat smaller in the RCM ensemble. For example, loss potentials in Germany are found to increase by 37.7% (15.1%) in the GCM (RCM) ensemble for the end of the 21st century.

7.2. Discussion and Outlook

It is likely that the considered multi-model simulations do not span the whole range of possible future developments. This is partly explained by the fact that members of a multi-model ensemble often share common systematic errors (Lambert and Boer, 2001). Such limitations may imply that distributions of climate responses from ensemble

simulations are themselves subject to uncertainty (Smith, 2002). Further, future scenario simulations have to be understood as conditional relations, i.e. the reaction of the climate system to a predefined forcing scenario (e.g. Nakićenović et al., 2000) is investigated. In this thesis, only one scenario is considered (SRES A1B) which assumes rather moderate GHG emissions during the 21st century. Observed GHG concentrations during the recent years, however, indicate considerable higher emissions, even higher than assumed in the worst-case scenarios (SRES A1F, A2). For the case that this development continuous, even stronger climate change signals than identified in this thesis should be expected. With regard to changes in extreme cyclones, wind speeds and also storm losses, Pinto et al. (2007a,b), for example, found that the intensity of the changes is in turn largely dependent on the intensity of the forcing.

Extra-tropical cyclones are generally connected to complex mesoscale features, such as frontal structures including subsynoptic-scale circulations, for example, or warm and cold conveyor belts (cf. Bosart et al., 1998; Wakimoto and Bosart, 2001; Roberts and Forbes, 2002; Forbes and Clark, 2003). Even sting jets can sometimes be observed, leading to extraordinarily high wind speeds at ground level (Browning and Field, 2004; Clark et al., 2005). Yet, using numerical models, those mesoscale dynamic and thermodynamic structures are only studied in some high-resolution case studies (e.g. Han et al., 2007; Kuwano-Yoshida and Asuma, 2008). Climate timescale integrations are generally still performed in spatial resolutions not resolving the mesoscale structure of frontal zones (e.g. Bauer and Del Genio, 2006). Thus, the small-scale characteristics of atmospheric features associated with storms are obviously not captured by the models analysed in this thesis, and one criticism may be that the climate models may not be completely realistic in simulating windstorms. Furthermore, processes relating to wind gusts are generally not resolved by the climate models, and thus – if gusts are calculated at all – they are subject to parameterisations (e.g. Schrodin, 1995; Brasseur, 2001; Goyette et al., 2003; White et al., 2003). Ongoing research and increasing computation power may allow for a more realistic simulation of these mesoscale processes in the future.

Due to these deficiencies, state-of-the-art climate models are not necessarily simulating realistic absolute values of wind speeds. For investigating the impacts of extreme wind events, it thus seems appropriate to use relative thresholds (as was done in this thesis). This approach is based on the assumption that at least the shape of the simulated wind

speed distribution is comparable to observations, even if the scale might be different (Thiele, 2008).

As shown in this thesis, the synoptic-scale atmospheric characteristics related to wind storms are well captured by the climate models. The (synoptic-scale) physical processes involved in cyclone development were not investigated in this thesis, but should be addressed in future studies. After analysing partly different model responses to increased GHG forcing with respect to winter storms and associated atmospheric circulation features in the different models, it will be necessary to examine reasons and investigate processes which lead to the different model behaviour. In particular, atmospheric conditions favouring the intensification of cyclones should be considered in the different models. Understanding the different behaviours of the individual models may help to identify and quantify the most important changes in atmospheric conditions explaining the identified signals with respect to European storminess. A contribution might also come from different characteristics of the ocean models. Recently, Pinto et al. (2009) investigated atmospheric growth factors associated with explosively deepening cyclones over the Atlantic. With respect to the increased cyclone intensity close to Europe, they found for one particular model (ECHAM5) contributions from increased values of baroclinicity, upper-tropospheric divergence and latent heating during the maximum deepening phase of the cyclones under ACC conditions, and an intensification of the jet stream close to Europe. Further, factors influencing the tracks of the cyclones should be investigated in detail in order to explain, for example, the accentuation of cyclones associated with storm events in Central Europe on a rather narrow “highway”, which was identified in this thesis.

Another issue is to examine and specify the detected differences of the change signal magnitudes between the RCM and GCM simulations found for extreme wind speeds and losses in some particular regions. In detail, effects related to RCM signals as compared to the large-scale results will have to be understood from future studies.

Further, availability of high-resolution insurance loss data allows for an improvement of the storm loss model. Increased accuracy of the loss estimations will permit more specific estimations of future risk changes, in particular considering changes on a more regional scale.

Bibliography

- Alcamo, J., J.M. Moreno, B. Nováky, M. Bindi, R. Corobov, R.J.N. Devoy, C. Giannakopoulos, E. Martin, J.E. Olesen, A. Shvidenko, 2007: Europe. Climate Change 2007: Impacts, Adaptation and Vulnerability. Contribution of Working Group II to the Fourth Assessment Report of the Intergovernmental Panel on Climate Change, M.L. Parry, O.F. Canziani, J.P. Palutikof, P.J. van der Linden and C.E. Hanson, Eds., Cambridge University Press, Cambridge, UK, 541-580.
- Alexandersson H, Tuomenvirta H, Schmith T, Iden K. 2000. Trends of storms in NW Europe derived from an updated pressure data set. *Clim Res* 14, 71-73
- Barring L, von Storch, H. 2004. Scandinavian storminess since about 1800. *Geophys. Res. Lett.* 31, L20202, doi:10.1029/2004GL020441
- Benedict JJ, Lee S, Feldstein SB. 2004. A synoptic view of the North Atlantic Oscillation. *J. Atmos. Sci.* 61:121-144
- Bengtsson L, Hodges KI, Roeckner E. 2006. Storm Tracks and Climate Change. *Journal of Climate* 19 : 3518-3543
- Berliner Wetterkarte, published by Verein BERLINER WETTERKARTE e.V., ISSN 0177-3984, <http://www.berliner-wetterkarte.de>
- Blessing S, Fraedrich K, Junge M, Kunz T, Lunkheit F. 2005. Daily North-Atlantic Oscillation (NAO) index: statistics and its stratospheric polar vortex dependence. *Meteorol. Z.* 14:763–769
- Bosart LF, Bracken WE, Seimon A. 1998. A study of cyclone mesoscale structure with emphasis on a large-amplitude inertia-gravity wave. *Monthly Weather Review*, 126, 1497-1527
- Brasseur O. 2001. Development and Application of a Physical Approach to Estimating Wind Gusts. *Mon Weather Rev*, 129: 5-25
- Browning KA, Field M. 2004. Evidence from Meteosat imagery of the interaction of sting jets with the boundary layer. *Meteorological Applications*, 11, 277-289.
- Bubnova R, Hello G, Benard P, Geleyn JF. 1995. Integration of the fully elastic equations cast in the hydrostatic-pressure terrain-following coordinate in the framework ARPEGE/ALADIN NWP System. *Mon Weather Rev*, 123: 515-535
- Buishand A, Brandsma T. 1997. Comparison of circulation classification schemes for predicting temperature and precipitation in the Netherlands. *Int. J. Climatol.* 17: 875-889
- Busch U, Beckmann BR, Roth R. 1998. Study of storm weather situations in observation and ECHAM3/T42 model simulation. *Tellus* 50A : 411-423.

- Cappel A, Emmerich P. 1975. Zwei Wetterkatastrophen des Jahres 1972: Der Niedersachsen-Orkan und das Gewitterunwetter von Stuttgart, Reports of the German weather service, 135, Offenbach.
- Carnell RE, Senior CA, Mitchell JFB. 1996. An assessment of measures of storminess: simulated changes in northern hemisphere winter due to increasing CO₂. *Clim. Dyn.* 12, 467-476
- Carnell RE, Senior CA. 1998: Changes in mid-latitude variability due to increasing greenhouse gases and sulphate aerosols. *Clim. Dyn.*, 14, 369–383.
- Center for International Earth Science Information Network (CIESIN), Columbia University; and Centro Internacional de Agricultura Tropical (CIAT) (2005) Gridded Population of the World Version 3 (GPWv3): Population Density Grids. Palisades, NY: Socioeconomic Data and Applications Center (SEDAC), Columbia University. Available at <http://sedac.ciesin.columbia.edu/gpw>. (date of download 2006-08-14).
- Christensen JH, Boberg F, Christensen OB, Lucas-Picher P. 2008. On the need for bias correction of regional climate change projections of temperature and precipitation. *Geophysical Research Letters* 35(L20709): doi:10.1029/2008GL034949.
- Christensen JH, Carter TR, Rummukainen M, Amanatidis G, 2007b. Evaluating the performance and utility of regional climate models: the PRUDENCE project, *Climatic Change*, 81:1–6, DOI 10.1007/s10584-006-9211-6
- Christensen JH, Christensen OB, Lopez P, van Meijgaard E, Botzet B (1996) The HIRHAM4: Regional atmospheric climate model. DMI Scientific Report 96-4.
- Christensen JH, Hewitson B, Busuioc A, Chen A, Gao X, Held I, Jones R, Kolli RK, Kwon WT, Laprise R, Magaña Rueda V, Mearns L, Menéndez CG, Räisänen J, Rinke A, Sarr A, Whetton P Regional Climate Projections. In: *Climate Change 2007: The Physical Science Basis. Contribution of Working Group I to the Fourth Assessment Report of the Intergovernmental Panel on Climate Change* [Solomon, S., Qin, D., Manning, M., Chen, Z., Marquis, M., Averyt, K. B., Tignor, M., and Miller, H. L. (eds.)]. Cambridge University Press, Cambridge, United Kingdom and New York, NY, USA, 2007.
- Clark PA, Browning KA, Wang C. 2005. The sting at the end of the tail: Model diagnostics of fine-scale three-dimensional structure of the cloud head. *Quarterly Journal of the Royal Meteorological Society*, 131, 2263-2292.
- Collins M, Booth BBB, Harris GR, Murphy JM, Sexton DMH, Webb MJ, 2006: Towards quantifying uncertainty in transient climate change. *Clim. Dyn.*, 27, 127–147.
- Collins M. 2007. Ensembles and probabilities: a new era in the prediction of climate change. *Philosophical Transactions of the Royal Society A* 365, 1957-1970

- Collins M, Booth BBB, Bhaskaran B, Harris GR, Murphy JM, Sexton DMH, Webb MJ. 2009. Climate model errors, feedbacks and forcings: A comparison of perturbed physics and multi-model ensembles. *Climate Dynamics* (submitted).
- Cornford SG. 2002. Human and economic impacts of weather events in 2001. *WMO Bull*, 51, 257–277.
- Coppin P, Bradley E, Finnigan J. 1994. Measurements of Flow over an Elongated Ridge and its Thermal Stability Dependence: the Mean Field. *Boundary-Layer Meteorol* 69: 173-199.
- D'Andrea F, Tibaldi S, Blackburn M, Boer G, Déqué M, Dix MR, Dugas B, Ferranti L, Iwasaki T, Kitoh A, Pope V, Randall D, Roeckner E, Straus D, Stern W, Van den Dool H, Williamson D. 1998. Northern Hemisphere atmospheric blocking as simulated by 15 atmospheric general circulation models in the period 1979-1988. *Climate Dynamics* 14(6) : 385-407.
- Della-Marta PM, Mathis H, Frei C, Liniger MA, Kleinn J, Appenzeller C. 2009a. The return period of wind storms over Europe. *Int. J. Climatol.* 29: 437-459 doi: 10.1002/joc.1794
- Della-Marta PM, Pinto JG. 2009b. The statistical uncertainty of changes in winter storms over the North Atlantic and Europe in an ensemble of transient climate simulations. *Geophys Res Lett* 36:L14703, doi:10.1029/2009GL038557
- Della-Marta PM, Liniger MA, Appenzeller C, Bresch DN, Koellner-Heck P, Muccione V. 2009c. Improved estimates of the European winter wind storm climate and the risk of reinsurance loss using climate model data. *Journal of Applied Meteorology and Climatology*, (revised).
- Demuzere M, Werner M, van Lipzig NPM., Roeckner E. 2008. An analysis of present and future ECHAM5 pressure fields using a classification of circulation patterns. *Int. J. Climatol.* in press doi: 10.1002/joc.1821
- Déqué M, Rowell DP, Luthi D, Giorgi F, Christensen JH, Rockel B, Jacob D, Kjellstrom E, de Castro M, van den Hurk B. 2007. An intercomparison of regional climate simulations for Europe: assessing uncertainties in model projections, *Climatic Change* 81 : 53-70.
- Donat, MG, Leckebusch, GC, Pinto, JG, Ulbrich, U. 2009: Examination of Wind Storms over Central Europe with respect to Circulation Weather Types and NAO phases. *International Journal of Climatology* in press doi: 10.1002/joc.1982, chapter 2 in this thesis.
- Donat MG, Leckebusch GC, Pinto JG, Uwe U. 2010a. European storminess and associated circulation weather types: future changes deduced from a multi-model ensemble of GCM simulations. *Climate Research* (in press) chapter 3 in this thesis.
- Donat, MG, Leckebusch GC, Wild S, Ulbrich U. 2010b: Benefits and limitations of regional multi-model ensembles for storm loss estimations. *Climate Research*. (submitted, revised), chapter 5 in this thesis.

- Dorland C, Tol RS J, Palutikof J. 1999. Vulnerability of the Netherlands and Northwest Europe to storm damage under climate change. *Clim Change* 43: 513–535
- Döscher, R, Willen U, Jones C, Rutgerson A, Meier HE, Hansson U, Graham LP. 2002. The development of the coupled regional ocean-atmosphere model RCAO. *Boreal Environ Res* 7: 183-192
- Efron B. 1979. Bootstrap Methods: Another Look at the Jackknife. *The Annals of Statistics* 7 (1), 1-26.
- Fink AH, Brücher T, Ermert E, Krüger A, Pinto JG. 2009. The European Storm Kyrill in January 2007: Synoptic Evolution, Meteorological Impacts and Some Considerations with Respect to Climate Change. *Nat Hazards Earth Syst Sci* 9: 405-423.
- Fink AH, Brücher T, Leckebusch GC, Krüger A, Pinto JG, Ulbrich U. 2004. The 2003 European summer heatwaves and drought—synoptic diagnosis and impacts. *Weather*, 59, 209–216.
- Forbes RM, Clark PA. 2003. Sensitivity of extratropical cyclone mesoscale structure to the parametrization of ice microphysical processes. *Quarterly Journal of the Royal Meteorological Society*, 129, 1123-1148.
- Furevik T, Bentsen M, Drange H, Kindem IKT, Kvamsto NG, Sorteberg A. 2003. Description and evaluation of the Bergen climate model: ARPEGE coupled with MICOM. *Clim. Dyn.* 21 : 27-51.
- Furrer R, Knutti R, Sain SR, Nychka DW, Meehl GA. 2007. Spatial patterns of probabilistic temperature change projections from a multivariate Bayesian analysis. *Geophys. Res. Lett.*, 34, L06711
- Gastineau G and Soden BJ, 2009. Model projected changes of extreme wind events in response to global warming, *Geophys. Res. Lett.*, 36, L10810, doi:10.1029/2009GL037500.
- GDV, 2006. Yearbook 2006 – The German Insurance Industry, published by: Gesamtverband der Deutschen Versicherungswirtschaft e.V. (German Insurance Association), www.gdv.de
- GDV, 2009. Yearbook 2009 – The German Insurance Industry, published by: Gesamtverband der Deutschen Versicherungswirtschaft e.V. (German Insurance Association), www.gdv.de
- Geng Q, Sugi M. 2003. Possible change of extratropical cyclone activity due to enhanced greenhouse gases and sulfate aerosols—study with a high-resolution AGCM. *J. Climate*, 16, 2262–2274.
- Gibelin AL, Déqué M. 2003. Anthropogenic climate change over the Mediterranean region simulated by a global variable resolution model. *Clim.Dyn.*, 20, 327-339.
- Giorgi F, Francisco R, 2000. Uncertainties in regional climate change prediction: a regional analysis of ensemble simulations with the HADCM2 coupled AOGCM. *Climate Dynamics*, 16, 169-182

- Goodess CM, Palutikof JP. 1998. Development of daily rainfall scenarios for southeast Spain using a circulation-type approach to downscaling. *Int. J. Climatol.* 10, 1051-1083
- Goyette S, Brasseur O, Beniston M. 2003. Application of a new wind gust parameterization: Multiscale case studies performed with the Canadian regional climate model. *Journal of Geophysical Research – Atmospheres*, 108 (D13), Article Number 4374.
- Hagedorn R, Doblas-Reyes FJ, Palmer TN. 2005. The rationale behind the success of multi-model ensembles in seasonal forecasting - I. Basic concept, *Tellus* 57 : 219-233, doi 10.1111/j.1600-0870.2005.00103.x
- Han M, Rauber RM, Ramamurthy MK, Jewett BF, Grim JA. 2007. Mesoscale dynamics of the trough and warm-frontal regions of two continental winter cyclones. *Monthly Weather Review*, 135, 1647-1670.
- Harris GR, Sexton DMH, Booth BBB, Collins M, Murphy JM, Webb MJ, 2006: Frequency distributions of transient regional climate change from perturbed physics ensembles of general circulation model simulations. *Clim. Dyn.*, 27, 357–375.
- Heneka P, Hofherr T, Ruck B, Kottmeier C. 2006. Winter storm risk of residential structures- model development and application to the German state of Baden-Württemberg. *Nat Hazards Earth Syst Sci*, 6: 721-733
- Hess P, Brezowsky H. 1969. Katalog der Großwetterlagen Europas, 3. Aufl, Berichte des Deutschen Wetterdienstes Nr. 113, Vol. 15, 2nd edn., Deutscher Wetterdienst, Offenbach am Main, 70pp. (In German.)
- Hewitt, CD. 2005. The ENSEMBLES Project: Providing ensemble-based predictions of climate changes and their impacts. *EGGS newsletter*, 13, 22-25
- Huebener H, Cubasch U, Langematz U, Spanghel T, Niehörster F, Fast I, Kunze M. 2007. Ensemble climate simulations using a fully coupled ocean-troposphere-stratosphere GCM. *Phil. Trans. Royal Soc. Series A* 365 : 2089-2101
- Hulme M, Jones PD. 1991. Temperatures and windiness over the United Kingdom during the winters of 1988/89 and 1989/1990 compared with previous years. *Weather* 46: 126-136
- Hurrell JW. 1995. Decadal trends in the North Atlantic Oscillation: regional temperatures and precipitation. *Science* 269:676–679
- IPCC, 2007a: Summary for Policymakers. In: *Climate Change 2007: The Physical Science Basis. Contribution of Working Group I to the Fourth Assessment Report of the Intergovernmental Panel on Climate Change* [Solomon, S., D. Qin, M. Manning, Z. Chen, M. Marquis, K.B. Averyt, M. Tignor and H.L. Miller (eds.)]. Cambridge University Press, Cambridge, United Kingdom and New York, NY, USA.
- IPCC, 2007b: Summary for Policymakers. In: *Climate Change 2007: Impacts, Adaptation and Vulnerability. Contribution of Working Group II to the Fourth Assessment Report of the*

- Intergovernmental Panel on Climate Change, M.L. Parry, O.F. Canziani, J.P. Palutikof, P.J. van der Linden and C.E. Hanson, Eds., Cambridge University Press, Cambridge, UK, 7-22.
- Jacob D, Podzun R. 1997. Sensitivity studies with the regional model REMO. *Meteor and Atmos Phys* 63: 119-129
- Jacob D. 2001. A note to the simulation of the annual and inter-annual variability of the water budget over the Baltic Sea drainage basin. *Meteorol Atmos Phys*, 77:61-73
- Jaeger EB, Anders I, Lüthi D, Rockel B, Schär C, Seneviratne SI. 2008. Analysis of ERA40-driven CLM simulations for Europe. *Meteorologische Zeitschrift* 17: 349-367.
- Jenkinson AF, Collison FP. 1977. An Initial Climatology of Gales over the North Sea, Synoptic Climatology Branch Memorandum no. 62, Meteorological Office, Bracknell (unpublished.) Available from the National Meteorological Library, Meteorological Office, Bracknell.
- Johns TC, Durman CF, Banks HT, Roberts MJ, McLaren AJ, Ridley JK, Senior CA, Williams KD, Jones A, Rickard GJ, Cusack S, Ingram WJ, Crucifix M, Sexton DMH, Joshi MM, Dong BW, Spencer H, Hill RSR, Gregory JM, Keen AB, Pardaens AK, Lowe JA, Bodas-Salcedo A, Stark S, Searl Y. 2006. The new Hadley Centre Climate Model (HadGEM1): Evaluation of coupled simulations. *J Climate* 19 : 1327-1353
- Jones PD, Hulme M, Briffa KR. 1993. A comparison of Lamb circulation types with an objective classification scheme. *Int. J. Climatol.* 13: 655-663.
- Jones RG, Murphy JM, Noguer M. 1995. Simulation of climate-change over Europe using a nested regional-climate model. Part I: Assessment of control climate, including sensitivity to location of lateral boundaries. *Q J R Meteor Soc*, 121: 1413-1449.
- Jones, PD, Horton EB, Folland CK, Hulme M, Parker DE, Basnett TA. 1999. The use of indices to identify changes in climatic extremes. *Clim. Change*, 42, 131–149.
- Jungclaus JH, Keenlyside H, Botzet M, Haak H, Luo J-J, Latif M, Marotzke J, Mikolajewicz U, Roeckner E. 2006. Ocean Circulation and tropical variability in the coupled model ECHAM5/MPI-OM. *J Climate* 19 : 3952-3972
- Kharin VV, Zwiers FW 2000. Changes in the extremes in an ensemble of transient climate simulations with a coupled atmosphere-ocean GCM. *J. Climate*, 13, 3760–3780.
- Klawa M, Ulbrich, U. 2003. A model for the estimation of storm losses and the identification of severe winter storms in Germany. *Nat. Hazards Earth Syst. Sci.* 3: 725– 732.
- Knippertz P, Ulbrich U, Speth P. 2000. Changing cyclones and surface wind speeds over the North Atlantic and Europe in a transient GHG experiment. *Clim. Res.* 15 : 109–122.
- Knutti R, Stocker TF, Joos F, Plattner G-K. 2002: Constraints on radiative forcing and future climate change from observations and climate model ensembles. *Nature*, 416, 719–723.
- Kuwano-Yoshida, A; Asuma, Y. 2008. Numerical study of explosively developing extratropical cyclones in the northwestern pacific region. *Monthly Weather Review*, 136, 712-740.

- Lamb HH. 1972. British Isles weather types and a register of the daily sequence of circulation patterns, 1861-1971, *Geophys. Mem.*, 116, 85 pp. (HMSO, London.)
- Lambert SJ. 1996. Intense extra-tropical Northern Hemisphere winter cyclone events: 1189-1991. *J. Geophys. Res.*, 101, 21319–21325.
- Lambert SJ, Boer GJ. 2001. CMIP1 evaluation and intercomparison of coupled climate models. *Clim. Dyn.*, 17, 83–106.
- Lambert SJ, Fyfe JC. 2006. Changes in winter cyclone frequencies and strengths simulated in enhanced greenhouse warming experiments: results from the models participating in the IPCC diagnostic exercise. *Clim Dyn* 26:713-728
- Leckebusch GC, Ulbrich U. 2004. On the relationship between cyclones and extreme windstorm events over Europe under climate change. *Global and Planetary Change* 44 : 181-193, doi:10.1016/j.gloplacha.2004.06.011
- Leckebusch GC, Koffi B, Ulbrich U, Pinto JG, Spanghel T, Zacharias S. 2006. Analysis of frequency and intensity of winter storm events in Europe on synoptic and regional scales from a multi-model perspective. *Clim Res* 31 : 59-74
- Leckebusch GC, Ulbrich U, Fröhlich L, Pinto JG. 2007. Property loss potentials for European midlatitude storms in a changing climate. *Geophys. Res. Lett.* Vol. 34, L05703, doi:10.1029/2006GL027663
- Leckebusch GC, Weimer A, Pinto JG, Reyers M, Speth P. 2008a. Extreme wind storms over Europe in present and future climate: a cluster analysis approach. *Meteorol. Z.* 17:67-82
- Leckebusch GC, Renggli D, Ulbrich U. 2008b. Development and application of an objective storm severity measure for the Northeast Atlantic region. *Meteorol. Z.* 17:575-587
- Leckebusch GC, Donat MG, Ulbrich U, Pinto JG. 2008c. Mid-latitude Cyclones and Storms in an Ensemble of European AOGCMs under ACC. *CLIVAR Exchanges* Vol. 13, No. 3, 3-5. ISSN 1026 – 0471, chapter 6 in this thesis.
- Legutke S, Voss R. 1999. The Hamburg Atmosphere-Ocean Coupled Circulation Model ECHO-G, Technical report, No. 18, 62 pp., German Climate Computer Centre (DKRZ)
- Lenderink G, van den Hurk B, van Meijgaard E, van Ulden A, Cuijpers H. 2003. Simulation of present-day climate in RACMO2: First results and model developments. *KNMI Technical Report* 252:24
- Lunkeit F, Ponater M, Sausen R, Sogalla M, Ulbrich U, Windelband M. 1996: Cyclonic activity in a warmer climate. *Contrib Atmos Phys*, 69, 393–407.
- Manzini E, McFarlane NA. 1998: The effect of varying the source spectrum of a gravity wave parameterization in a middle atmosphere general circulation model. *J. Geophys. Res.* 103 : 31.523-31.539

- Marshall J, Kushnir Y, Battisti D, Chang P, Czaja A, Dickson R, Hurrell J, McCartney M, Saravanan R, Visbeck M. 2001. North Atlantic climate variability: phenomena, impacts and mechanisms. *Int. J. Climatol.* 21:1863–1898
- Marti O, Braconnot P, Bellier J, Benshila R, Bony S, Brockmann P, Cadule P, Caubel A, Denvil S, Dufresne JL, Fairhead L, Filiberti MA, Foujols M-A, Fichet T, Friedlingstein P, Goosse H, Grandpeix JY, Hourdin F, Krinner G, Lévy C, Madec G, Musat I, deNoblet N, Polcher J, Talandier C. 2005. The new IPSL climate system model: IPSL-CM4. *Note du Pôle de Modélisation*, 26, ISSN 1288-1619.
- Martin GM, Ringer MA, Pope VD, Jones A, Dearden C, Hinton TJ. 2006. The Physical Properties of the Atmosphere in the New Hadley Centre Global Environmental Model (HadGEM1). Part I: Model Description and Global Climatology. *J. Climate* 19 : 1274–1301.
- Matulla C, Schöner W, Alexandersson H, von Storch H, Wang XL. 2008. European storminess: late nineteenth century to present. *Clim. Dyn.* 31:125–130
- McCabe GJ, Clark MP, Serreze MC. 2001. Trends in northern hemisphere surface cyclone frequency and intensity. *J. Climate*, 14, 2763–2768.
- McCallum E, Norris WJT (1990) The storms of January and February 1990. *Meteorol Mag.* 119: 201–210
- Meehl GA, Tebaldi C. 2004: More intense, more frequent, and longer lasting heat waves in the 21st century. *Science*, 305, 994–997.
- Munich Re. 1993. Winterstürme in Europa, Publication of the Munich Re, Order Number 2041-E-d, www.munichre.com
- Munich Re 1999, Naturkatastrophen in Deutschland: Schadenerfahrungen und Schadenpotentiale, Publication of the Munich Re, Order Number 2798-E-d www.munichre.com
- Munich Re 2007, Zwischen Hoch und Tief – Wetterrisiken in Mitteleuropa, Edition Wissen, Publication of the Munich Re, Order Number 302-05481, www.munichre.com
- Murphy JM, Sexton DM, Barnett DN, Jones GS, Webb MJ, Collins M, Stainforth DA. 2004. Quantification of modelling uncertainties in a large ensemble of climate change simulations. *Nature* 430(7001) : 768-772.
- Murray RJ, Simmonds I. 1991. A numerical scheme for tracking cyclone centres from digital data. Part I: Development and operation of the scheme. *Aust. Meteorol. Mag.* 39:155–166
- Nakićenović N, Alcamo J, Davis G, de Vries B, Fenhann J, Gaffin S, Gregory K, Grübler A, Jung TY, Kram T, La Rovere EL, Michaelis L, Mori S, Morita T, Pepper W, Pitcher H, Price L, Raihi K, Roehrl A, Rogner H-H, Sankovski A, Schlesinger M, Shukla P, Smith S, Swart R, van Rooijen S, Victor N, Dadi Z. 2000. Emission scenarios. A Special Report of

- Working Group III of the Intergovernmental Panel on Climate Change. Cambridge University Press, 599 pp
- Paciorek JC, Risbey JS, Ventura V, Rosen RD. 2002. Multiple indices of Northern Hemisphere cyclonic activity, Winters 1949–99. *J. Climate*, 15, 1573–1590.
- Palmer, TN and Hagedorn R (eds). 2006. *Predictability of weather and climate*. Cambridge, UK. Cambridge University Press. 718pp.
- Palmer TN, Shutts GJ, Hagedorn R, Doblas-Reyes E, Jung T, Leutbecher M. 2005. Representing model uncertainty in weather and climate prediction, *Annu- Rev. Earth Planet Sci.* 33 : 163-193
- Palmer TN, Räisänen J. 2002. Quantifying the risk of extreme seasonal precipitation events in a changing climate, *Nature* 415 : 512-514
- Palutikof JP, Skellern AR. 1991. *Storm Severity over Britain, A Report to Commercial Union General Insurance, Climatic Research Unit, School of Environmental Sciences, University of East Anglia, Norwich (UK)*
- Panofsky HA, Tennekes H, Lenschow DH, Wyngaard JC. 1977. The Characteristics of Turbulent Velocity Components in the Surface Layer under Convective Conditions. *Boundary-Layer Meteorol*, 11: 355-361
- Pinto JG, Spanghel T, Ulbrich U, Speth P. 2005. Sensitivities of a cyclone detection and tracking algorithm: individual tracks and climatology. *Meteorol. Z.*14:823–838
- Pinto JG, Spanghel T, Ulbrich U, Speth P. 2006. Assessment of winter cyclone activity in a transient ECHAM4-OPYC3 GHG experiment. *Meteorol Z* 15 : 279-291.
- Pinto JG, Fröhlich EL, Leckebusch GC, Ulbrich U. 2007a. Changing European storm loss potentials under modified climate conditions according to ensemble simulations of the ECHAM5/MPI-OM1 GCM., *Nat. Hazards Earth Syst. Sci.* 7:165–175
- Pinto JG, Ulbrich U, Leckebusch GC, Spanghel T, Reyers M, Zacharias S. 2007b. Changes in storm track and cyclone activity in three SRES ensemble experiments with the ECHAM5/MPI-OM1 GCM. *Clim. Dyn.* 29:195-210. doi 10.1007/s00382-007-0230-4
- Pinto JG, Zacharias S, Fink AH, Leckebusch GC, Ulbrich U. 2009. Factors contributing to the development of extreme North Atlantic cyclones and their relationship with the NAO. *Clim. Dyn.* 32:711-737 doi: 10.1007/s00382-008-0396-4
- Pinto JG, Neuhaus CP, Leckebusch GC, Reyers M, Kerschgens M. 2010. Estimation of wind storm impacts over West Germany under future climate conditions using a statistical-dynamical downscaling approach. *Tellus A* doi:10.1111/j.1600-0870.2009.00424.x (in press)
- Raible CC. 2007. On the relation between extremes of midlatitude cyclones and the atmospheric circulation using ERA40, *Geophys. Res. Lett.* 34, L07703, doi: 10.1029/2006GL029084

- Raible CC, Della-Marta PM, Schwierz C, Wernli H, Blender R. 2008. Northern hemisphere midlatitude cyclones: A comparison of detection and tracking methods and different reanalyses. *Mon. Wea. Rev.*, 136, 880-897.
- Räisänen J. 2005. Probability distributions of CO₂-induced global warming as inferred directly from multimodel ensemble simulations. *Geophysica*, 41, 19–30.
- Räisänen J. 2007. How reliable are climate models? *Tellus 59A* : 2–29
- Reichler T and Kim J. 2008. How Well Do Coupled Models Simulate Today's Climate? *Bull. Amer. Meteor. Soc*, 89, 303-311. DOI:10.1175/BAMS-89-3-303
- Reifen C and R Toumi, 2009. Climate projections: Past performance no guarantee of future skill?, *Geophys. Res. Lett.*, 36, L13704, doi: 10.1029/2009GL038082.
- Ringer MA, Martin GM, Greeves CZ, Hinton TJ, James PM, Pope VD, Scaife AA, Stratton RA, Inness PM, Slingo JM, Yang G-Y. 2006. The Physical Properties of the Atmosphere in the New Hadley Centre Global Environmental Model (HadGEM1). Part II: Aspects of Variability and Regional Climate. *J Climate* 19 : 1302–1326.
- Roberts NM, Forbes RM. 2002. An observational study of multiple cloud head structure in the FASTEX IOP 16 cyclone. *Atmospheric Science Letters*, 3, 59-70.
- Rockel B, Woth K. 2007. Extremes of near-surface wind speed over Europe and their future changes as estimated from an ensemble of RCM simulations. *Climatic Change*, 81: 267-280
- Rummukainen M, Raisanen J, Bringfelt B, Ullerstig A, Omstedt A, Willen U, Hansson U, Jones C. 2001. A regional climate model for northern Europe: model description and results from the downscaling of two GCM control simulations. *Clim. Dyn.*, 17: 339-359.
- Sánchez E, Romera R, Gaertner MA, Gallardo C, Castro M. 2009. A weighting proposal for an ensemble of regional climate models over Europe driven by 1961-2000 ERA40 based on monthly precipitation probability density functions. *Atmospheric Science Letters*, doi 10.1002/asl.230
- Schär C, Vidale PL, Luthi D, Frei C, Haberli C, Liniger MA, Appenzeller C. 2004. The role of increasing temperature variability in European summer heatwaves. *Nature*, 427, 332-336.
- Serreze MC, Carse F, Barry RG. 1997. Icelandic low cyclone activity climatological features, linkages with the NAO, and relationships with recent changes in the Northern Hemisphere circulation. *J. Climate*, 10, 453–464.
- Simmonds I, Keay K. 2000. Variability of Southern Hemisphere extra-tropical cyclone behaviour, 1958–97. *J. Climate*, 13, 550–561.
- Schmidtke H, Scherrer HU. 1997. *Sturmschäden im Wald*. Swiss National Science Foundation, NFP 31. vdf — Hochschulverlag AG: ETH Zürich; 38 pp.
- Schneidereit A, Blender R, Fraedrich K, Lunkheit F. 2007. Iceland climate and North Atlantic cyclones in ERA40 reanalyses. *Meteorol. Z.* 16:17-23.

- Schrodin R (ed). 1995. Dokumentation des EM/DM Systems, Deutscher Wetterdienst, Offenbach a. Main
- Schwierz C, Köllner-Heck P, Zenklusen Mutter E, Bresch DN, Vidale P-L, Wild M, Schär C. 2009. Modelling European winter wind storm losses in current and future climate. *Climatic Change* (in press) DOI 10.1007/s10584-009-9712-1.
- Selten FM, Branstator GW, Kliphuis M, Dijkstra HA. 2004. Tropical origins for recent and future northern hemisphere climate change. *Geophys. Res. Lett.*, 31, L21205, doi:10.1029/2004GL020739.
- Serreze MC, Carse F, Barry RG, Rogers JC. 1997. Icelandic Low cyclone activity: Climatological features, linkages with the NAO and relationships with recent changes elsewhere in the Northern Hemisphere circulation. *J. Clim.* 10: 453-464.
- Smith LA. 2002. What might we learn from climate forecasts? *Proc. Natl. Acad. Sci. U.S.A.*, 99, 2487-2492.
- Stephenson DB, Pavan V, Collins M, Junge MM, Quadrelli R, participating CMIP2 modelling groups. 2006. North Atlantic Oscillation response to transient greenhouse gas forcing and the impact on European winter climate: a CMIP2 multi-model assessment, *Climate Dynamics* 27 : 401-420, DOI 10.1007/s00382-006-0140-x
- Stappeler J, Dom G, Schättler U, Bitzer HW, Grassmann A, Damrath U, Gregoric G. 2003. Mesogamma scale forecasts using the nonhydrostatic model LM. *Meteorol Atmos Phys*, 82: 75-96.
- Swiss Re. 2008. Natur- und Man-made-Katastrophen im Jahr 2007: hohe Schäden in Europa. *Sigma*, Nr. 1/2008, Swiss Re publishing, Zürich (in German, <http://www.swissre.com>)
- Taylor PA, Teunissen HW. 1987. The Askevein Hill Project: Overview and Background Data. *Boundary-Layer Meteorol*, 39: 15-39
- Tebaldi C, Knutti R. 2007. The use of the multi-model ensemble in probabilistic climate projections. *Philosophical Transactions of the Royal Society A* Volume 365, Number 1857 : 2053-2075, doi: 10.1098/rsta.2007.2076
- Thiele D. 2008. Windgeschwindigkeiten in Stations-, Reanalyse und Klimamodelldaten in Abhängigkeit zur Orographie, Diploma Thesis, Institute for Meteorology, Freie Universität Berlin.
- Trigo RM, Dacamura CC. 2000. Circulation weather types and their influence on the precipitation regime in Portugal. *Int. J. Climatol.* 20: 1559-1581
- Ulbrich U, Fink A, Klawa M, Pinto JG. 2001: Three extreme storms over Europe in December 1999. *Weather* 56: 70-80
- Ulbrich U, Brücher T, Fink AH, Leckebusch GC, Krüger A, Pinto JG. 2003a. The central European floods of August 2002. Part I: rainfall periods and flood development. *Weather*, 58, 371-377.

- Ulbrich U, Brücher T, Fink AH, Leckebusch GC, Krüger A, Pinto JG. 2003b. The central European floods of August 2002. Part II: synoptic causes and considerations with respect to climatic change. *Weather*, 58, 434–442.
- Ulbrich U, Leckebusch GC, Pinto JG. 2009. Cyclones in the present and future climate: a review. *Theor. Appl. Climatol.*, 96:117-131
- Ulbrich U, Pinto JG, Kupfer H, Leckebusch GC, Spangehl T, Reyers M. 2008. Northern Hemisphere Storm Tracks in an ensemble of IPCC climate change simulations. *J Clim* 21 : 1669-1679
- Uppala SM, Allberg K, Simmons PW, Andrae AJ, Da Costa U, Bechtold V, Fiorino M, Gibson JK, Haseler J, Hernandez A, Kelly GA, Li X, Onogi K, Saarinen S, Sokka N, Allan RP, Andersson E, Arpe K, Balmaseda MA, Beljaars ACM, Van De Berg L, Bidlot J, Bormann N, Caires S, Chevallier F, Dethof A, Dragosavac M, Fisher M, Fuentes M, Hagemann S, Hólm E, Hoskins BJ, Isaksen I, Janssen PA, Jenne R, McNally AP, Mahfouf JF, Morcrette JJ, Rayner NA, Saunders RW, Simon P, Sterl A, Trenberth KE, Untch A, Vasiljevic D, Viterbo P, Woollen J. 2005. The ERA-40 re-analysis. *Q. J. Roy. Meteor. Soc.* 131: 2961-3012.
- van Bebber WJ. 1891, Die Zugstrassen der barometrischen Minima, *Meteorol. Z.*, Oktober 1891: 361-366
- van Ulden AP, van Oldenborgh GJ. 2006. Large-scale atmospheric circulation biases and changes in global climate model simulations and their importance for regional climate scenarios: a case study for West-Central Europe, *Atmospheric Chemistry and Physics* 6 : 863–881
- von Storch H, Langenberg H, Feser F. 2000. A spectral nudging technique for dynamical downscaling purposes. *Mon Weather Rev*, 128 (10): 3664-3673
- Wakimoto RM, Bosart BL. 2001. Airborne radar observations of a warm front during FASTEX. *Monthly Weather Review*, 129, 254-274
- Walker GT. 1924. Correlations in seasonal variations of weather IX. *Mem. India Meteorol. Dept.* 24: 275–332
- Wang XL, Zwiers FW, Swail VR, Feng Y. 2009. Trends and Variability of Storminess in the Northeast Atlantic Region, 1874-2007, *Clim. Dyn.* in press doi 10.1007/s00382-008-0504-5
- Wanner H, Bronnimann S, Casty C, Gyalistras D, Luterbacher J, Schmutz C, Stephenson DB, Xoplaki E. 2001. North Atlantic Oscillation—concepts and studies. *Surv. Geophys.* 22: 321–382
- WASA. 1998. Changing waves and storms in the Northeast Atlantic? *Bull. Am. Meteorol. Soc.* 79: 741–760
- Wernli H, Dirren S, Liniger MA, Zillig M. 2002. Dynamical aspects of the life cycle of the winter storm 'Lothar' (24-26 December 1999). *Q. J. Roy. Meteor. Soc.* 128: 405-429

- Weigel AP, Liniger MA, Appenzeller C. 2008. Can multi-model combination really enhance the prediction skill of probabilistic ensemble forecasts? *Quaternary Journal of the Royal Meteorological Society*, 134: 241-260.
- White PW and colleagues. 2003. IFS Documentation CY23r4. Part IV: Physical Processes (CY23r4). <http://www.ecmwf.int/research/ifsdocs/CY23r4/>
- Žagar N, Žagar M, Cedilnik J, Gregorič G, Rakovec J. 2006. Validation of mesoscale low-level winds obtained by dynamical downscaling of ERA40 over complex terrain. *Tellus A*, 58: 445-455. DOI: 10.1111/j.1600-0870.2006.00186.x

Acknowledgements

I would like to thank Prof. Dr. Uwe Ulbrich and PD Dr. Leckebusch for the opportunity to work on this interesting topic, for their support during the formation of this work, for fruitful discussions and for their goal-orientated supervision. I am grateful to Prof. Ulrich Cubasch for agreeing to be the second referee of this thesis. Special thanks go to all my dear colleagues from the working group *Climate Diagnostic and Meteorological Extreme Events* at Freie Universität Berlin for having a friendly and relaxed but focused and productive working atmosphere. Furthermore, I am thankful to my parents for their support and for being there. Last but not least, I am much obliged to the couple of important friends in my life for amiable diversion and company during the parts of life besides science.